Changes in the Shape of the Developing Vertebrate Nervous System Analyzed Experimentally, Mathematically and by Computer Simulation

ANTONE G. JACOBSON AND RICHARD GORDON
Department of Zoology, University of Texas, Austin, Texas 78712 and Image Processing Unit, National Cancer Institute, National Institutes of Health, Bethesda, Maryland 20014

ABSTRACT Two forces are necessary and sufficient to produce the transformation of the newt neural plate from a hemispheric sheet of cells one cell thick to a keyhole shape. These forces are: (1) a regionally programmed *shrinkage* of the surface of the neural plate (accomplished by contraction of the apical surfaces of the neural plate cells and elongation of these cells perpendicular to the plate); and (2) *displacement* of the whole sheet caused by elongation of either the notochord or the overlying neural plate cells in the antero-posterior direction. A computer simulation and mathematical analysis ("morphodynamics"), together with experiments and observations on embryos, were used to deduce the morphogenesis of the neural plate from these forces.

"The morphologist . . . will enquire whether two different but more or less obviously related forms can be so analysed and interpreted that each may be shown to be a transformed representation of the other. This once demonstrated, it will be a comparatively easy task (in all probability) to postulate the direction and magnitude of the force capable of effecting the required transformation . . . if such a simple alteration of the system of forces can be proved adequate to meet the case, we may find ourselves able to dispense with many widely current and more complicated hypotheses of biological causation. For it is a maxim in physics that an effect ought not to be ascribed to the joint operation of many causes if few are adequate to the production of it."—D'Arcy Thompson ('52)

I. INTRODUCTION

We have analyzed an example of one of the most common morphogenetic movements in embryos, the distortion of a coherent sheet of cells. In the newt, the central nervous system begins at gastrulation as a hemispheric sheet one cell thick. It then shrinks into a keyhole-shaped, thickened *neural plate*, while remaining a monolayer of cells in the process (fig. 1). We will demonstrate that the joint operation of two physical forces is necessary and sufficient to effect this transformation. These forces are: (1) *shrinkage* of the neural plate surface and (2) *displacement* of the region overlying the notochord. Shrinkage is accomplished by a regionally programmed contraction of the apical surfaces of the cells. (They are simultaneously undergoing an active elongation in a direction perpendicular to the sheet. See fig. 2) Displacement, the second force, results from elongation of the region of the neural plate attached to the notochord. This elongation in the antero-posterior direction results in reshaping of the whole sheet.

Morphogenesis is the consequence of the action of individual cells. Studies of morphogenesis are comparable to studies in statistical mechanics: both seek explanations of the dynamics and properties of the whole (an organism or bulk matter) in terms of the behavior and interactions of its parts (cells or molecules), (Gordon, '66). The urodele central nervous system provides an exemplary subject for such a study, because its early shaping can be analyzed in terms of the coordinated physical behavior of its individual cells.

As the neural plate changes shape, the apical shrinkage of each cell pulls the whole sheet towards itself, thus contributing to the motion of the whole sheet. The result is a complex relationship between the morphogenesis of the neural plate and the behavior of its component cells. In order to unravel this relationship, we created a computer simulation which allowed us to watch, in a completely controlled manner, how the physical interactions among

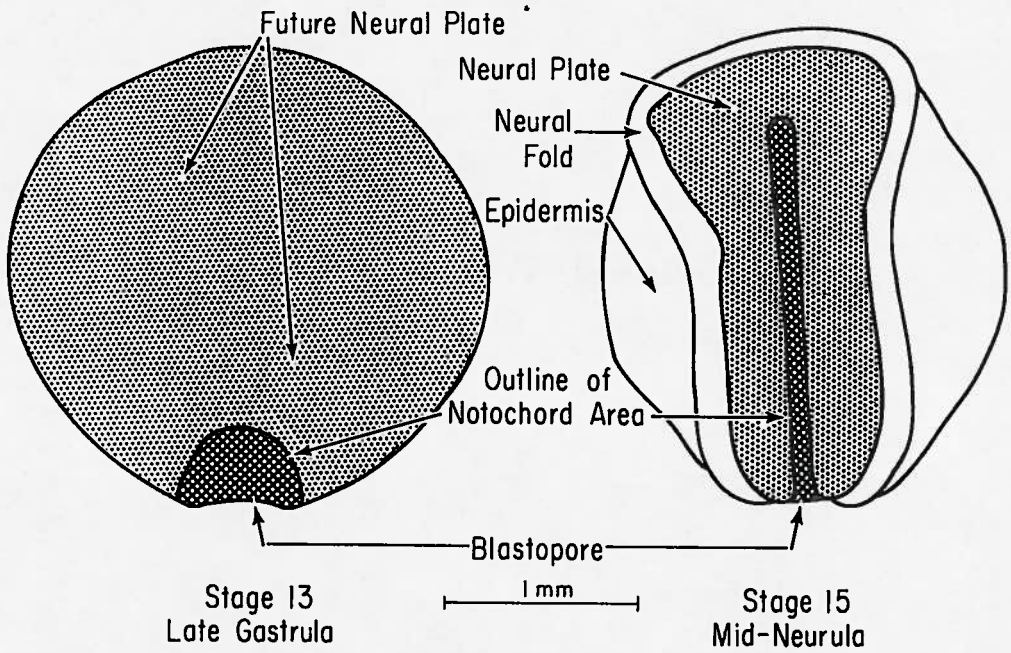

Fig. 1 In this paper we analyse the change in shape of the neural plate from a hemispheric shell at stage 13 to a keyhole shape at stage 15. These dorsal views of late gastrula and mid-neurula stages were drawn from projected movie frames of the same embryo at two stages of development. The outline of the notochordal area of the neural plate coincides with the outline of the notochord as seen through the neural ectoderm.

the cells lead to the keyhole shape of the neural plate. In constructing the logic for the computer simulation, it was necessary to formulate clear, quantitative statements of the principles governing cell behavior. Therefore, the act of creating the simulation sharpened our observations of the embryo.

In expressing cell behavior in mathematical terms, we have derived a formal mathematical description of the flow of tissues in the developing embryo which we call *morphodynamics*. This analysis contributed to the computer simulation and also provided experimentally testable predictions not derivable by simulation. Thus our investigation has utilized a full interplay of three modes of inquiry:

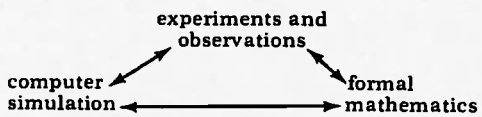

By defining the forces that shape the early neural plate, we describe, for the first time, the cellular basis for a D'Arcy Thompson grid transformation (Thompson, '52).

In the course of this work we have also uncovered the following:

We have found that shear lines correlate with major developmental boundaries in the embryo.

A spatial and temporal analysis was made of the unresolved tissue tensions in the ectoderm.

A new fate map of the neural plate, just after gastrulation, was constructed.

A new algorithm for flows of viscoelastic materials, such as embryonic tissues, was developed.

Burnside and Jacobson ('68) suggested that shape changes of the neural plate cells caused its morphogenesis. We will: (1) demonstrate that these cell shape changes are not sufficient to shape the neural plate (Section III); (2) show the role of the notochordal region in generating the necessary additional force (Section IV); and (3) compare the predictions of our resulting model with the observed transformation (Section VII).

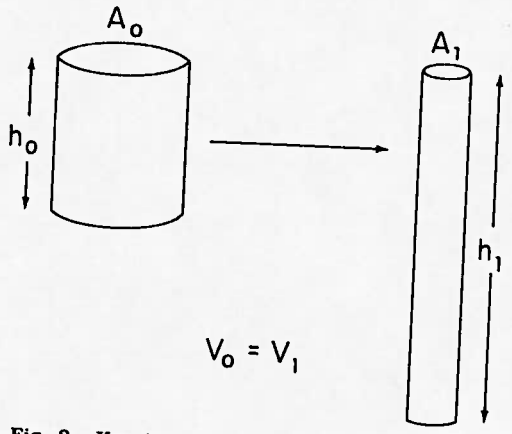

Fig. 2 Keeping the same volume, a cell increases its height (h_0 to h_1), while decreasing its apical surface (A_0 to A_1). The apical surfaces of the cells form the dorsal surface of the neural plate. The long axes of the cells are perpendicular to the surface of the plate. The apical area is inversely proportional to the height, $A = V/h$, since the cells retain a columnar shape during stages 13 to 15.

The rest of this paper contains: a brief description of the computer simulation in Sections V and VI; additional observations, ramifications and experiments in Section VIII; and discussion and historical background in Section IX. Details of the computer simulation and mathematics are given in APPENDICES 1 and 2. A few biological "Assumptions" were needed to specify details in the simulation. These are justified by experiments and observations in APPENDIX 3.

II. MATERIALS AND METHODS

We have studied primarily the California newt, *Taricha torosa* (also called *Triturus torosus*), from the San Francisco Bay area. The experiments, observations and references that follow apply to this animal unless otherwise stated. Morphological stages of the embryo were defined by Twitty and Bodenstein (in Rugh, '62) and a fate map of the nervous system in the late gastrula (stage 13) was constructed by Schechtman ('32) using vital dyes. The transformation investigated takes place between earliest neurula stage 13 and the mid-neurula stage 15 (fig. 1).

General methods for microsurgical operations on this species are described in detail by A. G. Jacobson ('67). Embryos were kept at 17°C.

Time-lapse movies of normal and experimental embryos were made in a constant temperature room at 17°C. A 42-mm Summar lens attached through a focussing telescope directly to a movie camera produced an image of the 2.4-mm diameter embryo that just filled the 16-mm movie frame. One-quarter second exposures were made at one minute intervals. Two heat-filtered microscope lamps provided incident illumination during the exposure period only. Movies were analysed with a stop motion projector equipped with a frame counter. Since each frame represented one minute, accurate timing of the embryos' development was possible.

Volume measurements of the neural plate were made from serial sections by projecting each section onto high quality paper which varied little in weight per unit area. The tissue outline was cut out and weighed. Projection was done through a side-arm drawing tube attached to a microscope with a Zeiss photochanger.

Simulation methods are described in detail in APPENDIX 1. During the 5-year development of this project we made use of the Sigma 7 computer at the Woods Hole Oceanographic Institution, the CDC 6600 and SDS 930 computers at the University of Texas at Austin, and the CDC 6400 at the State University of New York at Buffalo. The project has been completed using the PDP-10 computer at the National Institutes of Health at Bethesda, Maryland. The program is written in Fortran IV and is called *SHRINK for Simulated Hydrodynamic Reshaping Into Neural Keyhole*. Listings may be obtained from Richard Gordon.

III. SHRINKAGE ALONE IS INSUFFICIENT TO CAUSE THE SHAPE TRANSFORMATION

Both Gillette ('44) and C.-O. Jacobson ('62) noted a correlation between the increasing height of neural plate cells and the decreasing surface area of the plate. Burnside and A. G. Jacobson ('68) found that this correlation holds for each region and concluded:

> "Observed displacements of groups of neural plate cells are the consequence of deformations of the sheet . . . these deformations are the result of regional differences in the amounts of change of shape of the constituent cells.
>
> "Thus one consequence of primary embryonic induction is a patterned change in the height of cells in the forming neural plate. . . ."

Thus we postulated that nonuniform apical shrinkage of the neural plate cells (fig. 2) might be sufficient to account for its change of shape. This idea seemed reasonable because the future course of shrinkage of the apical surfaces of the cells is already determined at the beginning stage 13 (*Assumption* 4, APPENDIX 3) and the volumes of the cells do not change with time (*Assumption* 1).

Each of our three modes of inquiry led to the conclusion that no shrinkage pattern was adequate in itself to explain the observed shape transformation:

(1) *Computer simulation*

A computer program was designed which divided a disc-shaped sheet into a number of circles whose areas could decrease in any designated spatial and temporal pattern. After each increment of shrinkage the circles were moved so as to approximately retain their contiguity. A great many shrinkage patterns were tried; none generated a keyhole shape. At best, the simulation produced a slightly distorted disc narrowed at one end (fig. 3).

(2) *Experiment and observation*

A simulation using shrinkage only is equivalent to the experiment of isolating a stage 13 neural plate from all other tissues and following its subsequent development (Section IV). Isolated neural plates shrank, but did not form keyhole shapes (fig. 3).

(3) *Mathematics*

Since each cell pulls equally in all directions as it shrinks, to first approximation it should retain its apical shape. Mathematically, the transformation would then be *conformal.* One property of a conformal transformation is that the angle between two intersecting lines drawn on the sheet of cells would not change during the deformation (APPENDIX 2). However, considerable angle changes *are* observed in some regions of the plate (fig. 4), contradicting the hypothesis that isotropic shrinkage could be the sole driving force for the transformation. (This argument is analysed more critically in APPENDIX 2).

IV. THE ROLE OF THE NOTOCHORDAL REGION

Since a patterned shrinkage of the apical surface was not sufficient by itself to produce a keyhole-shaped neural plate, it became clear that at least one other force

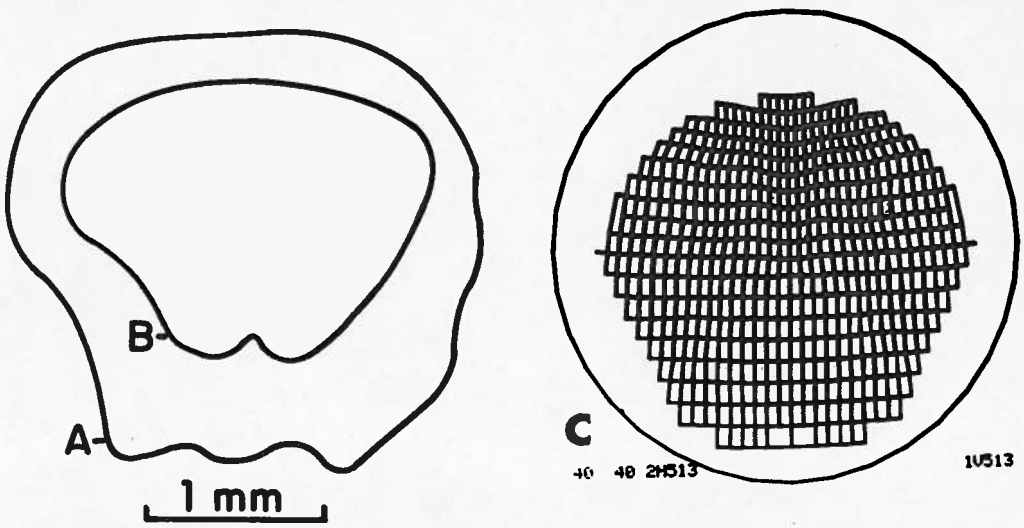

Fig. 3 A. Appearance of the neural plate immediately after isolation without notochord at stage 13. B. Shape attained in the same explant when controls had reached mid-neurula stage 15. C. Results of a computer simulation using shrinkage alone, which should be compared to B. This simulation is the same as SIM 1 in figure 16, Section VII, except no notochordal area is included. The simulation is explained in sections V and VI. The outer circle shows the neural plate perimeter at stage 13, the inner grid is the shape attained by stage 15. A and B are outline drawings made from projected frames of a time-lapse movie. Posterior is at the bottom of each figure. C is a photo from a computer graphics terminal.

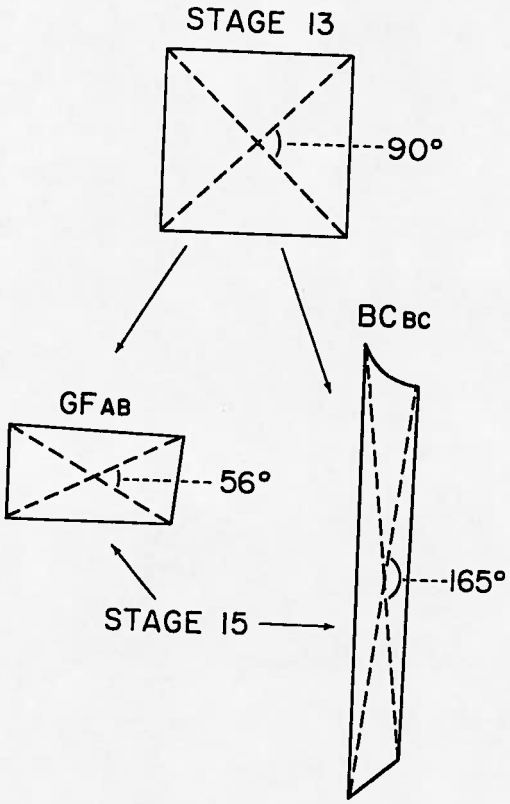

Fig. 4 In Burnside and Jacobson ('68) (our fig. 22) a stage 13 neural plate is marked off in a square coordinate grid. The distortion of two regions (GFab and BCbc) at stage 15 is shown here. The angles of the intersecting diagonals change between stages 13 and 15 so the mapping is not conformal.

was necessary to explain the shape transformation. We postulated that the notochordal area of the neural plate might provide the additional driving force. Some of the neural plate cells are closely associated with the underlying notochord. The following eight sets of observations and experiments implicate the notochordal area (fig. 1) as a causative agent in shaping the neural plate:

(1) *Fate mapping of the notochord and overlying neural plate*

C.-O. Jacobson and Löfberg ('69) mapped the movements of the dorsal mesoderm, using vital dye techniques, and compared the movements in the mesoderm with cell displacements in the overlying neural plate. They found that the notochord and the neural plate cells that overlie it follow almost identical paths of displacement. The remaining mesoderm and overlying neural plate showed considerable differences in amount and to some extent direction of displacement. (These experiments were done on *Amblystoma punctatum* and *A. mexicanum*. Movements were followed between stages 14 and 17.)

(2) *Movements of the neural plate over notochord observed with time-lapse movies*

Between stages 13 and 15, as seen in time-lapse movies, the notochord and the region of the neural plate overlying it move in unison. Individual neural plate cells were followed by taking advantage of the natural variegations in pigmentation. The shape of the notochord could be seen through the neural plate and was especially apparent in color movies. The two regions clearly move together. Following a lag of approximately 600 minutes, elongation is linear with time to stage 15 (fig. 5).

The notochord and overlying neural plate cells do not elongate from one end, but

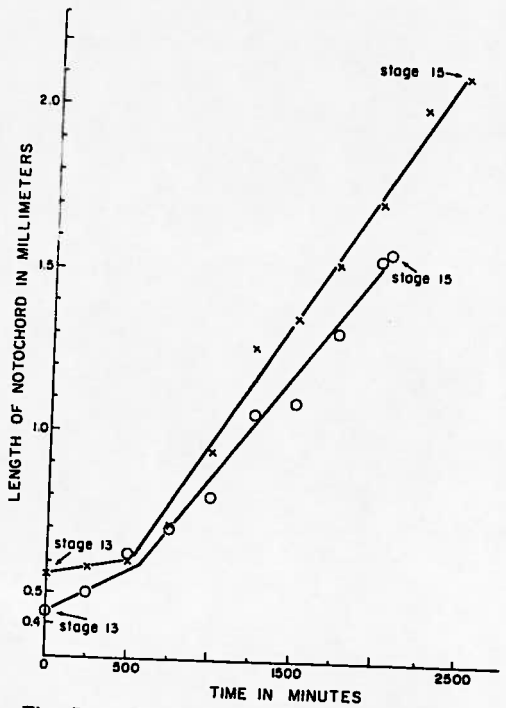

Fig. 5 The length of the notochordal region of the neural plate, and of the underlying notochord seen through the neural ectoderm, was measured at different time intervals from projected frames of time-lapse movies of two embryos (x,o).

rather the elongation is uniform along the whole length (fig. 6).

(3) *Histology*

Figure 7 shows a section through a stage 15 neural plate and the underlying mesoderm and endoderm. The bases of neural plate cells attach firmly to the notochord, but not directly to other subjacent mesoderm. At earlier stages, the attachment of the notochord to the neural plate is less intimate, but always close, and always more than with lateral mesoderm. (At stage 13, the most intimate attachment between neural plate and notochord is at the anterior end of the notochord.)

(4) *Mechanical attachment*

When the neural plate is excised, the plate is readily separated from all mesoderm except the notochord. Separation of the notochord from the neural plate requires dissection, usually with some injury to the cells. (Separation is more easily accomplished at stage 13 except for the anterior end of the notochord. Here the attachment is sufficiently strong that separation almost always damages both plate and notochord cells of that region. See fig. 9.)

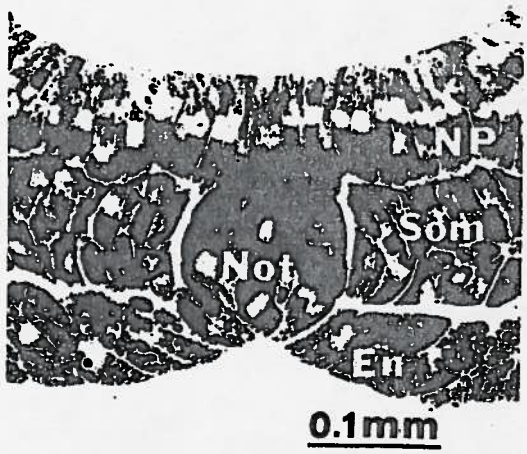

Fig. 7 Cross section (thick section, 1 μ) through the neural plate (NP) and underlying notochord (NOT), somite mesoderm (SOM), and endoderm (EN) of a stage 15 embryo. The neural plate cells are bound tightly to the notochord, but are separated from the somite mesoderm by extracellular space. Note that the neural plate is just one cell thick and each cell stretches from the top to the bottom of the plate. (Photo courtesy of Beth Burnside).

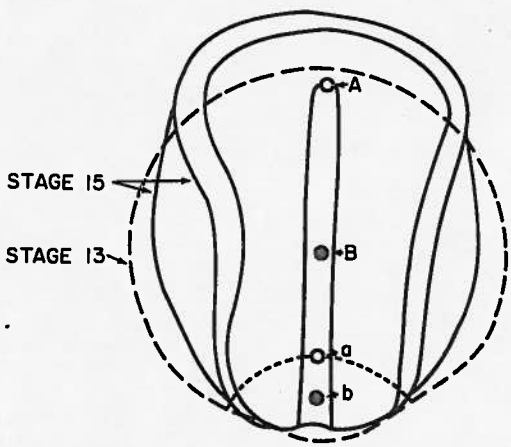

Fig. 6 The outline of the embryo and notochordal region are shown at stage 13 (dashes) and at stage 15 (solid lines). On a movie of development of the embryo, cells were located at stage 15 at the anterior end of the notochordal area and half way to the blastopore (A and B). These cells were then followed as the movie was run backwards to stage 13. The two cells then occupied positions a and b. Point a was still at the top of the notochordal area and point b half way to the blastopore. Thus, the regions between a and b and between b and the blastopore appear to elongate proportionately.

(5) *Isolated neural plate*

We have found that the prospective neural plate, isolated by itself at stage 13, will not generate a keyhole shape. The neural ectoderm of stage 13 embryos was excised and cleaned of underlying tissues. The tissue was placed on a bed of neutral (pH 7) agar (to which the basal ends of the cells do not attach). These plates were prevented from curling by placing over them pieces of cover slips with beaded edges that supported the weight of the slips. (The apical surface of the neural plate is non-adhesive.) The morphogenesis of these explants (19 cases) was recorded either by time-lapse cinematography or with a sequence of photographs. The typical shape assumed by such explants when control embryos reared in the same dishes had reached stage 15 (keyhole shape) is shown in figure 3. The shape of the isolated neural plate is comparable to a computer simulation which includes no notochordal region (fig. 3).

(6) *Neural plate isolated with notochord*

We have made numerous isolations of the entire neural plate of stage 13 late gastrulae leaving attached various combinations that include notochord. The neural plate and attached notochord, with no other tissues, will generate a keyhole-shaped plate (fig. 8). These explants (5 cases) were held flat against neutral agar and recorded as above. Control embryos were reared in the same dishes.

These results indicate that only neural ectoderm and notochord are essential to obtain a keyhole-shaped plate. Any contribution that other tissues, such as epidermis and presumptive somites, may make to the process is not essential after stage 13.

(7) *Whole embryo without notochord*

Two stage 13+ embryos were slit along the ventral midline and all the endoderm removed to expose the notochord, which was then removed with as little damage to the neural plate as possible.

These embryos did not form a keyhole shape at stage 15. They had a neural fold-like structure only around the anterior half of the plate. The posterior half changed very little and did not narrow (fig. 9). The somite, prechordal, mandibular, etc., mesoderm and epidermis were present in the embryo in these experiments.

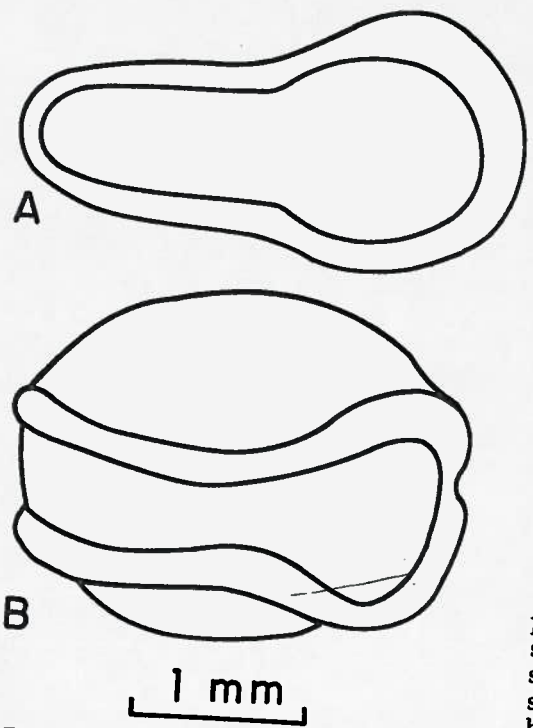

Fig. 8 At stage 13 the neural plate and attached underlying notochord were isolated. These outline drawings are from projected movie frames showing (A) the keyhole shape attained by the isolated neural plate with notochord by the time a control embryo (B) in the same dish had reached stage 15+.

Fig. 9 Dorsal view of the neural plate of an embryo at stage 15 that was deprived of notochord and the entire endoderm at stage 13. The injured area is at the anterior tip of the notochordal area, posterior is at the bottom. The notochordal region of the neural plate remains spread out posteriorly rather than forming a narrow midline rod.

(8) *Isolation of notochord with only those neural plate cells that overlie it*

This combination of tissues was explanted onto neutral agar in Holtfreter's solution (fig. 10). The neural ectoderm spreads over the exposed notochordal tissue, then the whole complex elongates and bends. The amount and rate of elongation of this isolate compares well with the elongation of the neural plate region overlying the notochord in the intact embryo. (Compare fig. 11 to fig. 5. Both elongated 1 mm in 2,000 minutes.)

We conclude that anterior-posterior elon-

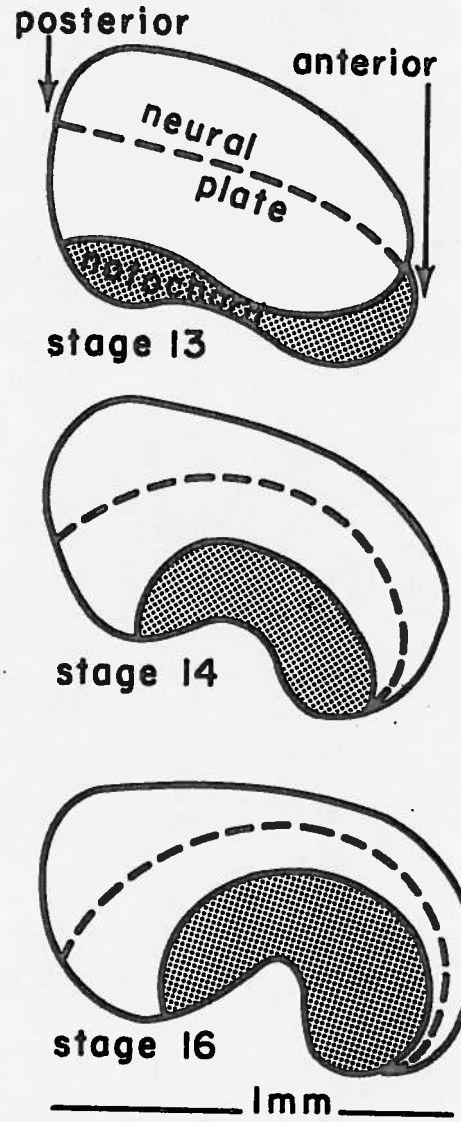

Fig. 10 Drawings from projected frames of a time-lapse movie of side views of isolated notochord and that region only of the neural plate that directly overlies the notochord. The explant is shown at three times when controls were at the stages indicated. The length of the notochordal area of the neural plate was measured with a map measurer along the dashed lines at the stages shown and at intermediate times (fig. 11). The lines are chosen somewhat arbitrarily, but are consistent from stage to stage. Since the explant bent on itself, the top and bottom edges of the neural portion had different lengths, thus a position half-way between was chosen for measurement.

gation of the neural plate requires the attached notochord. We have not observed elongation in notochord isolated alone at stage 13. But the two tissues together do elongate.

The notochord could be responsible for providing the sole force for the elongation. Alternatively, whatever mechanisms redistribute the notochord cells into an elongated rod may be duplicated in the neural plate cells that overlie it. In this case the motive forces would be generated partly or entirely within the plate. Whatever the case, we have demonstrated that continued association between notochord and overlying plate cells after stage 13 is required for elongation; i.e., the notochordal region of the neural plate and the underlying notochord act in concert.

V. BRIEF DESCRIPTION OF THE COMPUTER SIMULATION

The neural plate is represented in the SHRINK computer program as a sheet of about 300 circular *shrinkage units*, each

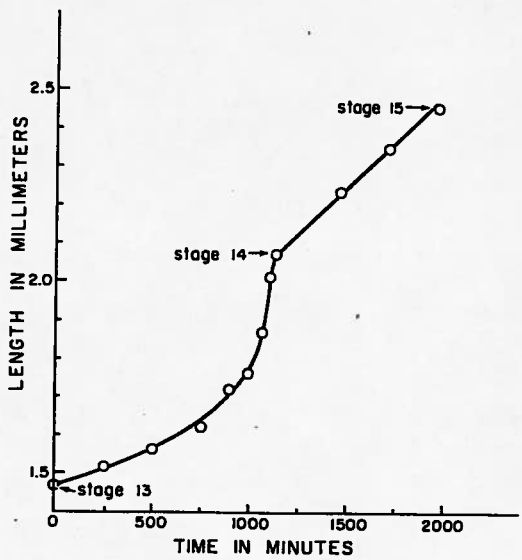

Fig. 11 Lengths of notochordal region (dashed lines in fig. 10) plotted against time. Compare to the increase in length of the notochordal region of the intact embryo (fig. 5). The initial lag is more pronounced in the explant, but notochordal regions of both explant and intact embryos eventually elongate about 1 mm in 2,000 minutes. The lengths measured on the isolate are longer, due probably to the technique (fig. 10).

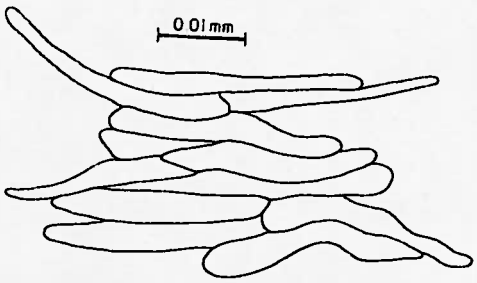

Fig. 12 Diagrammatic representation of apical surfaces of maximally stretched neural plate cells in the spinal cord (narrow) region near the neural fold of a stage 15 embryo. The cells are stretched in the medio-lateral direction. The drawing is taken from a projection of a high magnification time-lapse film.

corresponding on average to approximately 30 cells in the embryo. Initially, the shrinkage units are closely packed and have the same radius (cf. fig. 29B). Each unit is assigned one of nine *height programs* indicating how its height, perpendicular to the sheet, will increase with time. (A unit's area is inversely proportional to the height, and its radius proportional to the square root of the area. Thus we may interchangeably speak of either a height or shrinkage program.) We define the *shrinkage pattern* to mean the initial spatial distribution of height programs. The shrinkage pattern may be altered to imitate surgical manipulations.

Nearest neighbor units are connected by *bonds*. As the units shrink, these bonds are used to pull them together, as if they were connected by rubber bands.

The notochordal region of the neural plate is represented by an inverted parabola containing shrinkage units that are arranged uniformly along its perimeter. Bonds are established across the notochordal region to represent the indirect connection between the two sides. The parabola is elongated in 40 small steps and reconfigured so the notochordal region always has the same area, as we have observed in the embryo (*Assumption* 9, APPENDIX 3).

The simulation proceeds by elongating the notochordal region, shrinking each unit, and then pulling all the units together via their network of bonds (until the repacking approximates a continuous sheet). Pulling starts at the perimeter of the notochordal region and propagates outward. Bonds at equivalent distances from the notochordal region are considered in random order to avoid systematic effects. Departures from bilateral symmetry are corrected.

The large distortions of the sheet sometimes lead to excessively long bonds and crossed bonds which we then break and connect to new nearest neighbors. This simulates the *viscoelastic* nature of the sheet. The change of nearest neighbors indicates *shear*.

Some numerical parameters had to be estimated to guarantee numerical stability of the computation.

Full details of the simulation are given in APPENDIX 1.

VI. EMPIRICAL PARAMETERS FOR THE COMPUTER SIMULATION

Only a few biological parameters need to be measured for the computer simulation. These involve certain physical dimensions versus time, the height programs and shrinkage pattern, and the distensibility of the cells in the plane of the neural plate:

(1) *Dimensions*

The parabolic area of the neural plate representing the notochord is given an initial width and length and a final length that are measured from time-lapse movies. This area is kept constant (*Assumption* 9, APPENDIX 3). At the beginning of stage 13 the notochord is 0.54 mm long and 0.54 mm wide at its base. At stage 15 it reaches a length of 2.07 mm and is 0.14 mm wide at its base.

We assume that the neural plate may be represented as a flat disc (*Assumption* 2). Its radius is 1.2 mm, equal to the radius of the embryo. In the embryos, the neural plate is not flat until late stage 13, at which time the notochord is 0.98 mm long and 0.3 mm wide. These dimensions were taken as the *initial conditions* for the simulation, which thus extends from late stage 13 to stage 15. (Late stage 13 is designated as the "beginning" of stage 13 by Burnside and Jacobson, '68.)

(2) *Distensibility of cells*

The computer simulation requires a *relative cutoff distance*, (defined in APPENDIX 1), at which two bound units break apart.

No analagous event has yet been observed in the embryo, probably because high magnification movies have only been made of regions where such breakage would not be expected. However, considerable stretching does occur in these regions. Cells elongate *in the plane* of the neural plate, so that their apical surfaces become spindle shaped (fig. 12). Long axes are always in the medio-lateral direction. We calculated the average length to width ratio for a group of such cells which were undergoing the maximum observed stretching. The ratio averaged 9.6 for ten cells. We may regard two such cells end to end as ellipses with major half axes l_1 and minor half axes l_2. If we assume that their surface areas are unchanged by the stretching, then $\pi l_1 l_2 = \pi r^2$, where r is the apical radius of the unstretched cell. The *relaxed distance* between the cells is $2r$ (APPENDIX 1) while the actual distance is $2l_1$: the *relative distance* $2l_1/(2r) = \sqrt{l_1/l_2} = \sqrt{9.6} = 3.1$ is taken as the cutoff. We assume that two cells stretched more than this distance cease to be connected. The simulation treats shrinkage units in this manner.

It should be noted that the observed apical elongation occurs approximately at right angles to that required for a quasi-conformal representation of the neural plate, and probably reflects stresses imposed by the epidermis (APPENDIX 2).

(3) *Derivation of the height programs and the shrinkage pattern*

Height patterns and a shrinkage pattern were derived from the illustrations and data in Burnside and Jacobson ('68: figs. 3, 4; table 3) and from our collection of sectioned and staged embryos and time-lapse movies of neural plate formation (figs. 13–15).

Between stages 13 and 15, cells of the neural plate are displaced considerable distances, some as much as 0.9 mm on a 2.4-mm diameter embryo (Burnside and Jacobson, '68). To derive height programs and a shrinkage pattern it is necessary to measure the height of cells at stage 13, locate the same cells at stage 15, and measure their new heights. This was done at 24 lateral points and nine points along the midline, mostly at the intersections of coordinate grid lines (fig. 22). The heights for the remaining areas were interpolated from observed cell pathways.

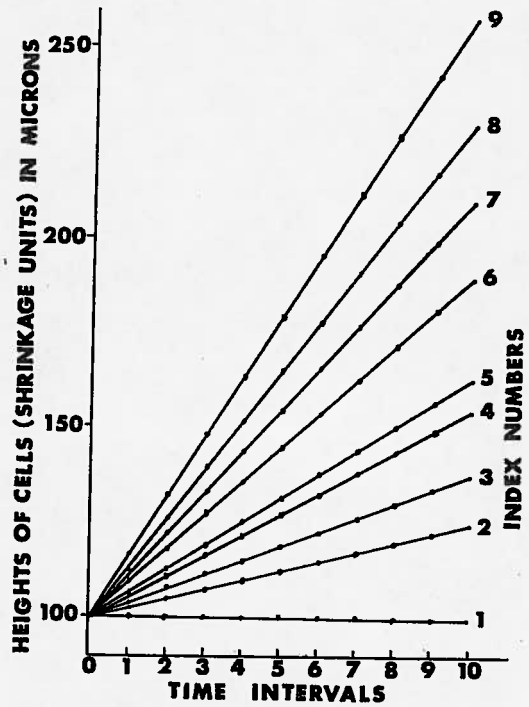

Fig. 13 Starting heights (time 0) and change in height at ten time intervals of shrinkage units (height programs 1–9). Heights closely approximate actual cell heights at stage 13 (0) and stage 15 (time 10). In this set of height programs the height increase between the two stages is made linear.

Nearly every cell differed from every other cell in its starting and final heights. Height data were normalized to a uniform starting height of 100 microns. The dynamics of the shape depends on the *ratio* of the height of a cell at a given time to its initial height, and, therefore, is unaffected by this normalization (APPENDIX 1, equation 1.7).

For convenience, the resulting data were divided into nine categories (discrete height programs). Height program 1 is a constant and is reserved to symbolize epidermal cells just outside the neural plate whose heights would either not change or would decrease rather than increase. Height program 9 has the greatest increase in height (and hence the greatest shrinkage of apical surface). Height programs 1 to 9 increase monotonically in amount and rate of height change, but not necessarily linearly. The groupings were chosen to best fit the measured values.

These measurements gave us the start-

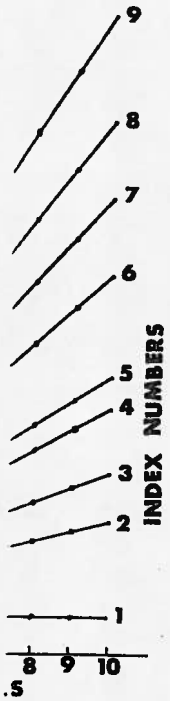

0) and change
shrinkage units
losely approxi-
3 (0) and stage
: programs the
stages is made

from every
inal heights.
to a uniform
ons. The dy-
on the *ratio*
en time to its
is unaffected
DIX 1, equa-

ng data were
screte height
is a constant
idermal cells
hose heights
uld decrease
: program 9
height (and
of apical sur-
9 increase
rate of height
linearly. The
t fit the mea-

us the start-

ing and final heights for each height program but not the intermediate values. That is, we do not yet have a direct measure of the temporal course of each height program. To make up for this lack, in one set of height programs we assume a linear change in height through time (fig. 13). In another we have made the heights through time inversely proportional to the area of the entire neural plate (fig. 14). In both cases, the height programs match the known initial and final heights.

Our inability to accurately stage different embryos at intermediate stages between stages 13 and 15 makes it extremely difficult to use sectioned material to derive height programs.

VII. RESULTS OF THE SIMULATION

The simulation which we obtained using the parameters described above compares well with the normal embryo (fig. 16). Results compare even more favorably with the shape transformation in a neural plate isolated together with underlying notochord (fig. 17).

Two forces, programmed shrinkage of plate cells and of the notochordal region elongation, produce the shape transformation in the simulation. The relative contribution of these forces is illustrated by running the simulation with either one force or the other. Using shrinkage alone compares to the experiment of isolating the neural plate without a notochord (fig. 3). Simulation of notochordal elongation alone cannot be duplicated by experiment, so only simulation results are presented (fig. 16: SIM 3, and fig. 18). Although both forces are necessary and sufficient to duplicate the normal shape transformation, it is also clear that elongation of the notochordal region contributes most during the conversion to a keyhole shape.

Both linear and nonlinear height programs have produced good simulations (fig. 16: SIM 1 and 2). Thus it appears that the shape of the neural plate depends mostly on the *total* height changes of the cells, rather than on the detailed course of the height programs.

Leaving a border of units that do not shrink is comparable to leaving a ring of epidermis around an isolated neural plate. However, this has little effect on the shape conversion (fig. 19).

Duplicate computer runs, differing only in the random number input, give essentially the same shape (fig. 20). Therefore, we conclude that the simulation is stable in the presence of continual small perturbations.

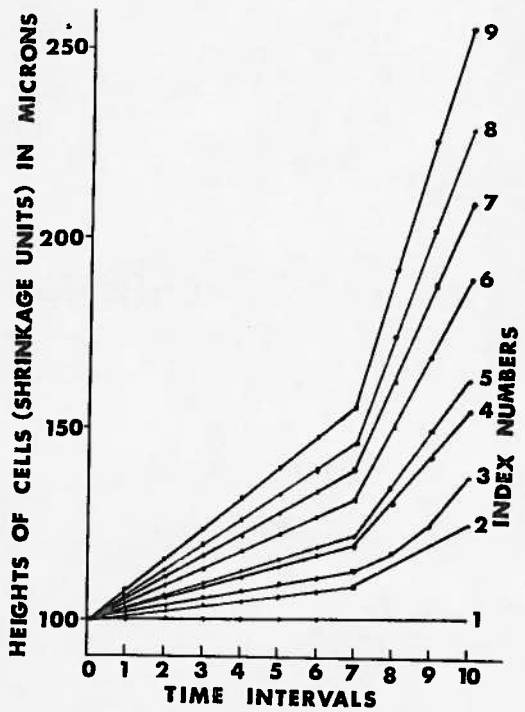

Fig. 14 This set of height programs has the same starting and ending heights as those in figure 13, but rather than increasing linearly through time the height is inversely proportional to the area of the neural plate (nonlinear).

Bilateral symmetrization was important to the quality of the final shape (fig. 21). Without it the random perturbations accumulating unequally on the two sides distort the overall shape. This is a deficiency of our numerical method, which might be alleviated by alternative computational schemes (APPENDIX 1).

The distortion of the coordinate grid in the simulation closely tracked the empirical distortion illustrated by Burnside and Jacobson ('68) for a normally forming neural plate (fig. 22). Similarly, trajectories of shrinkage units in the simulation are close to empirical pathways (fig. 23). The major discrepancy occurs in the blastopore region and is due to a continued involution of posterior tissue that is not simulated. (At the anterior end, the empirical trajectories are optically foreshortened.)

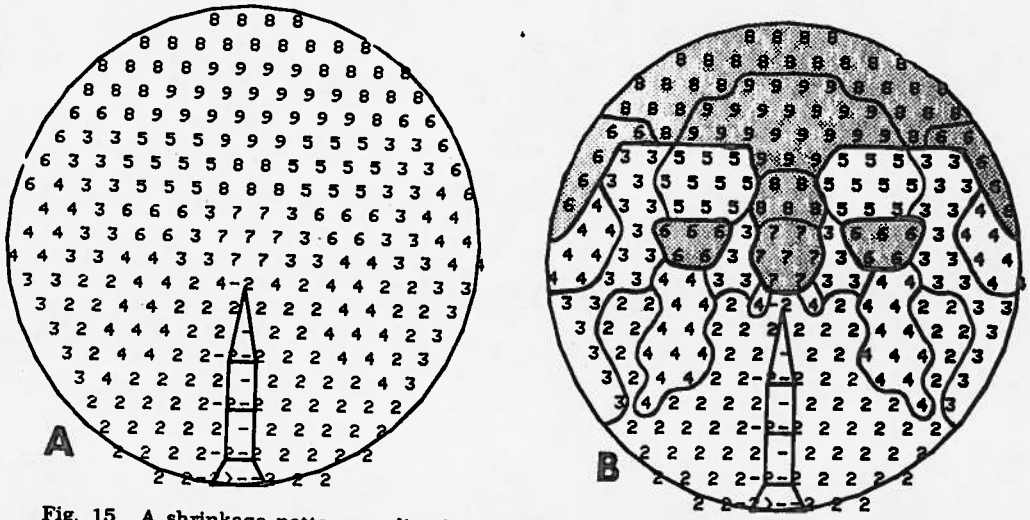

Fig. 15 A shrinkage pattern or distribution of height programs on a starting disc representing a stage 13 neural plate. Shrinkage units with higher numbers shrink more than units with lower numbers, as specified by the height programs (e.g., figs. 13, 14). Minus signs indicate units on the perimeter of the notochordal region. (Isolated minus signs indicate units over the notochord which are removed before the simulation proceeds.) The bottom of the figure represents the posterior or blastoporal end of the embryo. Note greater shrinkage will occur anteriorly at the edge of the embryo, and directly anterior to the notochordal region. B. Contour lines have been added to make the pattern more visible. Those areas that will shrink most (height programs 6–9) are shaded. (Compare to fig. 36.)

The visual agreement between our simulations and our various experimental preparations of the neural plate appears good. A more quantitative comparison would be difficult because of the irregular foreshortening of the neural plate on the intact embryo. Moreover, the wrinkling of the excised plate during keyhole formation would distort its projected transformation grid. Thus we leave precise measures of our numerical accuracy for future work.

VIII. ADDITIONAL OBSERVATIONS, RAMIFICATIONS AND EXPERIMENTS

In this section we present additional observations and experiments that have increased our understanding of the mechanisms of early neural plate morphogenesis.

(1) *Fate map of nervous system at stage 13*

We have made a fate map of the earliest neural plate by a new method of extending known fate map boundaries back in time using a time-lapse movie.

The "stage 13" embryo operationally defined as 19 hours and 17 minutes prior to first contact of the neural folds by Burnside and Jacobson ('68) is actually a very late stage 13. In that paper, the time, at 17°C, between stage 13 and stage 15 was 766 minutes (12.8 hours).

In three recent movies, we started with embryos staged as stage 13 by choosing those whose blastopore dimensions matched exactly the stage 13 illustrated by Twitty and Bodenstein (Rugh, '62). The average time between such a beginning stage 13 and stage 15 was 33.8 hours (individual measurements: 42.2, 33.8, 25.4 hours).

Fig. 16 Normal development of the neural plate as recorded by outline drawings from projected frames of a time-lapse movie (left) is compared to computer simulations (right). The simulations proceed in 40 equal steps and are shown at every ten steps. Normal development is shown at equivalent stages from late stage 13 to stage 15.

SIM 1: A successful simulation whose starting parameters are listed above (section VI). The linear height programs are used (fig. 13).

SIM 2: This simulation is the same as SIM 1 except that non-linear height programs are used (fig. 14).

SIM 3: All parameters are the same as SIM 1 except the height program was a constant for all units so no shrinkage occurred. Thus we can isolate and see the effect of the elongation of the notochordal region on the neural plate.

isc repre-
ıan units
igns indi-
ınits over
he figure
vill occur
ı. B. Con-
ill shrink

lds by Burn-
ually a very
the time, at
tage 15 was

started with
by choosing
ons matched
ed by Twitty
The average
ing stage 13
s (individual
25.4 hours).

---

of the neural
vings from pro-
ie (left) is com-
ght). The simu-
and are shown
oment is shown
e 13 to stage 15.
whose starting
n VI). The linear

same as SIM 1
grams are used

same as SIM 1
constant for all
Thus we can iso-
ation of the noto-

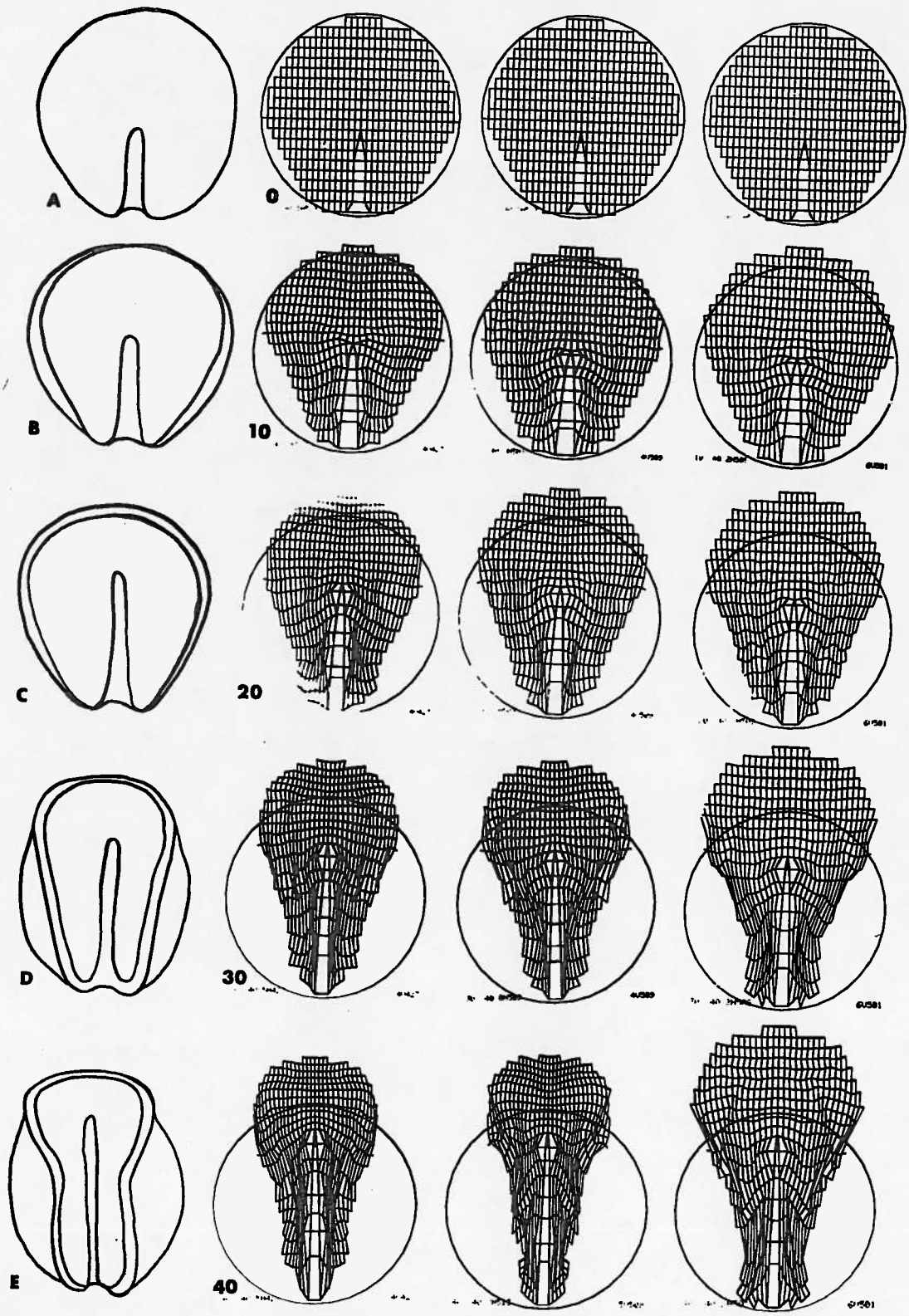

Figure 16

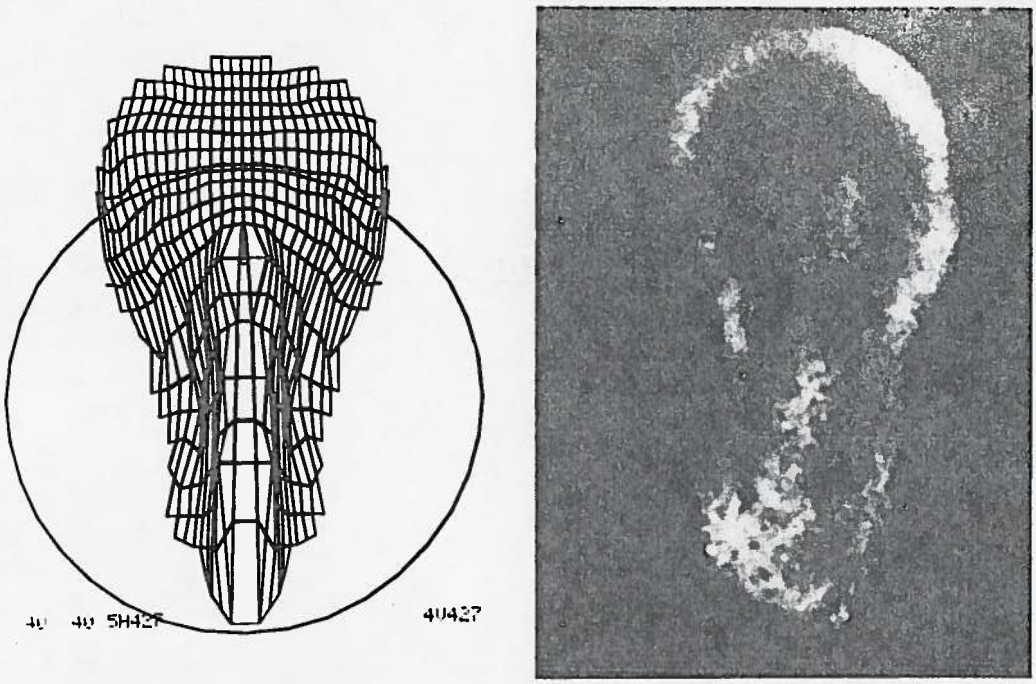

Fig. 17 The end result of the same simulation shown in figure 16 (SIM 1) is compared here to a neural plate with underlying notochord that was isolated at stage 13 and photographed at a stage equivalent to stage 15. The circle in the simulation is representative of the stage 13 starting disc, with a diameter of 2.4 mm. The neural plate is shown at an equivalent magnification.

During the first two-thirds of this period, not followed in the Burnside and Jacobson ('68) paper, there is considerable displacement of cells. We have mapped these and later movements to make a first approximation to a fate map of the nervous system on an early stage 13 embryo.

C.-O. Jacobson ('59) has mapped the positions of parts of the nervous system on a stage 15 Axolotl embryo (*Ambystoma mexicanum*). We assume the map at stage 15 to be the same in Axolotl and *Taricha*. We superimposed boundary lines from C.-O. Jacobson's fate map onto a projected image from a time-lapse movie of a stage 15 *Taricha torosa* embryo. We chose points

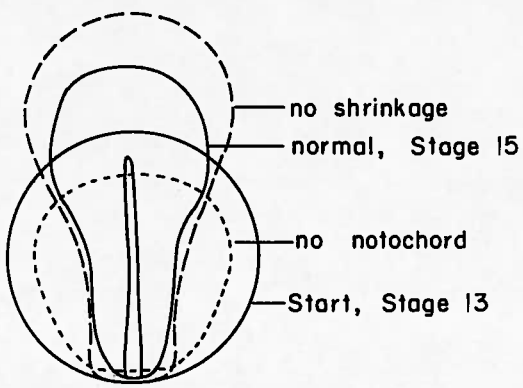

Fig. 18 A composite drawing comparing the outline of the normal stage 15 neural plate, and simulation of the same, to simulations that were identical except one of the driving forces was eliminated. "No notochord" shows the effect of shrinkage alone, "no shrinkage" shows the effect of the notochordal region acting alone.

Fig. 19 This simulation is identical to SIM 1 in figure 16, except an extra ring of units with height program 1 was added around the perimeter to represent epidermis. Units with height program 1 do not shrink. The simulation took 40 steps. A. The starting shrinkage pattern, stage 13. B. Tenth step. C. Twentieth step. D. Thirtieth step. E. Fortieth step (end stage 15). Each horizontal row is at the same step. F–Q illustrate other display modes. F–I, distortion of coordinate grid. K–N, nearest neighbor connections. N–Q, circular shrinkage units are represented by their circumscribed hexagons (N shows connections and units simultaneously.) J, magnified region of N showing overlaps and slippage of units.

ared here
ographed
stage 13
ent mag-

rst approxi-
nervous sys-
o.
pped the po-
system on a
stoma mexi-
t stage 15 to
Taricha. We
from C.-O.
jected image
a stage 15
hose points

tical to SIM 1
of units with
the perimeter
ight program 1
0 steps. A. The
B. Tenth step.
ep. E. Fortieth
l row is at the
lay modes. F–I,
nearest neigh-
nkage units are
l hexagons (N
ltaneously.) J,
rlaps and slip-

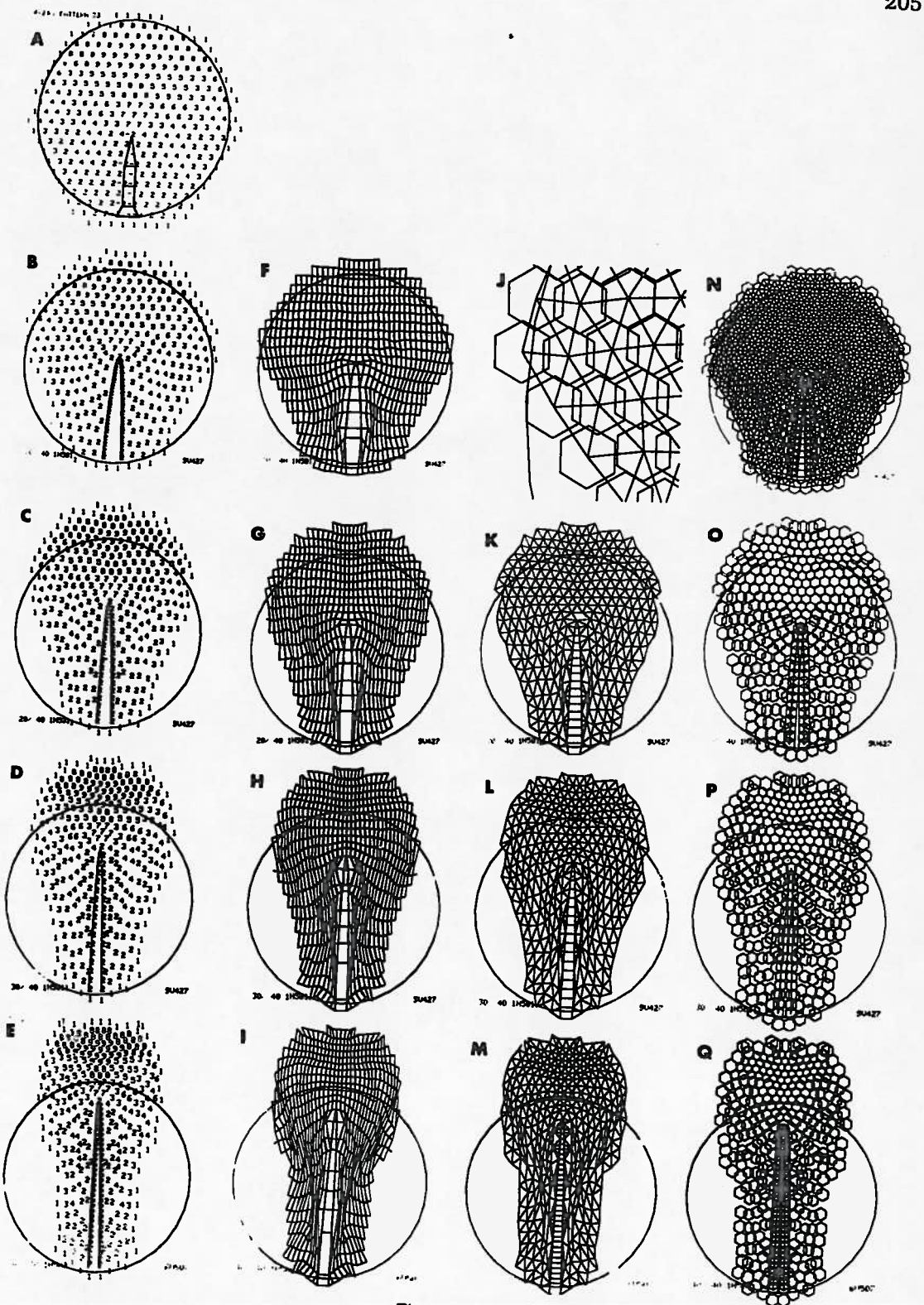

Figure 19

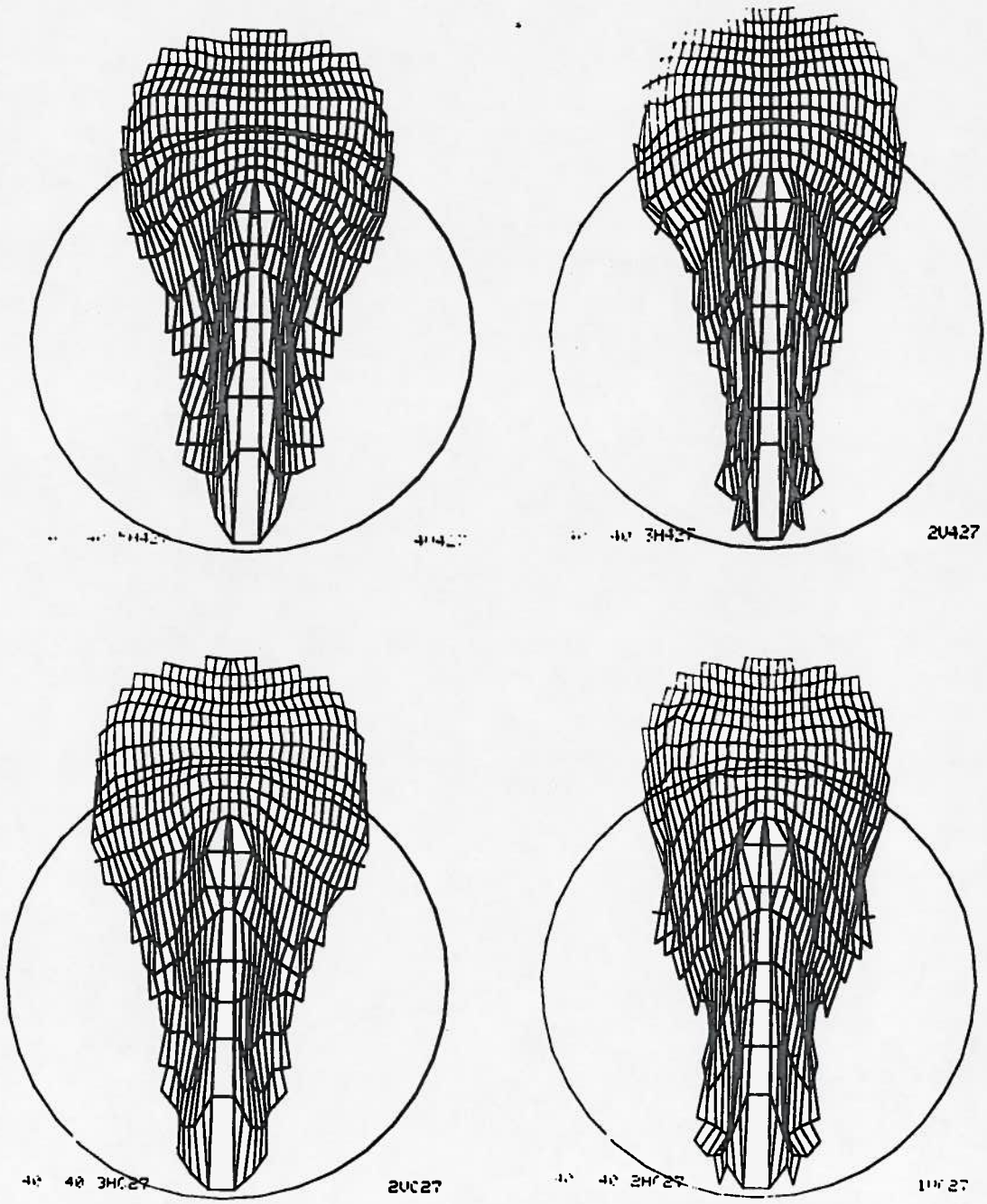

Fig. 20 Four runs of the simulation are shown all made with identical initial parameters. They differ only in the sequence of random numbers used. This comparison illustrates the amount of shape variation the simulation generates. (Upper left simulation is from fig. 16, SIM 1, step 40.)

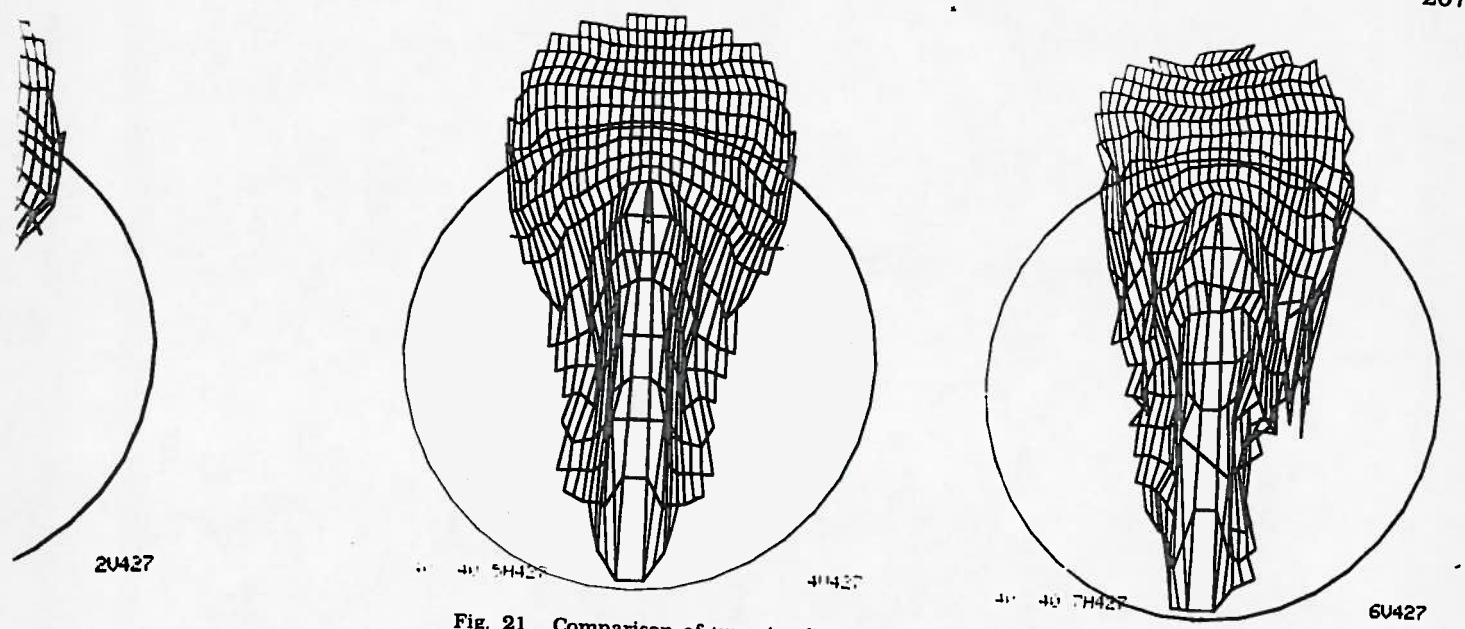

Fig. 21 Comparison of two simulations with (left, from fig. 16, SIM 1, step 40) and without (right) bilateral symmetrization. The same form is obtained (cf. fig. 20).

rameters.
trates the
m fig. 16,

(pigmented cells or groups of cells) that fell on the boundary lines of the stage 15 fate map and traced them back, frame by frame, to their earlier positions at stage 13 (fig. 24).

The stage 13 fate map was surprising in that most of the area of the future neural plate is brain. Much of the salamander's brain originates near its rear end. The future hind brain arises nearly adjacent to the blastopore. The spinal cord comes from a thin sliver of tissue next to the blastopore that extends ventrally around under the curve of the embryo.

According to Schechtman's ('32) fate map for *Taricha torosa*, at the end of gastrulation (stage 13+) the future neural plate is located in the dorsal hemisphere of the ectoderm. We have found, to the contrary, that at late gastrula stage 12 and beginning stage 13 some cells that will form part of the neural plate are located ventral to the equator near the blastopore (fig. 24: label numbers 25, 26, 29, 30).

(2) *Cell placement and dynamics during early plate formation*

The surface area of a hemisphere is $2\pi r^2$. The area of a disc or plate of the same radius r is πr^2. Hence the neural plate must shrink 50% to convert from a hemisphere at stage 12 to a disc of the same radius (1.2 mm) at a late stage 13 (from 9.05 mm² to 4.52 mm²). Measurements of neural plate surfaces of stage 15 embryos projected from our time-lapse movies show an additional area decrease of 39% from stage 13 (from 4.52 mm² to 2.76 mm²). This additional decrease is 19.5% of the area at stage 12. Thus, between stages 12 and 15, from the hemispheric shell to the keyhole-shaped plate, there is a total decrease in area of 69.5%. Most of the decrease is due to the conversion from a hemisphere to a disc (fig. 25).

Just before the neural plate begins to change from a disc with the radius of the embryo to a plate of lesser area, the cells of the neural plate must be, on the average, twice the height of the cells of the epidermis. By stage 15 the disparity has increased.

In the neural disc of the late stage 13 embryos, cell heights in the neural plate vary. The taller cells are found near the rim of the disc (Burnside and Jacobson, '68: their fig. 3). The disc decreases its area primarily by increasing the heights of the cells near the rim (Burnside and

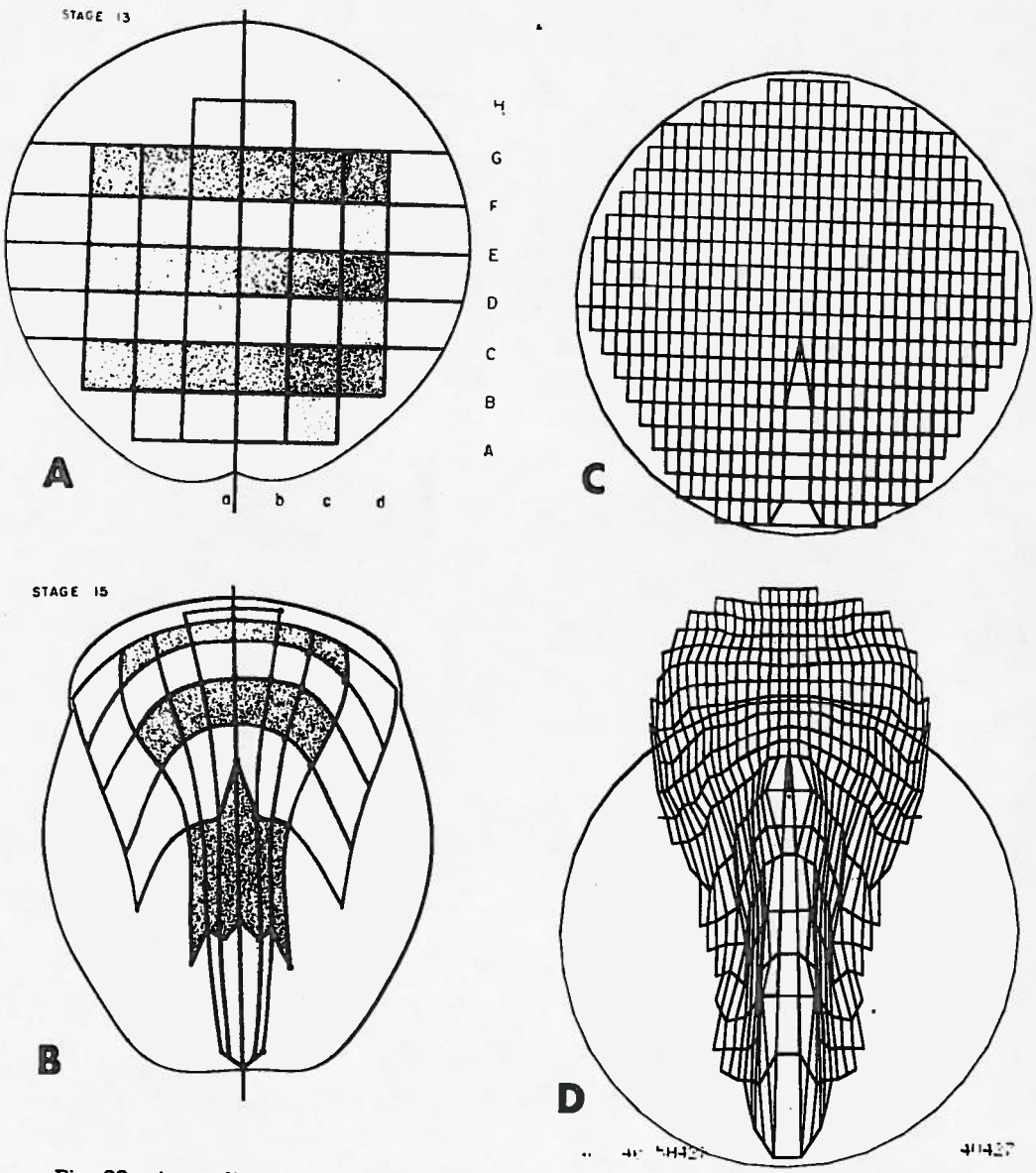

Fig. 22 A coordinate grid is placed on the outline of a stage 13 embryo (A) and the distortion of that grid shown at stage 15 (B). These are compared to the starting coordinate grid of our simulation (C), and its distorted grid (D) (fig. 16, SIM 1, step 40). A and B are from figure 2 of Burnside and Jacobson, '68. Note that the anterior end of the neural plate in B is seen in perspective, wrapped over a flattened spherical surface.

Jacobson, '68: their fig. 4). The cells of the epidermis flatten and spread, covering more than half of the embryo. The boundary cells along the rim become the neural fold and give rise to that peculiar cell population, the neural crest.

(3) *Breaking of cell-cell contacts during neural plate formation and possible implications*

Is the neural plate a simple elastic sheet during its formation, or do the cells that

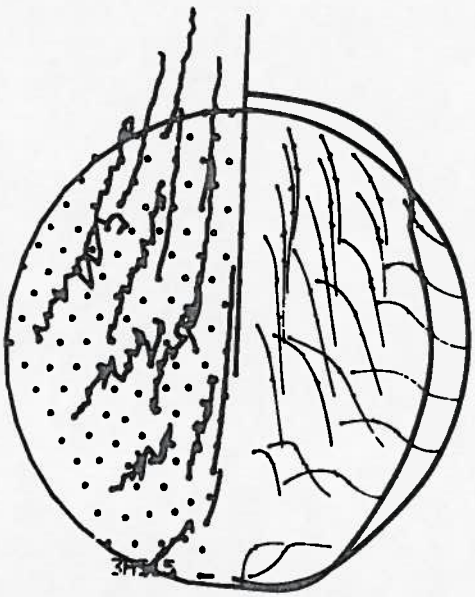

Fig. 23 Pathways of movement of simulation shrinkage units (left half of figure) are compared to pathways of cell movements in normal embryo through same time period (right half of figure). Cell pathways are from Burnside and Jacobson ('68), their figure 1. Along the midline, in both simulation and normal embryo, units (cells) move directly anteriorly (toward top of figure).

compose the forming neural plate break contact with neighboring cells and assume new relationships with new neighbors? In the mathematical section of this paper (APPENDIX 2), we demonstrate that the transformation of the neural plate from a disc to a keyhole shape is not conformal — that shearing must occur. In these calculations, as in most hydrodynamic analyses, fluid elements are considered to be infinitely small (though assumed at the same time to be large in comparison to molecules). In our simulation, the units that compose the system are, by contrast, actually large, about 33 cells each at stage 15.

During the simulation, regions where unit-unit contacts are broken became apparent (fig. 26). We believe these reflect regions in which cells change nearest neighbors. The regions that showed most slippage or cracking were near the notochord, especially toward the anterior end.

In the simulation the notochordal region had to be handled in a special way because rearrangement of the units in this area was so dramatic. Only the units at the changing perimeter of the notochordal region were simulated because only the perimeter transmits motion of the notochordal region to the rest of the neural plate. The problems in this region are illustrated in figure 27. As the shape of the notochord region becomes more elongated, most internal units become part of the perimeter. Extensive rearrangement is necessary. That cell neighbors do in fact change in this region in real embryos is illustrated by tracing the movements of some cells in the region. (See, for example, numbers 14, 21, 22 in fig. 24.) How this rearrangement is accomplished with the basal ends of the neural plate cells attached to notochord cells remains an enigma.

The edge of the forming neural plate is another region where many cell-cell contacts may be broken and new neighbors made through rearrangement of cell positions. This perimeter corresponds to the position of the neural folds.

At stage 13 the perimeter of the neural plate is a circle with no evidence as yet of a neural fold. During the transformation to the keyhole shape of stage 15, the length of the perimeter remains constant. Perimeter measurements were made with a map measurer using projected movie images of an embryo developing from stage 13 to stage 15. Since a circle is the geometrical configuration with minimal perimeter for a given area, any planar change in the shape of the sheet should increase the perimeter. Decreasing the area of the neural plate would compensate for the shape change and tend to keep the perimeter constant. The embryo somehow achieves exactly such a balance.

Although the perimeter of the plate remains about constant in total length, the cells that compose the perimeter are those that reduce their diameter the most. At the boundary between the epidermis and the plate, while the epidermal cells are enlarging in diameter, the plate cells are shrinking. In the normal embryo the boundary is very abrupt (fig. 52A). The probable consequence is that cells change neighbors at the boundary. Thus the boundary may be a line of shear.

In the embryo, there are several ways in which cells could adjust to the abrupt

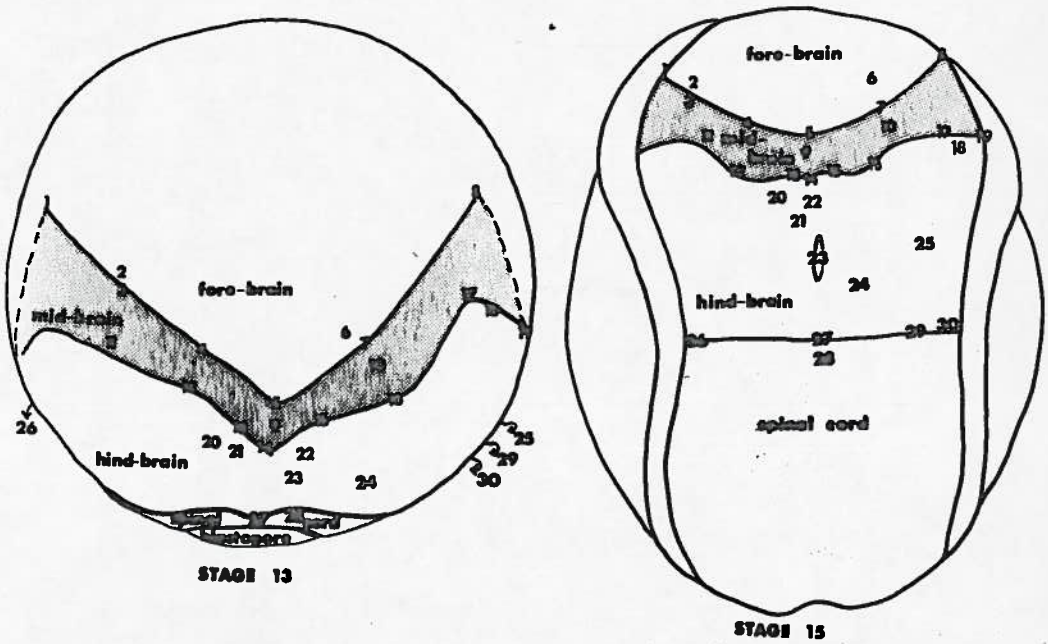

Fig. 24 The fate map of C.-O. Jacobson ('59) was projected onto a stage 15 *Taricha torosa* (right). Naturally pigmented regions at the positions indicated by the numbers were followed back in time on a time-lapse movie to their positions at stage 13 (left), providing a fate map at this earlier stage. Some regions (25, 26, 29, 30) emerge from beneath the equator. Number 23 was a small circular group of cells at stage 13. This same group has become an oriented ellipse, as indicated, at stage 15. This shows that the transformation is quasiconformal (APPENDIX 2).

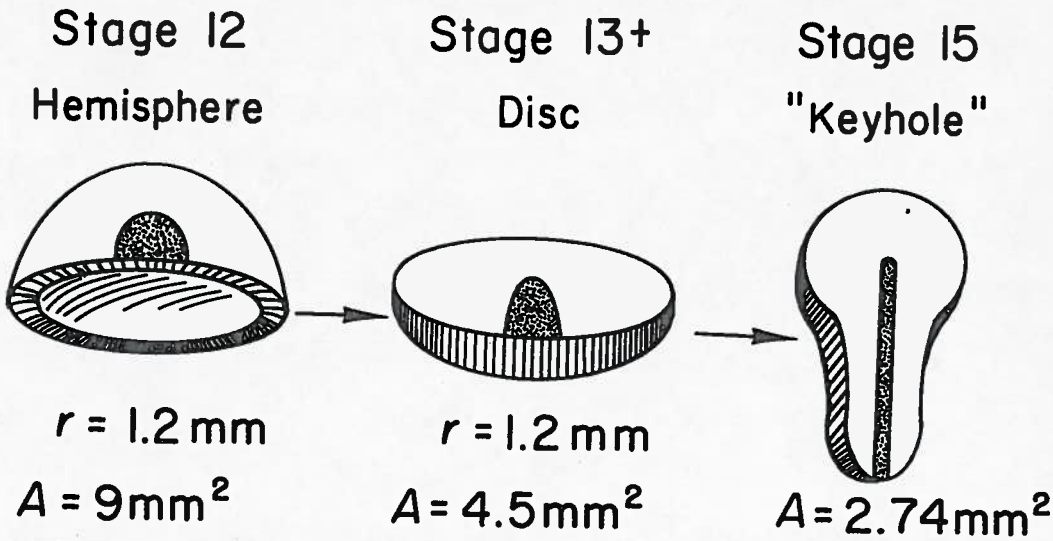

Fig. 25 The areas of the prospective neural plate was calculated at stage 12 ($A = 2\pi r^2$) and at stage 13+ ($A = \pi r^2$) and measured at stage 15. Between stages 12 and 13+ the area decreases 50%; between stages 12 and 15 the area decreases 70%. Hence most change in area occurs in the conversion from a hemisphere to a disc. Between stages 13+ and 15 the length of the neural plate perimeter remains constant.

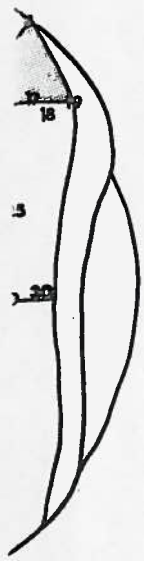

ia torosa
followed
fate map
Number
oriented
rmal (AP-

15

ole"

74mm²

$(A = 2\pi r^2)$
+ the area
nge in area
the length

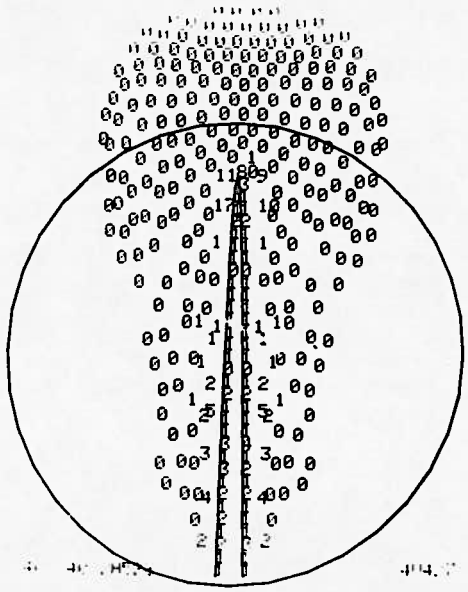

Fig. 26 The simulation (SIM 1, fig. 16, step 40), at a stage comparable to embryo stage 15, in a display mode that lists the number of times each shrinkage unit has changed neighbors (sheared). Most frequent shearing is at the anterior end and sides of the notochordal region. Some of the shearing is attributable to the making and breaking of bonds to new units intercalated on the notochordal region's perimeter as it elongates.

boundary between epidermis and neural plate. Besides tearing and binding new cell neighbors, the epidermis-neural plate boundary could bend or slip (fig. 28), the shapes of the apical surfaces of the cells could alter, or the cells at the boundary could round up, perhaps divide, and remain as an intermediate cell population (neural crest) between epidermis and neural plate. None of these possibilities can be completely eliminated at this time. Further high magnification studies are needed.

In order to test the behavior of such a boundary of cells in the simulation, we use an artificial shrinkage pattern (fig. 29A). Below a horizontal line all units change heights from 100 μ to 258 μ. Above the line all units remain a constant 100 μ long. Results of this simulation (fig. 29) show that bending occurs at the boundary. Shearing among units along the boundary is also evident. The simulation takes 40 steps. Slippage between units at the boundary is evident after 10 steps and increases at 20, 30, and 40 steps. Most rearrangements of units across the boundary occur at the two ends. The center of the boundary is least disturbed.

The only region of the neural plate in which little or no changing of cell neighbors occurs is in the anterior (brain) plate. This region floats uppermost at these stages and is thus easiest to photograph at high magnification. It was examination of this region that led to the erroneous conclusion in a previous publication (Burnside and Jacobson, '68) that cells of the neural plate always retain their neighbors.

The changing of cell neighbors at the perimeter of the neural plate, where the neural folds arise, follows a very sharp boundary between domains of cells that are very different. How cell domains in embryos become isolated from one another is still unresolved. Shear could be an important factor. Shear may, for example, sever tight junctions or other intimate cell contacts at the boundary between epidermis and neural plate. This could, in turn, lead to subsequent changes in cell behavior (Loewenstein, '68). The eventual ap-

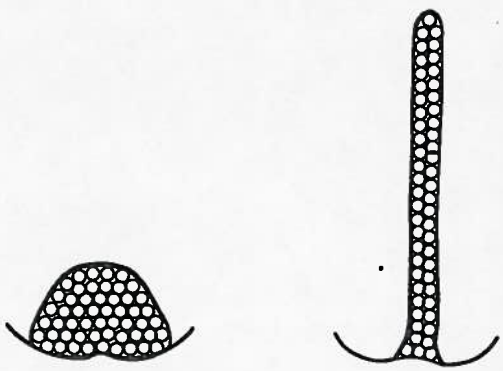

Fig. 27 The region of the neural plate that overlies, and is attached to, the notochord is shown at two stages. "Cells" are shown diagrammatically in the notochordal area in equal numbers at each stage. As the notochord elongates, cells from the interior of the planar region intercalate to take positions as perimeter cells. In this example, there are 15 cells that abut the top and sides of the notochordal area at stage 13 and 52 cells on the perimeter at stage 15. This diagram illustrates the immense amount of shear (changing of neighbors) that is necessary during the change in shape of the notochordal region of the neural plate.

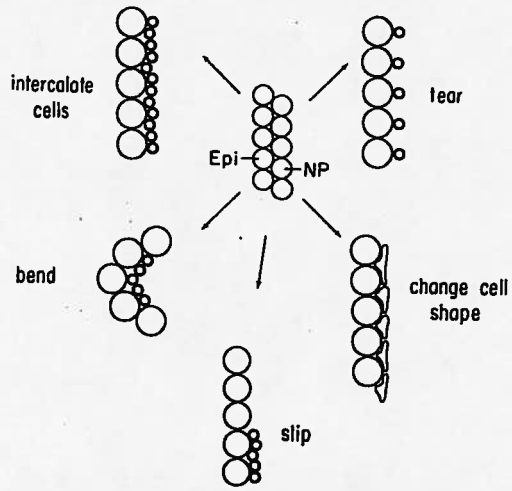

Fig. 28 At the future boundary between neural plate and epidermis, cells have, at first, the same apical areas (center). As neural plate cells (NP) shrink (lengthen) and epidermal cells (epi) expand (flatten) five possible means of accomodating the resulting shear are shown.

pearance of a special population of cells, the neural crest, at this boundary could well be due to shear. The massive amount of shear in the notochordal region similarly may have a role in dividing the neural field into two bilaterally symmetrical equivalents.

The region of the neural plate that overlies the notochord approximately maps into the future floor plate of the spinal cord and hind brain. The notochord extends only to beneath the myelencephalon by early tail-bud stages, and does not reach its ultimate anterior extent abutting the infundibulum until late tail bud stages (Witschi, '56: his fig. 58 and p. 106).

The exact anterior extent of the notochord during neurulation is not known. Histological differentiation is not by then sufficient to accurately judge, but sections and movies suggest that the notochord extends well up beneath the future hind brain.

At the blastula stage, the notochord maps as a crescent whose long axis is at a right angle to the axis of the future notochord. Notochord cells in the mesoderm and the supra-chordal area of the neural plate make the same movements during neurulation (C.-O. Jacobson and Löfberg, '69).

If one follows the pathways of cells located over the notochord from stages 13 to 15 in a time-lapse movie, the cells at the midline invariably move in the anterior direction for considerable distances. If, on the other hand, one follows midline cells over the notochord from stage 15 backwards to stage 13, some cells are more posterior on the midline at the earlier stage, but many cells move posteriorly, then diverge laterally. This implies that in early stages, the neural plate cells over the notochord are arranged in a crescent adjacent to the crescent of future notochord cells (fig. 1). It also suggests that cells along the midline had to change neighbors to arrive there.

(4) *Spatial and temporal analysis of unresolved tissue tensions in the ectoderm*

The forces exerted by shrinkage of apical surfaces of cells and thrusting and elongating of the notochordal region of the neural plate eventually result in the displacement of other cells of the neural plate. The possibility exists that these forces could merely stretch rather than move cells relative to one another resulting in elastic tensions that remain unresolved for some period of time.

We found a simple experimental approach that gives some information of a semiquantitative nature about the presence, direction and gross amplitude of such tensions: When we made small slits in the neural plate and epidermis, the immediate response was for the wound to gape. The extent of the gape varied with the position and direction of the slit and the age of the embryo. We have recorded the results of these experiments with photographs made within one minute of slitting the embryo. (The gape reaches its maximum extent in

Fig. 29 This simulation run shows the behavior of a boundary between shrinking and non-shrinking cells. A. Initially, the boundary between shrinkage units with height programs 1 and 9 is a straight line. Units with height program 1 do not shrink; units labelled 9 shrink greatly (heights change from 100 μ to 258 μ, using the height program in fig. 13). The simulation was completed in 40 steps. B, step 10; C, step 20; D, step 30; E, step 40 (End). F. Step 40 in a display mode that gives the number of times each unit changed neighbors (shear). Units changing neighbors were at the edges near the boundary in the area that shrinks. At step 40 the curved boundary between the two areas is five-sixths its original length.

stages 13 to
cells at the
ie anterior
aces. If, on
idline cells
e 15 back-
e more pos-
rlier stage,
ly, then di-
at in early
er the noto-
nt adjacent
chord cells
cells along
eighbors to

is of

age of api-
usting and
egion of the
in the dis-
the neural
that these
ather than
ther result-
main unre-

mental ap-
nation of a
t the pres-
ude of such
l slits in the
e immediate
o gape. The
the position
e age of the
e results of
raphs made
the embryo.
m extent in

ws the behav-
ing and non-
ndary between
ms 1 and 9 is
program 1 do
reatly (heights
the height pro-
s completed in
tep 30; E, step
ode that gives
nged neighbors
s were at the
a that shrinks.
tween the two
).

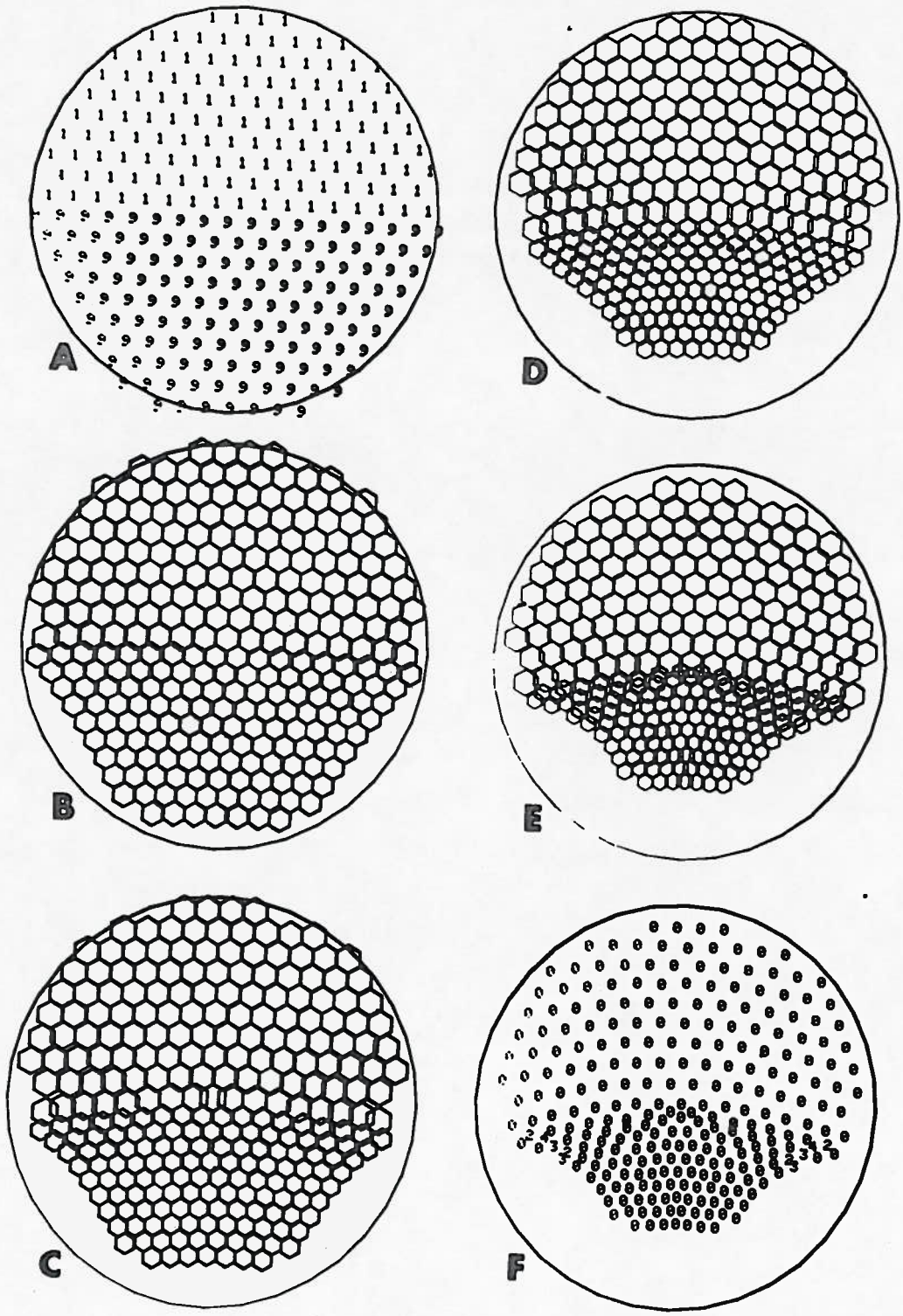

Figure 29

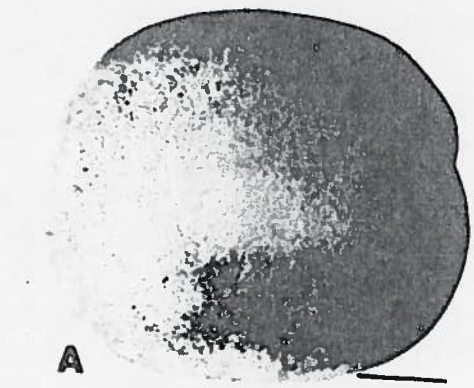

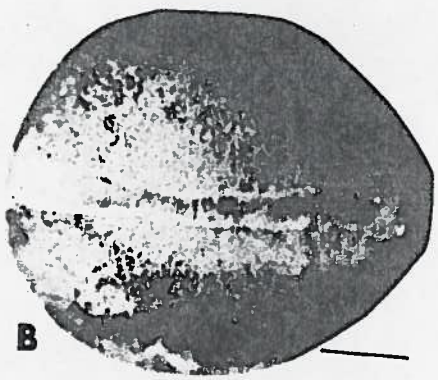

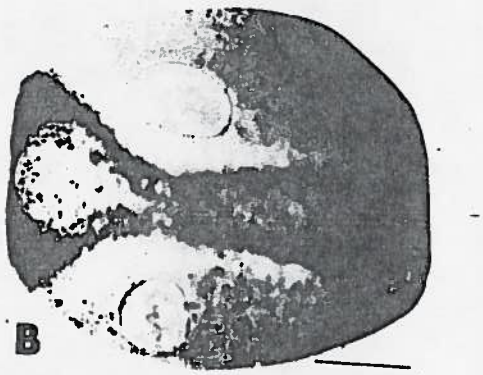

Fig. 31 A. Ventral surface of a stage 13 embryo showing gaping resulting from slits made in the epidermis in the medio-lateral direction (top) and in the antero-posterior direction (bottom). The photographs were made one minute after the operation. B. Gaping resulting from slits made in dorso-lateral epidermis of a stage 15 embryo. The slits were made antero-posterior (top) and medio-lateral (bottom). Bars are 0.5 mm.

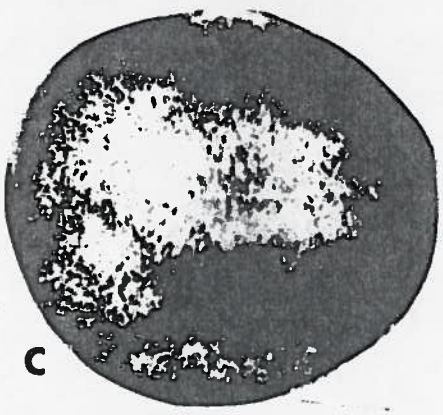

Fig. 30 A. Dorsal view of a stage 13 embryo. Posterior is at right. B. Same embryo photographed one minute after a slit was made along midline showing resulting gaping. C. The same embryo photographed one hour after the slit was made showing complete healing. Bar equals 0.5 mm.

a few seconds). Gaping occurs to some extent in nearly every case indicating that unresolved elastic tensions do exist through most of neurulation.

Within an hour after making a slit, the gaping wounds have closed and healed, or are in the process of doing so (fig. 30).

Several sets of conclusions can be made from these experiments:

(a) *Epidermis.* Wherever and whenever the epidermis is slit, the gape is large. The direction of slit makes no difference in the epidermis. The result is always a large round gape (fig. 31). One can conclude that

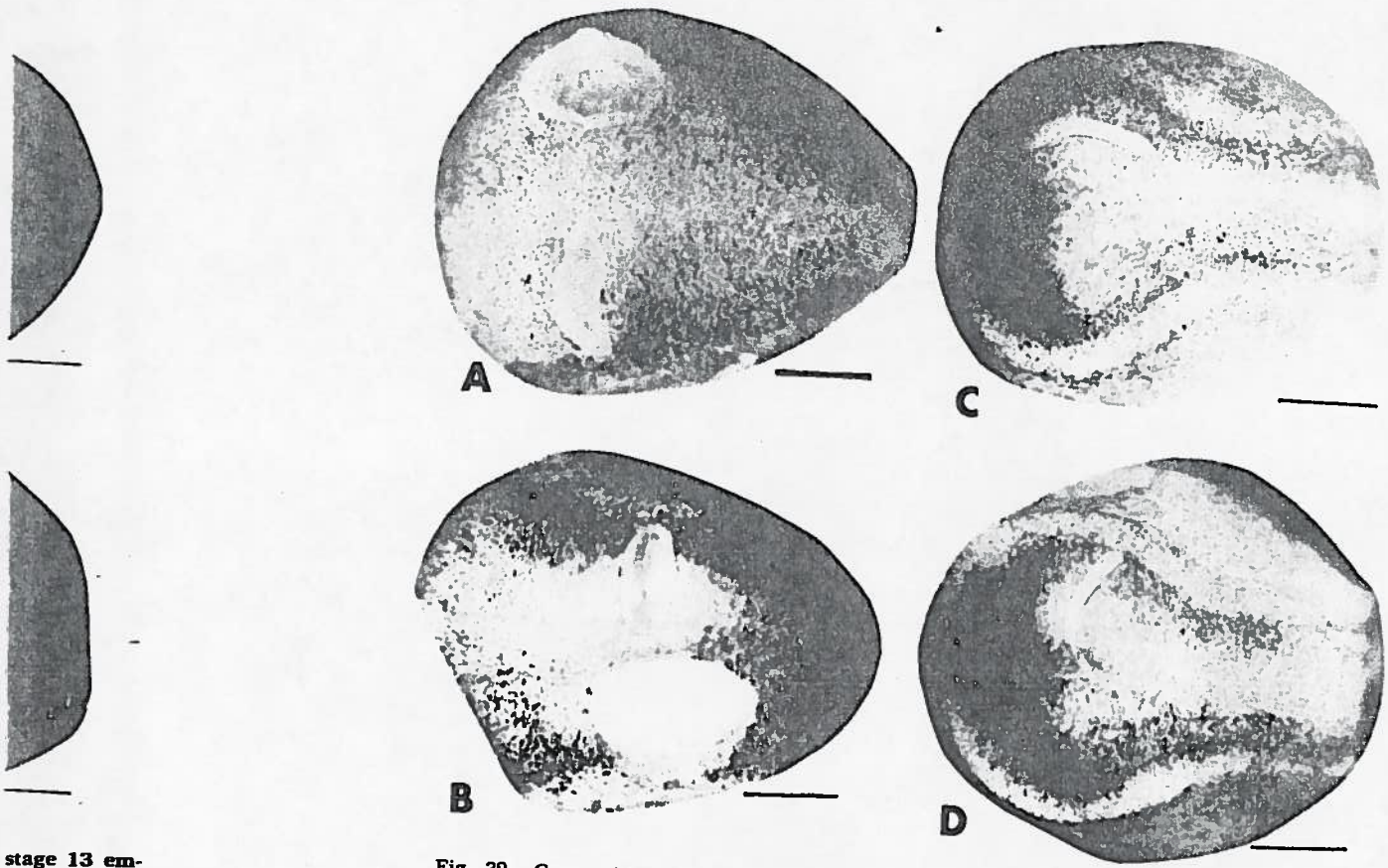

Fig. 32 Comparison of gaping resulting from slits made in the neural plate in different directions and at different ages. The photographs were made one minute after slitting. Bars equal 0.5 mm. A. Stage 13 embryo. Slits made antero-posterior (top) and medio-lateral (bottom). B. Stage 14 embryo, slits made medio-lateral (top) and antero-posterior (bottom). C. Stage 15 embryo, slit made antero-posterior. D. Stage 15 embryo, slit made medio-lateral.

from stage 13 to stage 15, the epidermis is under a considerable tension which is uniform in every direction. These experiments suggest that the epidermis cannot possibly be "pushing" on the neural folds to augment neurulation movements.

(b) *Neural plate.* In early neural plates at stages 13 and 14, there are considerable unresolved tensions. The tensions are definitely greater in the medio-lateral direction than in the antero-posterior direction (fig. 32).

(c) *Age of the embryo.* While unresolved tensions are great in early neurula stages, by stages 15 and 16 these tensions are mostly resolved. The gaping following slitting at these older stages is minimal in the brain plate (fig. 32C,D), but still occurs in the spinal region (fig. 33).

(d) *Removal of neural plate from spherical embryo.* The forming neural plate is wrapped on a sphere and is pulled by the epidermis at all edges. Unresolved elastic tensions in the neural plate could be due to this pulling. To test this, we removed the neural plate from the embryo and epidermis. Slits made anywhere in the neural plate did not cause gaping (fig. 34).

(e) *Notochord thrusting.* Another possibility we considered was that rather than tension there could be compression directly anterior to the thrusting notochord region. To test this, a slit was made in the neural plate at right angles to the long axis of the

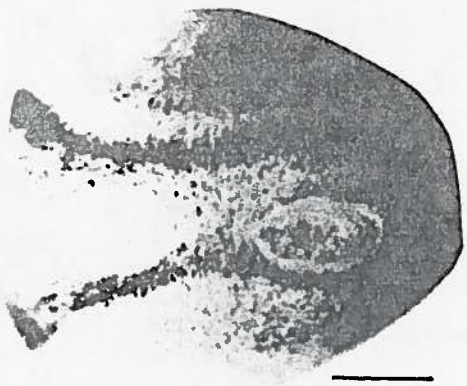

Fig. 33 Gaping follows slitting in the spinal cord region of a stage 15 embryo. Compare to figure 32C,D where very little gaping results from slitting the brain plate at stage 15. Bar equals 0.5 mm.

notochord and anterior to it. The slit gaped; hence, even here, there is elastic tension and no compression.

(f) *The role of the epidermis in neurulation.* C.-O. Jacobson ('62) and others have noted that the epidermis closes mediad if the neural plate is removed. This does not prove that the epidermis may "push" to add to neurulation movements. It seems more likely that this closure of the epidermis could be simply a healing response, or alternatively a passive tracking of movements in the underlying mesoderm (cf. Karfunkel, '74).

C.-O. Jacobson ('62) showed that the epidermis would not close to the dorsal midline following neural plate removal if the notochord is removed or if the archenteron roof is excised. It has been shown (C.-O. Jacobson and Löfberg, '69) that the mesoderm beneath the neural plate converges mediad very much as the overlying neural plate does, especially in the notochordal region. We suggest that the epidermis may be drawn mediad by these mesodermal movements in the absence of the neural plate. This motion would fail if the notochord rudiment were removed as well.

The intact epidermis is always pulling on the neural plate. This may hold the neural plate wrapped around the nearly spherical embryo and may prevent the plate from buckling and folding (as it does when isolated unrestrained). The anisotropy of the tensions within the neural plate may be due to its non-circular shape. Since isolated early neural plates will complete neurulation, including forming a neural tube, in the absence of the epidermis, the tension provided normally by the epidermis appears not to be an essential force in neurulation.

(5) *Coordination of the shrinkage pattern with elongation of the notochordal region*

One of the remarkable features of neural plate morphogenesis is the accommodation of the anterior regions of the plate to the thrusting of the notochordal region. The notochordal region does not cleave through the plate, but rather displaces cells anteriad. The thrust of the notochord-

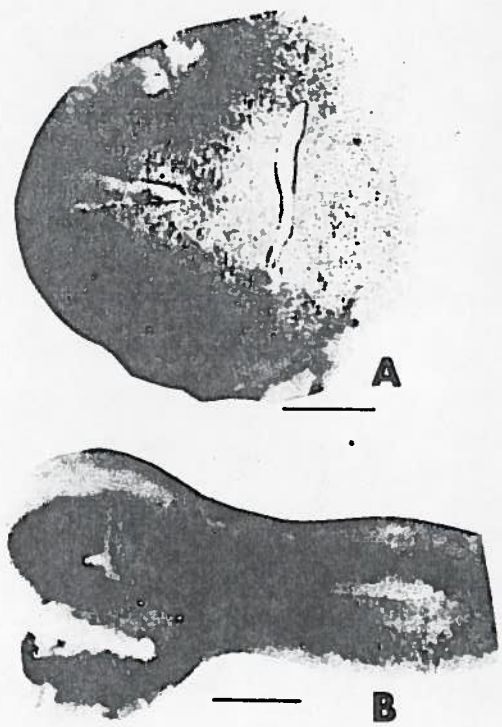

Fig. 34 A. The neural plate was removed from a stage 13 embryo, placed on a bed of neutral agar, then slit in two directions. The photograph, taken one minute later, shows very little gaping occurs (compare to fig. 32A). B. Almost no gaping results from slitting a removed stage 15 neural plate (compare to fig. 32C,D and fig. 33). Bar equals 0.5 mm.

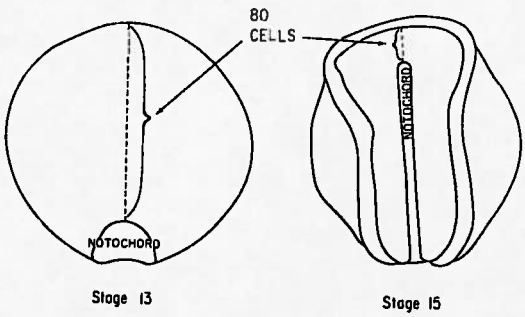

Fig. 35 Counts of cells in mid-sagittal sections of stage 13 and stage 15 embryos show the same number of cells occupy the midline between the anterior end of the notochord and the anterior edge of the neural plate at each stage.

al region is mainly responsible for the massive concentration of cells in the future brain region.

Nevertheless, the shrinkage pattern of the plate is intimately interrelated to notochordal area elongation. A region of great shrinkage extends down the midline anterior to the notochord. We made a simple cell count (fig. 35) and found that 80 neural plate cells occupy the midline between the anterior end of the notochord and the anterior point of the neural plate both at stage 13 and at stage 15 after notochord elongation.

The shrinkage pattern (fig. 15) has a tongue of greatly shrinking cells that extends from the anterior border to the anterior tip of the notochordal region. This is evident also in neural plates isolated at stage 13. These plates shrink with only slight distortion of the programmed shrinkage pattern which is revealed by concentrated egg pigment in those cells that shrink most (fig. 36). When the notochordal region elongates in normal embryos, the tongue of greatly shrinking cells is moved to the anterior border (fig. 37).

(6) *Elongation of the entire neural plate during neurulation*

Much of the elongation of the notochordal region is offset by shrinkage of the cells anterior to the notochord. Nevertheless, the entire neural plate gets longer. This elongation of the plate was not very dramatic between stages 13 and 15, but becomes

Fig. 36 A neural plate with no other tissue was explanted onto neutral agar at stage 13 and held flat by a piece of beaded covered slip. The pigment concentration that results by the time controls have reached stage 15 is a distorted version of the stage 13 shrinkage pattern (cf. fig. 15). Posterior is at the bottom. × 33.

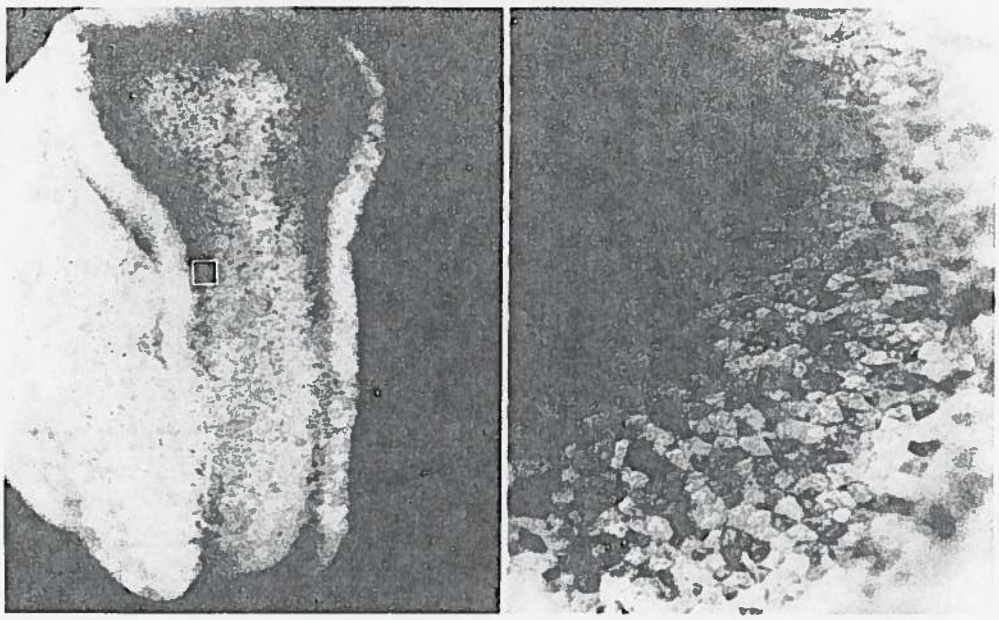

Fig. 37 Dorsal view of a stage 15 embryo (left) showing pigment concentration where cells have shrunk the most (cf. fig. 39). The area outlined by the square is enlarged (right) to show details of apical cell surfaces. Left, × 31; right, × 606.

very important after stage 15 and for the remainder of the neurulation process.

We removed the neural plates of embryos at successively older stages, laid them flat and measured their lengths along the midline. Results are shown in figure 38. Length of the nervous system rapidly decreases from stages 12 to 13 as the hemisphere of presumptive nervous tissue converts to a disc. From stages 13 to 15, elongation of the plate procedes at about 0.01 mm/hr. At stage 15, the rate of elongation increases abruptly tenfold or more to 0.15 mm/hr and this rate continues until the plate is closed into a tube at stage 19. The rate of nervous system elongation then drops tenfold to 0.015 mm/hr thereafter. We believe the rapid elongation of the neural plate during the latter stages of neurulation plays a major role in the folding of the plate into a tube.

(7) *Density of cells in various regions of the neural plate*

While it was not possible to measure apical cell surface areas over the whole plate, it was possible to measure cell densities (numbers of cells in a given unit of area) at some points in the plate, fold and epidermis. These counts were made from enlargements of high magnification photographs of living stage 15 embryos (fig. 39). The abrupt transition in cell densities between plate and fold is apparent, as are the greater densities at the edge of the plate and anterior regions compared to the midline or more posterior regions.

IX. DISCUSSION

In this section we consider other models of neurulation and the subcellular origins of the two forces which we find responsible for shaping the neural plate. We also discuss the role of shear in morphogenesis and give a detailed summary of the development of the neural plate.

(1) *Other studies of neurulation*

Past studies of neurulation have concentrated more on the closure of the neural plate into a tube than on its initial shaping. The two forces for its initial shaping from a flattened hemispheric shell to a keyhole shaped plate appear to be sufficient to explain the remaining transformation into a neural tube. These two forces, shrink-

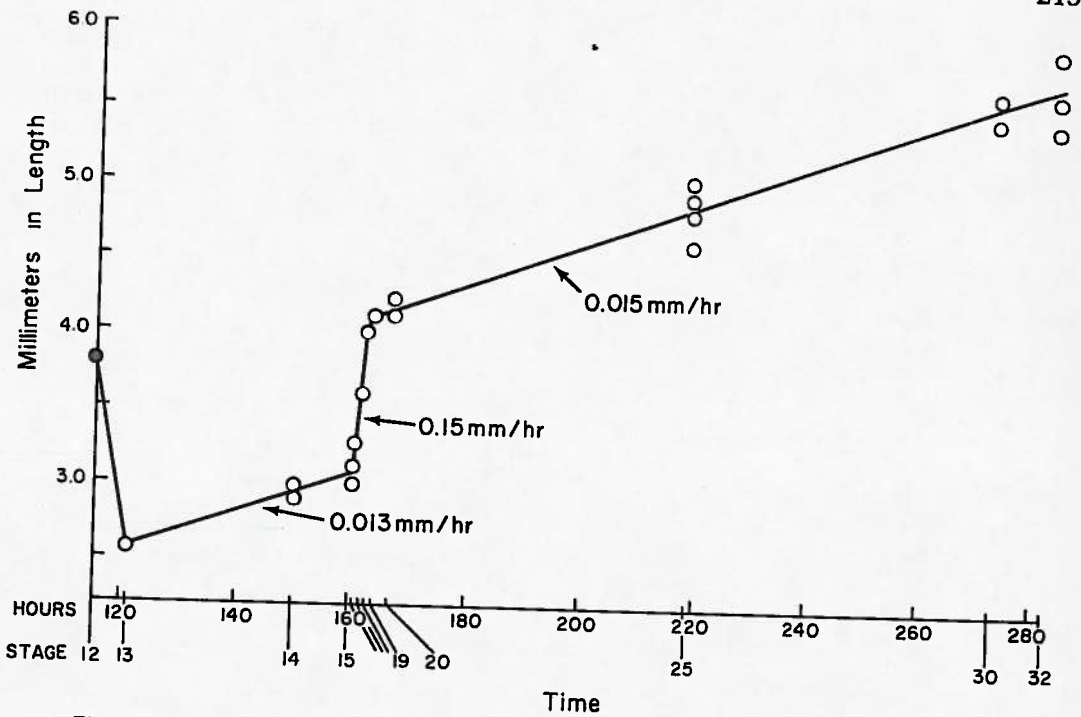

Fig. 38 Length of excised nervous system at different stages of development. The point at stage 12 is the calculated hemicircumference of the spherical embryo (radius = 1.2 mm). Between stages 12 and 13 the length of the nervous system decreases as the hemisphere converts to a disc. Thereafter the length increases at the rates shown. Most rapid elongation is from mid-neurula stage 15 to neural tube closure at stage 19.

age of apical cell surfaces and rearrangement of the cells in the notochordal region certainly continue after stage 15. Burnside ('71, '73a) has shown that apical surface shrinkage and concomitant cell shape changes occur in the later neurula stages of *Taricha torosa*. C.-O. Jacobson ('62) illustrated midline elongation of the neural plate through stage 17 in the axolotl, *Ambystoma (Siredon) mexicanum*. We have shown that the nervous system elongates throughout neurulation in *Taricha torosa* (Section VIII, fig. 38). Thus we suspect that the same forces form a tube from the keyhole-shaped plate.

Schroeder ('70) analysed neurulation in the anuran *Xenopus laevis* and proposed a model to explain it. Anuran neurulation is complicated by the presence of two layers of ectoderm in the neural plate region. Schroeder was mainly concerned with explaining the closure of the neural plate into a tube. His model included: (1) cell shape changes mediated by microtubules and contracting microfilaments, (2) pushing upward by the myotomes, (3) pushing mediad by the epidermal ectoderm that "migrates mediad by a mechanism akin to mass amoeboid movement," (4) a role of the elongating notochord in actively opposing the longitudinal shortening of the neural plate during in-folding.

Schroeder's model agrees with our analysis of urodele neurulation in two ways: the roles of cell shape changes and an involvement of the notochord. The "pushing" by myotomes and epidermis that he proposes is either absent or non-essential in the urodele. Isolated neural plates and notochords will complete neurulation through to the closed tube stage. Moreover, the epidermis is actually pulling.

A serious defect of a number of papers (Schroeder, '70; Baker and Schroeder, '67; Waddington and Perry, '62; and others) is that cell shapes are compared at different

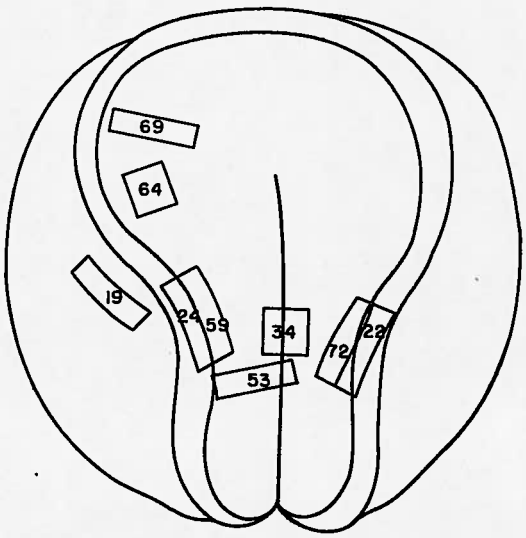

Fig. 39 The rectangles and squares are equal areas (0.036 mm²). Cell counts were made from high magnification photographs of living stage 15 embryos and are recorded in each area.

stages without first deriving maps of cell movements. The cells compared are not necessarily the same cells.

(2) *Cellular basis of the height programs*

The contraction of the apical surface of a neural plate cell and the concomitant elongation of the cell perpendicular to the plate involve microfilaments and microtubules. This has been demonstrated for *Taricha torosa* by Burnside ('72, '73a) and for numerous other species (cf. Burnside, '73a; Wessells et al., '71, for review). Microfilaments are arranged in a purse-string fashion around the cell perimeter at the apical end. These bundles of filaments are united through the desmosomes in a network that joins cell to cell. This microfilament network ensures that shrinkage of each cell surface pulls on the neighboring cells. Burnside ('72, '73a) presented evidence and arguments that the ring of microfilaments is contractile. She also demonstrated, by colchicine experiments, that the microtubules oriented in the long axis of the neural plate are necessary for cell elongation. (She favors a mechanism of basally directed transport of cytoplasmic constituents along the microtubules.) Thus it seems that microfilaments and microtubules acting together may be responsible for each cell's height program. Therefore, we may envision a molecular basis for the shrinkage pattern. Accounting for the details of the shrinkage pattern (fig. 15) presents a challenging problem.

(3) *Cellular basis for elongation of the notochordal region*

Cell rearrangements (changes of neighbors), rather than cell shape changes, are principally involved in the elongation of the notochordal region. The origin and development of the notochord and the notochordal region of the neural plate may give us some insights into the mechanisms involved.

The presumptive notochord is first localized, within hours of fertilization, in a crescent (at first, the gray crescent) lying at right angles to the antero-posterior axis of the embryo. This position is maintained through cleavage and blastula stages. In the embryo of the anuran *Xenopus*, gray crescent cortical cytoplasm of the uncleaved or recently cleaved egg shares a property of the later notochord: the ability to induce the central nervous system and other axial structures. This was shown by removing or transplanting the gray crescent cortical cytoplasm (Curtis, '60, '62, '63) or by implanting gray crescent cortical cytoplasm into the blastocoel of a host embryo (Tompkins and Rodman, '71) where it induced a secondary axis.

During gastrulation the crescent of notochordal cells involutes around the dorsal lip of the blastopore to assume an internal position underlying prospective neural plate. (Involution involves well-known cell shape changes. See Waddington, '40, '42; Holtfreter, '43.)

During neurulation the crescent of notochordal cells is rearranged into a rod oriented along the antero-posterior midline. This dramatic rearrangement must involve numerous changes in cell neighbors (shear). During neurulation there is an ever increasing contact among future notochordal cells (Mookerjee et al., '53). This observation has been confirmed by electron microscopy (Waddington and Perry, '62). By stage 15, the notochord forms a sheath around itself. The expansion characteristic of later stages involving formation and growth of intracellular vacuoles (Mookerjee et al., '53) has not yet begun.

The neural plate cells that come to overlie the notochord are positioned at the beginning of neurulation like the notochord, in a crescent at right angles to the antero-posterior axis. They lie at the posterior end of the prospective neural plate contiguous with the crescent of pre-notochordal cells around the dorsal lip of the blastopore. These overlying neural plate cells make the same rearrangements as the subjacent notochord to become a long rod at the antero-posterior midline. (They are the future floor plate cells of the spinal cord and posterior brain.)

(4) *Origin of the shrinkage pattern*

It has been suggested (A. G. Jacobson, '66) that determination of the nervous system depends about half on predetermination and about half on induction by the chordamesoderm. We have done a simple experiment in an attempt to assess the relative roles of "predetermination" and induction by the chordamesoderm in establishing the shrinkage pattern. We severed the dorsal hemisphere of ectoderm (the future neural plate) with a cut around the equator of stage 12 embryos and rotated only the ectoderm by 90° (20 cases). If predetermination had a role in fixing the pattern, then the pattern would now have been rotated 90°. If the pattern is fixed mainly by induction from the underlying unrotated chordamesoderm then, since that induction occurs mostly after the stage at which the ectoderm was rotated, a normal, unrotated shrinkage pattern should have been imposed on the rotated ectoderm.

We observed these embryos by time-lapse cinematography. Rather than forming a normal neural plate, the rotated prospective neural plate ectoderm made extensive abnormal convolutions and assumed an abnormal appearance (fig. 40). Sections of these embryos showed a complete lack of nervous tissue. It is most unusual to get no nervous tissue when chordamesoderm is underlying competent ectoderm. Predetermination and induction may be giving conflicting instructions in these cases.

(5) *The function of lines of shear*

Cell domains in an embryo may be integrated or controlled through junctional communication among the cells (Loewenstein, '68; Furshpan and Potter, '68). We have found that the abrupt boundaries between cell domains in the stage 15 neural plate correlate with lines of shear in the notochordal region and at the boundary between the neural plate and epidermis. These lines of shear could break junctions between cells and serve to isolate domains of cells from one another, allowing them to pursue different developmental pathways. This mechanism may be seen in other developmental systems: lines of shear must occur at the edge of the optic cup, (the future iris), which is the boundary between sensory retina and pigmented retinal epithelium (A. G. Jacobson, in preparation); the regression of the primitive streak in the chick creates a line of shear down the midline that has a role in somite formation (Lipton and Jacobson, '74a,b).

Fig. 40 External view of an embryo whose neural hemisphere was rotated 90° at gastrula stage 12. The picture was taken when control embryos had reached tail bud stage 21. This grotesque embryo completely lacks a brain and spinal cord. × 33.

(6) *Summary of neural plate shaping*

During blastula stages the prospective neural plate maps as a spherical quadrant above the gray crescent. During gastrula-

tion all ectoderm, including the prospective neural portion, behaves the same. The ectoderm thins and spreads, the movement being away from the animal pole and toward the forming blastopore. This is the process called epiboly. The quadrant of ectoderm that represented the future neural plate of the blastula is converted to a hemispheric shell during gastrulation. This hemispheric shell is underlain by prospective chordamesoderm that involutes around the dorsal and lateral blastopore lips. This mesodermal sheet thins and spreads rapidly to completely underlie the prospective neural plate by the end of stage 12.

As stage 13 begins, each cell of the prospective neural plate acquires a height program that it executes regardless of where it is transplanted. The spatial distribution of height programs, the shrinkage pattern, is quite complex (fig. 15). The notochord and overlying notochordal area of the neural plate become a determined system that will together elongate along the antero-posterior midline.

The chordamesoderm probably also has a shrinkage pattern, since this extended sheet of cells contracts with movements similar to those in the neural plate, and with identical motions in the notochordal areas (C.-O. Jacobson, '69). Moreover, the fate map we have produced for the neural plate (fig. 24) is most likely reflected in the underlying chordamesoderm. Much mesoderm located in posterior regions at late stage 12 is actually future anterior mesoderm (and inductor of anterior neural plate).

We assume that the shrinkage pattern is imposed through induction by the underlying chordamesoderm, and from predetermination. The cell rearrangements that produce the thrust of the notochordal region of the neural plate are induced by, and require the continued cooperation of, the notochord.

Near the end of stage 12, the ectodermal cells in the area of the future neural plate stop their epibolic motion toward the blastopore and reverse direction to head back toward the animal pole with a component also toward the dorsal midline. When the neural plate cells make this change, they stop getting flatter and begin to get taller.

From late stage 12 through late stage 13 (about 21 hours of development at 17° C) the boundary of the neural plate is approximately circular. This circle corresponds to the equator between dorsal and ventral halves of the embryo, except near the blastopore where the boundary between neural and epidermal ectoderm drops below the equator. Much shrinkage occurs during this time. Its effect is to convert the hemispheric shell of the neural area into an approximate disc. During this period there is also considerable rearrangement of cells in the notochordal region. The notochord and the notochordal region of the neural plate are elongated crescents in the medio-lateral direction at early stage 12 and have rearranged into regions about as wide as they are long by late stage 13. The effect of this on the shape of the plate is not great. This rearrangement is responsible for much of the decrease in extent of the blastoporal rim which has essentially become a slit by late stage 13.

At about the end of stage 13 and the beginning of stage 14, the antero-posterior length of the neural plate becomes minimal as shrinkage in the plate draws the anterior boundary up over the equator and back slightly toward the blastopore. The anterior boundary stops this retrograde motion at beginning stage 14 and returns to the equator, then slowly the antero-posterior axis elongates (fig. 38). At the end of stage 15 this elongation increases rapidly.

Both the shrinkage pattern (fig. 15) and the notochordal thrusting (figs. 1, 27) are necessary and sufficient to convert the neural hemispheric shell into a flattened keyhole shape. We believe these same forces continue to operate and shape the neural plate into a neural tube.

ACKNOWLEDGMENTS

This work was mainly supported by a grant from the National Institutes of Health (HD-03803). R. Gordon's work was supported in part by the State University of New York at Buffalo through the Einstein Chair budget of the late Prof. C. H. Waddington, NASA Grant NGR-33-015-016 to the Center for Theoretical Biology, and NIH Grant HD-05136 to Dr. Robert Rosen. We also thank the Information Processing Center of the Woods Hole Oceanographic Institution for some computing time (NSF Grant GJ-133).

For discussions and cooperation we thank

Beth Burnside, Robert S. Schechter and the staff of the Engineering Computer Center of the University of Texas at Austin, and the PDP 10 systems staff at the National Institutes of Health. For helpful comments we thank David Beebe, Leslie J. Biberman, Richard Campbell, Alfred J. Coulombre, Bruce Kellogg, Maurice Klee and Joram Piatigorski.

LITERATURE CITED

Avery, C. S., Jr. 1933 Structure and development of the tobacco leaf. Amer. J. Bot., 20: 565–592.

Baker, P. C., and T. E. Schroeder 1967 Cytoplasmic filaments and morphogenetic movement in the amphibian neural tube. Develop. Biol., 15: 432–450.

Burnside, B. 1968 Morphogenetic Movements in the Neural Plate of the Newt *Taricha torosa*. Ph.D. dissertation, The University of Texas at Austin, 113 pp.

Burnside, B. 1971 Microtubules and microfilaments in newt neurulation. Develop. Biol., 26: 416–441.

——— 1972 Experimental induction of microfilament formation and contraction. J. Cell. Biol., 55: 33a.

——— 1973a Microtubules and microfilaments in amphibian neurulation. Amer. Zool., 13: 989–1006.

——— 1973b *In vitro* elongation of isolated neural plate cells: possible roles of microtubules and contractility. J. Cell Biol., 59: 40a.

Burnside, B., and A. G. Jacobson 1968 Analysis of morphogenetic movements in the neural plate of the newt *Taricha torosa*. Develop. Biol., 18: 537–552.

Curtis, A. S. G. 1960 Cortical grafting in *Xenopus laevis*. J. Embryol. Exp. Morph., 8: 163–173.

——— 1962 Morphogenetic interactions before gastrulation in the amphibian *Xenopus laevis* — the cortical field. J. Embryol. Exp. Morph., 10: 410–422.

——— 1963 The cell cortex. Endeavour, 22: 134–137.

da Riva Ricci, D., and B. Kendrick 1972 Computer modelling of hyphal tip growth in fungi. Canadian J. Bot., 50: 2455–2462.

Erickson, R. O. 1966 Relative elemental rates and anisotrophy in growth in area: a computer programme. J. Exp. Bot., 17: 390–403.

Flügge, W. 1967 "Viscoelasticity." Blaisdell, Waltham, Massachusetts.

Furshpan, E. J., and D. D. Potter 1968 Low resistance junctions between cells in embryos and tissue culture. In: Current Topics in Developmental Biology. Vol. 3. A. A. Moscona and A. Monroy, eds. Academic Press, New York, pp. 95–127.

Gillette, R. 1944 Cell number and cell size in the ectoderm during neurulation. (*Amblystoma maculatum*). J. Exp. Zool., 96: 201–222.

Glaser, O. 1914 On the mechanism of morphological differentiation in the nervous system. I. The transformation of a neural plate into a neural tube. Anat. Rec., 8: 525–551.

——— 1916 The theory of autonomous folding in embryogenesis. Science, 44: 505–509.

Glasstone, S., K. J. Laidler and H. Eyring 1941 The Theory of Rate Process. McGraw-Hill, New York.

Gordon, R. 1966 On stochastic growth and form. Proc. Natl. Acad. Sci. (U.S.A.), 56: 1497–1504.

Gordon, R., N. S. Goel, M. S. Steinberg and L. L. Wiseman 1972 A rheological mechanism sufficient to explain the kinetics of cell sorting. J. Theor. Biol., 37: 43–73. (Reprinted in: Mathematical Models for Cell Rearrangements. G. G. Mostow, ed. Yale Univ. Press, New Haven, Connecticut, 1975, pp. 196–230.)

Happel, J., and H. Brenner 1965 Low Reynolds Number Hydrodynamics. Prentice-Hall Englewood Cliffs, New Jersey.

Harris, T. H. 1964 Pregastrular mechanisms in the morphogenesis of the salamander *Amblystoma maculatum*. Develop. Biol., 10: 247–268.

Hildebrand, F. B. 1956 Introduction to Numerical Analysis. McGraw-Hill, New York.

Hodgman, C. D. 1943 Handbook of Chemistry and Physics. Twenty-seventh ed. Chemical Rubber Publ. Co., Cleveland, Ohio, p. 266.

Holtfreter, J. 1943 A study of the mechanics of gastrulation. I. J. Exp. Zool., 94: 261–318.

——— 1946 Structure, mobility and locomotion in isolated embryonic amphibian cells. J. Morph., 79: 27–62.

——— 1947 Observations on the migration, aggregation and phagocytosis of embryonic cells. J. Morph., 80: 25–55.

Holman, R. M., and W. W. Robbins 1947 A textbook of General Botany for Colleges and Universities. John Wiley and Sons, New York, p. 189.

Jacobson, A. G. 1958 The roles of neural and non-neural tissues in lens induction. J. Exp. Zool., 139: 525–557.

——— 1966 Inductive processes in embryonic development. Science, 152: 25–34.

——— 1967 Amphibian cell culture, organ culture, and tissue dissociation. In: Methods in Developmental Biology. F. H. Wilt and N. K. Wessells, eds. Crowell, New York, pp. 531–542.

Jacobson, C.-O. 1959 The localization of the presumptive cerebral regions in the neural plate of the axolotl larva. J. Embryol. Exp. Morph., 7: 1–21.

——— 1962 Cell migration in the neural plate and the process of neurulation in the axolotl larva. Zool. Bidrag ((Uppsala)), 35: 433–449.

Jacobson, C.-O., and J. Löfberg 1969 Mesoderm movements in the amphibian neurula. Zool. Bidrag ((Uppsala)), 38: 233–239.

Kantorowich, L. V., and G. P. Akilow 1964 Functional Analysis in Normed Spaces. Pergamon, Oxford.

Kaufmann, P. 1974 The mechanisms of neural tube formation. Int. Rev. Cytol., 38: 2465–2772.

Lehto, O., and K. I. Wittanen 1973 Quasiconformal Mappings in the Plane. Springer, Berlin.

Lin, C. C., and L. A. Segel 1974 Mathematics Applied to Deterministic Problems in the Natural Sciences. Macmillan, New York.

Lipton, B. H., and A. G. Jacobson 1974a Analysis of neural somite development. Develop. Biol., 38: 73–90.

——— 1974b Experimental analysis of the mechanisms of somite morphogenesis. Develop. Biol., *38:* 91–103.

Loewenstein, W. R. 1968 Communication through cell junctions. Implications in growth control and differentiation. Develop. Biol. (Suppl.), *2:* 151–183.

Manchot, E. 1929 Abgrenzung des Augenmaterials und anderer Tielbezirke der Medullarplatte; die Teilbewegungen wärend der Auffaltung (Farbmarkierungsversuche an Kiemen von Urodelen) Roux' Arch. f. Entwmech., *116:* 689–708.

Milnor, J. W. 1965 Topology from the Differentiable Viewpoint. Univ. Press of Virginia, Charlottesville.

Mookerjee, S., E. M. Deuchar and C. H. Waddington 1953 The morphogenesis of the notochord in amphibia. J. Embryol. Exp. Morph., *1:* 399–409.

Ortega, J. M., and W. C. Rheinboldt 1970 Iterative Solution of Nonlinear Equations in Several Variables. Academic, New York.

Prandtl, L., and O. G. Tietjens 1934 Fundamentals of Hydro- and Aeromechanics. Dover, New York.

Richards, O. W., and A. J. Kavanaugh 1945 The analysis of growing form. In: Essays on Growth and Form Presented to D'Arcy Wentworth Thompson. W. E. LeGros Clark and P. B. Medawar, eds. Clarendon, Oxford, pp. 188–230.

Rugh, R. 1962 Experimental Embryology. Burgess, Minneapolis, Minnesota, p. 90.

Saaty, T. L., and J. Bram 1964 Nonlinear Mathematics. McGraw-Hill, New York.

Schechtman, A. M. 1932 Movement and localization of the presumptive epidermis in *Triturus torosus* (Rathke). Univ. Calif. Publ. Zool., *36:* 325–346.

Schroeder, T. E. 1970 Neurulation in *Xenopus laevis*. An analysis and model based upon light and electron microscopy. J. Embryol. Exp. Morph., *23:* 427–462.

Schulz, W. D. 1964 Two-dimensional Lagrangian hydrodynamic difference equations. Meth. Computational Physics, *3:* 1–45.

Smith, G. D. 1965 Numerical Solutions of Partial Differential Equations. Oxford Univ. Press, New York.

Thompson, D'Arcy W. 1952 On Growth and Form. Cambridge Univ. Press, Cambridge.

Thompkins, R., and W. P. Rodman 1971 The cortex of *Xenopus laevis* embryos: Regional differences in composition and biological activity. Proc. Nat. Acad. Sci. (U.S.A.), *68:* 2921–2923.

Turing, A. M. 1952 The chemical basis of morphogenesis. Phil. Trans. Roy. Soc., *B237:* 5–72.

Waddington, C. H. 1940 Organisers and Genes. Cambridge Univ. Press, Cambridge.

——— 1942 Observations on the forces of morphogenesis in the amphibian embryo. J. Exp. Biol., *19:* 284–293.

Waddington, C. H., and M. M. Perry 1962 The ultrastructure of the developing urodele notochord. Proc. Roy. Soc. London B., *156:* 459–482.

Wessells, N. K., B. S. Spooner, J. F. Ash, M. O. Bradley, M. A. Luduena, E. L. Taylor, J. T. Wrenn and K. M. Yamada 1971 Microfilaments in cellular and developmental processes. Science, *171:* 135–143.

Witschi, E. 1956 Development of Vertebrates. W. B. Saunders, Philadelphia, pp. 106, 109.

APPENDIX 1

Evolution of the computer simulation

This section describes in detail how the various physical parameters of a distorting sheet of cells are handled in our computer simulation. It also discusses alternative approaches that were considered and found inadequate and the resolutions of computer-specific problems encountered. For the final simulation see *Summary of the SHRINK Computer Program* in this APPENDIX.

(1) *Quantitative statement of the problem*

We begin by precisely defining the concepts of *height program* and *shrinkage pattern*. Let us assume that each cell maintains a constant volume V during shaping of the neural plate (*Assumption* 1 in APPENDIX 3). If $h(t)$ is the height of the cell as a function of time (its height program), and $A(t)$ is its contribution to the surface area of the sheet at time t, then these quantities are inversely related by

$$h(t)\cdot A(t) = V \tag{1.1}$$

or

$$A(t) = V/h(t) \tag{1.2}$$

(fig. 2).

Equation (1.2) is strictly valid only for a flat sheet of columnar cells which remain in contact from their basal to their apical ends. The forming neural plate may be approximated as a flat disc at late stage 13 (*Assumption* 2). The columnar cells are in close contact along their lengths (*Assumption* 3). We assume that the height programs are determined by stage 13 (*Assumption* 4).

Let (x_0,y_0) be the position of a cell at the initial time t_0. Its volume depends on its initial position (Gillette, '44), but will be independent of time (*Assumption* 1). Thus we let $V(x_0,y_0)$ designate the volume of a cell which was initially at (x_0,y_0). Let $h(x_0,y_0,t)$ and $A(x_0,y_0,t)$ be the height and apical area of this cell at time t. Then we have the relationship:

$$A(x_0,y_0,t) = V(x_0,y_0)/h(x_0,y_0,t) \tag{1.3}$$

$h(x_0,y_0,t)$ will be designated the *height transformation* and $A(x_0,y_0,t)$ will be called the *shrinkage transformation*. Each is a pattern in both space and time. They may be used interchangeably because of their reciprocal relationship, Equation (1.3). For a given (x_0,y_0), $h(x_0,y_0,t)$ is a *height program*; at time t_0, either $A(x_0,y_0,t_0)$ or $h(x_0,y_0,t_0)$ may be called the *shrinkage pattern*.

As the sheet shrinks each cell will move. We can express the path of a cell by its consecutive positions (x,y) where

$$x = x(x_0,y_0,t) \tag{1.4}$$
$$y = y(x_0,y_0,t).$$

The unknown functions (x,y) have initial values

$$x(x_0,y_0,t_0) = x_0 \tag{1.5}$$
$$y(x_0,y_0,t_0) = y_0.$$

If we could solve for the functions in Equations (1.4), we would have a complete description of the trajectories of all the cells. This is the aim of morphodynamics. The solutions must make use of information such as that provided by the relationship in Equation (1.3). The complexity of the problem arises from the fact that each cell contributes to the motion of the whole sheet. Thus the path of each cell depends on the behavior of all the other cells.

(2) *Digital representation of a sheet of cells*

We divide the sheet of cells into a number of circular shrinkage units. At the beginning of a simulation all shrinkage units have the same radius and the units are hexagonally close-packed. Together they approximate a disc representing the neural plate (fig. 15).

The initial radius of the units, r_0, is set by two criteria. It must be small enough so that *after* neural plate formation the narrowest regions of the neural plate, to the left and right of the notochord, remain at least a few units wide. It must be large enough so that the number of shrinkage units, N, is kept in reason. N is approximately $A/(\pi r_0^2)$, where A is the initial area of the neural plate. Thus N increases rapidly as r_0 is decreased. Moreover, the pro-

gra n consumes computer time proportional to $N^{3/2}$ (see below). We found $N \simeq 300$ satisfied both the needs for a fine spatial division of the neural plate and plausible computing time (about 15 minutes CPU time per run on the PDP10).

To obtain $N \simeq 300$, r_0 was set at 0.07 mm, representing about 22–33 cells per shrinkage unit on the average. (Initial non-uniformities in *cell* apical widths would cause this figure to vary over the neural plate.)

This method of representing a continuous sheet of cells in a digital computer has the advantage that the area of each unit is designated by only three geometric parameters: its x and y coordinates and its radius. (See below, *Future Computational Procedures*, for alternatives.) On the other hand, there are open spaces between the initially close packed circular units amounting to $1 - \pi\sqrt{3/8} = 32\%$ of the total area, which are not accounted for. As units move in the course of the simulation, they of necessity acquire overlaps with or gaps between their neighbors (fig. 19J). The open spaces and doubly represented areas may contribute to the problems with numerical convergence discussed below. Also, units which are apart have space between them into which other units may intrude.

(3) *Representation of the height programs*

A shrinkage unit represents a cylinder of tissue whose height varies with time. Each shrinkage unit is assigned a digit from 1 to 9, representing one of the nine height programs it could follow, $h_p(t)$, $p = 1, \ldots, 9$. The $h_p(t)$ are set in microns at 11 time points $t(j) = t_0 + j(t_1 - t_0)/10$, $j = 0, \ldots, 10$, where t_0 and t_1 are the initial and final times covered by the simulation. The heights at intermediate times are calculated by linear interpolation of h_p between $t(j)$ and $t(j+1)$ for the appropriate value of j.

The radius of each shrinkage unit, $r_p(t)$, is calculated using the assumption (Equation (1.3)) that the volume of the cylinder remains constant:

$$\pi r_0^2 h_p(t_0) = \pi r_p^2(t) h_p(t) \tag{1.6}$$

or

$$r_p(t) = r_0 \sqrt{\frac{h_p(t_0)}{h_p(t)}} \tag{1.7}$$

The *spatial* pattern of he.g.t programs, or shrinkage pattern, is established by hand using interactive "computer surgery." An initial pattern is displayed on a computer graphic terminal. This consists of hexagonally close packed units lying within the disc representing the embryo, which are labelled with height programs 1 to 9 (fig. 15). A pointer can be moved from unit to unit using keys sensed by the computer. The height program of the indicated unit may be changed to any other. If the label is set to 0, then the unit will be removed before the simulation proceeds. If the pointer is moved to a space not containing a unit, a new unit may be inserted at that position. Thus any surgical operation involving excisions, transplantations, or inversions may be imitated.

For convenience each new shrinkage pattern is recorded as a file on the computer disc storage, from which it may be retrieved for later simulation runs.

(4) *Repacking of the units during shrinkage*

Although the shrinkage units are initially hexagonally close-packed, as soon as their radii change by different amounts in accordance with the height programs (Equations (1.7)), this arrangement is disrupted. Two features of hexagonal close-packing are lost. First, it is no longer possible for each unit to just contact each of its neighboring units. Second, as a consequence, the position of a unit is no longer uniquely specified by the positions of its neighbors. Thus any algorithm which moves or "repacks" the units in an attempt to retain them in a contiguous sheet must make compromises about the positioning of the units and will be arbitrary to some degree. This explains, in retrospect, the considerable difficulties we had in designing an adequate algorithm.

In our first repacking algorithm we attempted to move all units simultaneously. A vector was calculated from a unit to its neighbors, of a length just long enough to bring them in contact. The actual motion of the unit in one iteration was taken as the vector sum of the vectors towards all its neighbors. Consider the ith unit of radius r_i at a given moment. Let the index

j represent its nearest neighbors. The distance between unit i and a neighbor is

$$d_{ij}^q = \sqrt{(x_i^q - x_j^q)^2 + (y_i^q - y_j^q)^2} \tag{1.8}$$

where (x_i^q, y_i^q) is the position of the center of unit i at the qth iteration during a single repacking. If the units were in contact, the distance between their centers would be the sum of their radii, $r_i + r_j$, which we shall call the *relaxed distance* between two adjoining units. A vector which would bring unit i into contact with unit j could be defined to have components

$$\Delta x_{ij}^q = \left(1 - \frac{r_i + r_j}{d_{ij}^q}\right)(x_j^q - x_i^q) \tag{1.9}$$

$$\Delta y_{ij}^q = \left(1 - \frac{r_i + r_j}{d_{ij}^q}\right)(y_j^q - y_i^q)$$

and the net motion, (the sum of the vectors towards all neighbors), is given by

$$x_i^{q+1} - x_i^q = \sum_j \Delta x_{ij}^q$$
$$y_i^{q+1} - y_i^q = \sum_j \Delta y_{ij}^q \tag{1.10}$$

At the beginning of the simulation each unit inside the disc is nearly symmetrically surrounded by six neighbors pulling it in opposite directions, so that the *net* motion by this algorithm, Equation (1.10), will be very small. Units at the edge of the disc, on the other hand, do not have balancing neighbors, and would have a significant net motion. Thus one would need a large number of iterations to propagate the motion at the edge inwards. Because of this slow convergence and consequently long computer time needed, the algorithm of Equation (1.10) was abandoned.

We adopted another point of view in which we attempted to calculate the effect of each shrinkage unit on the rest of the sheet. Insofar as the behavior of a shrinkage unit is similar to the behavior of the cells it represents, we may regard this as an attempt to simulate the deformation of the sheet caused by the pulling of a single shrinking cell.

We temporarily designate one shrinkage unit as a *packing center* and move all the other units towards it. At first, we calculated the motion of each unit towards a packing center by treating the rest of the sheet as continuous. Only the packing center, designated by the subscript k, was shrunk, say by an area

$$\Delta A_k = \pi r_k^2(t) - \pi r_k^2(t - \Delta t) \tag{1.11}$$

where Δt is the time between iterations. Consider a point at a large distance μ from the packing center. It will move towards the packing center by a distance

$$\Delta\mu = -\Delta A_k/(2\pi\mu) \tag{1.12}$$

(fig. 41). To first order, this is the effect of a single cell on the sheet as a whole.

Each shrinkage unit was moved towards the packing center by this amount. Unfortunately, this procedure does not account for the finite size of the neighboring shrinkage units, so that it leads to large amounts of overlap of units near the packing center. However, a correction for this effect did not help much.

Instead of using a formula, such as Equation (1.12), the following more discrete approach was taken. We moved the units toward the packing center in consecutive rings of units, attempting to adjust the distances so that neighboring units just touched. All the nearest neighbors were adjusted to the packing center. Then *their* nearest neighbors, the next ring, were adjusted to them, etc., so the adjustments propagated outwards from the packing center. Within a given ring the units were adjusted in random order to avoid any systematic effects. This method prevented most local overlapping and was retained. Each shrinkage unit had to be considered as a packing center in turn so that each could be shrunk. We found that any sys-

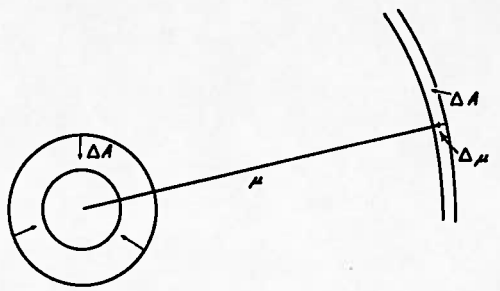

Fig. 41 When a circular unit decreases its area by ΔA, a point at a large distance μ from its center will move towards it by a distance $\Delta\mu = -A/(2\pi\mu)$.

tematic order of choosing units as packing centers made the overall shape of the disc lopsided, because of the impossibility of obtaining a unique packing of circles with varying radii. Therefore, we chose the packing centers in a random order to evenly distribute the empty space between the units. Later, we noted that *all* of the units could be shrunk slightly before starting a repacking, which necessitated far fewer repackings.

Because hexagonal close-packing could not be retained, if we moved any pair of neighbors into perfect contact we would disrupt other pairs. Thus a compromise was made in which only a partial correction towards the relaxed pair distance is made with each repacking q:

$$d_{ij}^{q+1} = (1-c)\, d_{ij}^{q} + c(r_i + r_j) \qquad (1.13)$$

The parameter c determines the amount of adjustment per repacking. If $c = 0$ no adjustment is made. If $c = 1$ a perfect adjustment would be made. When $c > 0.9$ we found that cracks propagated through the disc, as if it were brittle. By trial and error we found $c = 0.5$ to be satisfactory.

Suppose that we were simulating only a single pair of units, i and j. Let the *relative distance* between them be

$$\delta_{ij}^{q} = \frac{d_{ij}^{q}}{r_i + r_j} \qquad (1.14)$$

(Note that δ_{ij}^{q} is a dimensionless quantity.) Then equation (1.13) becomes

$$\delta_{ij}^{q+1} = (1-c)\,\delta_{ij}^{q} + c \qquad (1.15)$$

and consecutive repackings would change the relative distance in steps toward the relaxed value 1, as shown in figure 42.

δ_{ij}^{q+1} could have been any monotonically increasing function of δ_{ij}^{q} passing through the unshaded region of figure 42. For simplicity we chose the linear function of Equation (1.15). Since $\delta_{ij}^{q+1} = c$ when $\delta_{ij}^{q} = 0$, the parameter c is analogous to a "hard core potential" in molecular dynamics computations.

By solving Equation (1.15) recursively, we find that

$$\delta_{ij}^{q} = 1 + (\delta_{ij}^{0} - 1)(1-c)^{q} \qquad (1.16)$$

which approaches 1 as q increases, independently of the value of c, if $0 < c < 1$.

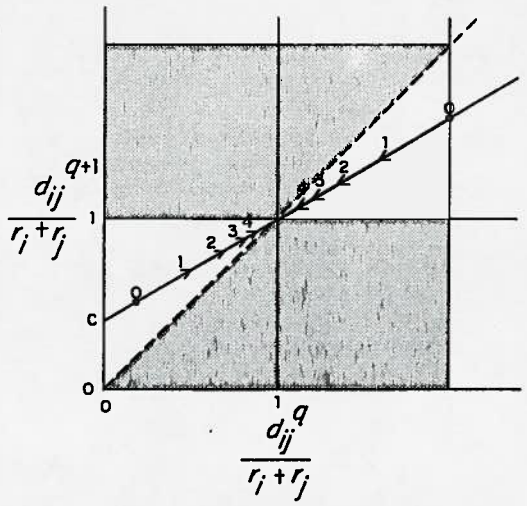

Fig. 42 New relative distance between units versus previous relative distance (Equations (1.14) and (1.15)). For an isolated pair the relative distance would converge towards 1 whether initially less than 1 or greater than 1, as shown by the labels for consecutive iterations in the two cases. Any monotonically increasing function through the unshaded region would share this property.

Let us return to the full disc of shrinkage units. If unit j is being adjusted to unit i at the qth repacking, it could be placed anywhere on a circle of radius d_{ij}^{q+1} centered on shrinkage unit i. We choose a position on this circle such that the motion of unit j would be towards the packing center. The geometry of this situation is depicted in figure 43. Let the subscript k again designate the packing center. In algebraic terms the new coordinates of unit j are

$$x_j^{q+1} = x_k + (x_j^{q} - x_k) d_{kj}^{q+1}/d_{kj}^{q}$$
$$y_j^{q+1} = y_k + (y_j^{q} - y_k) d_{kj}^{q+1}/d_{kj}^{q} \qquad (1.17)$$

where, by using the law of cosines

$$d_{kj}^{q+1} = \Big\{ d_{ik}^2 + (d_{kj}^{q})^2 - (d_{ij}^{q})^2 \pm \sqrt{[d_{ik}^2 + (d_{kj}^{q})^2 - (d_{ij}^{q})^2]^2 + 4(d_{kj}^{q})^2 [(d_{ij}^{q+1})^2 - d^2 ik]} \Big\} / (2\, d_{kj}^{q}) \qquad (1.18)$$

Two roots of Equation (1.18) exist because the circle of radius d_{ij}^{q+1} centered on unit i generally intersects the line between unit j and the packing center at two points (fig. 43). The root which results in smallest

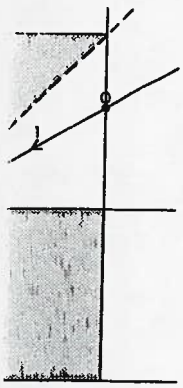

e between units
Equations (1.14)
the relative dis-
whether initially
shown by the la-
the two cases.
unction through
his property.

isc of shrink-
g adjusted to
, it could be
f radius d_{ij}^{q+1}
We choose a
that the mo-
's the packing
s situation is
e subscript k
center. In al-
inates of unit

$$l_{kj}^{q}$$

$$_{kj}^{q} \qquad (1.17)$$

ines

$$\overline{l_{kj}^{q})^2 + (d_{ij}^{q+1})^2}$$

(1.18)
exist because
centered on
line between
at two points
lts in smallest

displacement of unit j is chosen. If the roots are complex numbers, then the line does not intersect the circle. In this case units i and j are adjusted along the line between their centers.

If two units being adjusted to one another are in the same ring, then they are also adjusted along the line between their centers instead of along the line to the packing center. This can be justified heuristically in terms of the orthogonality between radial and tangential adjustments. Inclusion of this nuance led to considerable improvement in the results of repacking.

In detail, the simulation utilized three consecutive rings, each one bond further from the packing center. Initially the first ring contains only the packing center; the second contains its nearest neighbors. The third ring is built from neighbors of units in the second ring which are not in the first two rings. These rings propagate by deriving the first ring from the second, the second from the third, and calculating a new third ring.

Each unit in the first ring is considered, but in random order. When one unit is chosen, it is considered to be *anchored*, and will no longer be moved during this repacking. Each of its unanchored first nearest neighbors, belonging to the first or second ring, is adjusted to it. When the ith unit is anchored, its net displacement since the last repacking is calculated. We can consider this as the *local displacement* of the sheet. When a unit is anchored, its second nearest neighbors which are in the third ring are moved according to this local displacement. In this way the relative positioning of the units, the *local structure* of the sheet, is preserved. If local displacements were not taken into account, units of consecutive rings could overlap more and more severely with increasing distance from the packing center.

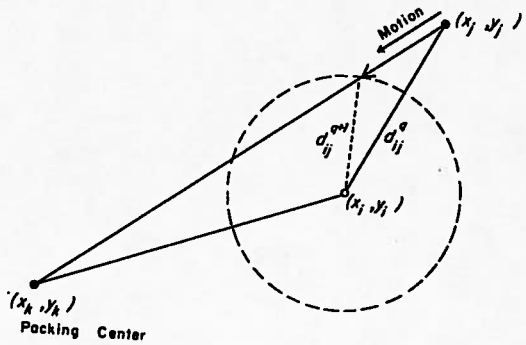

Fig. 43 Geometry for calculating the motion of unit j towards the packing center k so that it ends up at distance d_{ij}^{q+1} from unit i after the qth repacking with the motion directed toward the packing center.

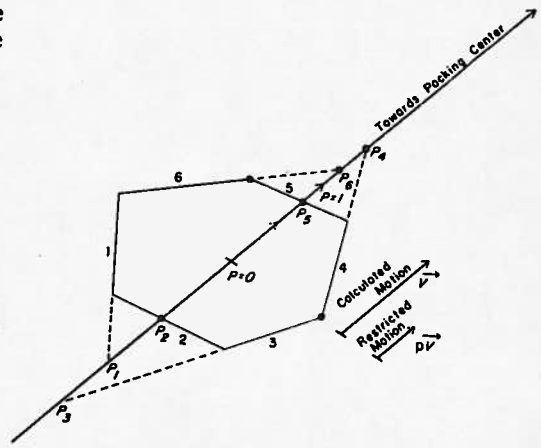

Fig. 44 The motion of a shrinkage unit located at $p = 0$ is restricted to remain within the polygon formed by the bonds between its nearest neighbors, numbered 1 to 6 here. (Their centers are at the vertices of the polygon.) The vector of motion is parametrized so that it lies along the line of motion from $p = 0$ to $p = 1$. Each bond intersects this line at a given value of p. Here p_1, p_2 and $p_3 < 0$, and are ignored in Equation (1.19), so that $p_{min} = p_5$. The restricted motion is then $p = \min(p_5/2, r/v)$ (Equation 1.20). Note $v = d_{ij}^{q+1}$, Equation (1.13).

The lines between the centers of nearest neighbors, which we shall call *bonds* or *connections*, initially form a net or *planar graph*. In other words, they do not cross. We found it essential to restrict the motion of adjustment to hinder bond crossing from developing. If the graph of connections is not kept planar, the topological equivalents of folds and wrinkles may develop.

Consider a unit about to be moved. Its center lies inside the polygon formed by the bonds between its nearest neighbors. If the motion would carry it outside the polygon or near an edge, it is restricted to

an appropriate magnitude less than that given by Equation (1.13) (fig. 44). (The direction is maintained.)

The motion is restricted to remain within the polygon in the following way. First a list is made containing each bond between nearest neighbors of the unit to be moved. The vector of motion is described by a linear parameter p so that $p = 0$ corresponds to no motion, and $p = 1$ corresponds to the full motion of Equation (1.13). The vector of motion may be considered as a line segment [0,1] along a line described by the parameter p (fig. 44). Each bond l between nearest neighbors intersects this line at a point describable by $p = p_l$. If the intersection falls behind the vector of motion, i.e., $p_l < 0$, it is ignored. Let

$$p_{\min} = \min [p_l \text{ such that } p_l > 0] \quad (1.19)$$

where l ranges over the bonds. Then the restricted length of the vector of motion is given by the parameter

$$p = \min(1, p_{\min}/2, r/v) \quad (1.20)$$

where r is the radius of the unit and v is the length of the unrestricted vector. The second term keeps the motion away from a bond between neighbors. The third term restricts the motion to less than one radius.

(5) *Simulating the notochord*

When we concluded that the notochordal region provides an essential driving force to the shaping of the neural plate, we were faced with the problem of appending its effect to the computer simulation.

Utilizing the notion of "tissue hydrodynamics" (Gordon et al., '72), we began to think of the neural plate as a two dimensional fluid in which the notochordal region acted as a moving boundary. The lengthening of the notochordal region is sufficiently slow so that effects of inertia or momentum would be entirely negligible (Gordon et al., '72: their APPENDIX B). Thus if we regard the sheet as a fluid, transmission of motion from the notochord to the rest of the sheet would require that it be either of exceedingly high viscosity or viscoelastic.

It is clear that there ought to be flows away from the anterior end of the lengthening notochord and towards its narrowing sides. It was suggested that we could approximate this pattern of flow of representing the notochordal region by a rectangle whose anterior edge is a line of sources of an ideal *non-viscous* fluid and whose sides are sinks (R. Schecter, personal communication) (fig. 45). The lineal densities of sources and sinks along the sides of the rectangle can be balanced so that there is no net production of fluid. The flow can be normalized so that the velocity at the anterior end of the notochord equals its rate of elongation. The flow pattern is easily calculated by superposition of the complex potential functions for the velocity fields emanating from the sources and sinks (Prandtl and Tietjens, '34: Chapter X). Thus the motion of any shrinkage unit due to the change of shape of the notochord could be estimated. The computer program was fixed to alternate between repackings and such flow calculations. At each alternation the notochord elongated by an appropriate increment.

This continuous treatment of the sheet for the purpose of calculating the effect of notochord elongation was abandoned when we realized that the repacking algorithm calculates the "flow" of units due to their shrinkage and thus should also be able to repack the units to accommodate small motions of the notochord. To accomplish this the perimeter of the notochord region of the neural plate was represented by a line of shrinkage units along an inverted parabola (O in fig. 19). Pairs of units on the left and right sides of the notochord perimeter were regarded as nearest neighbors so that waves of repacking could propagate across the notochord (*Assumption* 5, APPENDIX 3). (cf. fig. 19K.)

As the notochord elongates its perimeter increases. Thus new units have to be intercalated between the old ones along the perimeter. These may be considered to have come from cells within the perimeter.

As discussed above, enormous rearrangements of the neural plate cells over the notochord must occur. Such motions were not simulated because they have not yet been adequately observed and because they are of no consequence to the motions of the rest of the neural plate. Only the motion of the perimeter of the notochordal region affects the rest of the sheet, and that is obtained by observation.

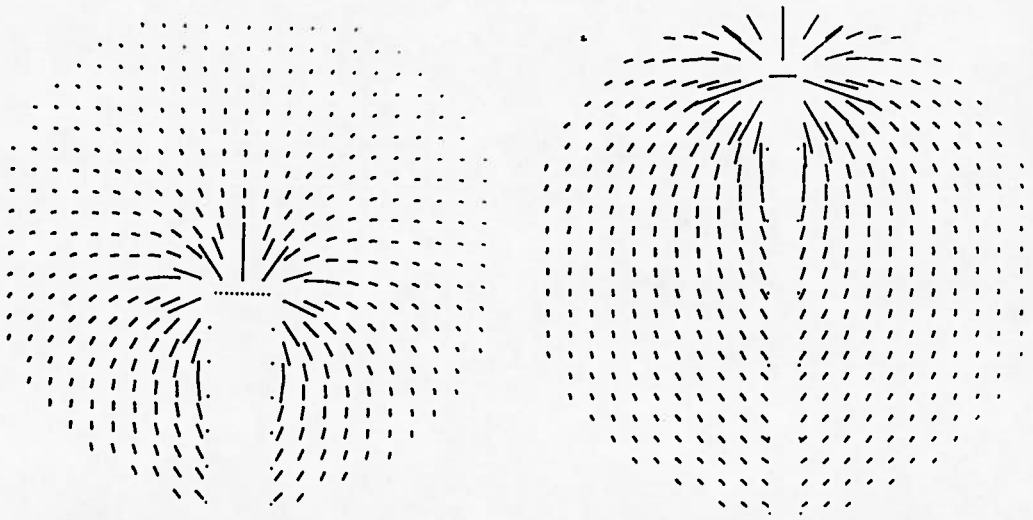

Fig. 45 Flow pattern in the neural plate caused by a notochordal region modeled as a row of sources of fluid at the top of a rectangle and as rows of sinks along the sides. The method of reflection about the x-axis was used, with the origin at the blastopore (bottom). Dimensions of the notochord (rows of dots) correspond to the initial (left) and final (right) widths and heights of the parabolas used in later simulations.

The initial notochord units were chosen by taking the outermost units falling within a parabola of appropriate size placed over the initial hexagonal close-packed array of units (fig. 15). The chosen units were then moved to the parabola (cf. fig. 19B). This generally caused some initial overlapping of units which was worked out by subsequent repackings. Because we required an odd number of notochord units intersected by the parabola, it was necessary to adjust the initial notochord dimensions and the vertical displacement of all the units until this condition could be met. Thus the initial notochord dimensions depart slightly from the empirical ones.

When units repack towards a packing center, the notochord ought to move with them. However, the notochord should retain its momentary shape, so the units representing the perimeter of the notochord must be moved as a group. Concerted motion of the notochord was achieved by first allowing the notochord units to move individually during a repacking, with the exception that they do not readjust to one another. Then their average displacement was calculated, the notochord units restored to their former positions along the parabola, and the non-notochord units moved by the opposite displacement.

(6) *The problem of getting deformation rather than splitting from thrusting of the notochord*

If the neural plate were a fluid without any viscosity, the elongating notochord would grow right through it, cleaving it in two. At the other extreme, if the array of shrinkage units representing the neural plate were to act like a crystal, the thrusting notochord would crack through as if it were brittle. We want the notochord to carry the "fluid" along, the intermediate case. Quantification and computer implementation of this concept proved to be elusive.

Viscosity is a measure of the difficulty for molecules within a fluid to slip past one another (Glasstone et al., '41). There are many ways to introduce viscous-like behavior into the simulated sheet of units. In our first attempt we allowed the bonds between units to be one of two types: breakable and permanent. Breakable bonds snapped if the relative distance between two units exceeded some set *cutoff distance*. Permanent bonds could be stretched indefinitely.

Permanently binding some units and not others made the sheet inhomogenous in its properties and required arbitrary decisions about which units to bind. Thus instead, a larger relative cutoff distance was invoked for *all* units, and permanent bindings were no longer used.

In order to allow shrinkage units to change neighbors, once a bond was broken, it was necessary to allow new bonds to form. This was done by allowing a unit with a free bond to attach to any other shrinkage unit within some present relative *cut-on distance*.

Because these steps did not eliminate cleavage, we turned to the concept of the *boundary layer* in continuum fluid mechanics. It is ordinarily assumed that a boundary layer of fluid has zero velocity relative to a boundary. Thus we moved those shrinkage units directly attached to notochord units along with the notochord during its elongation (*Assumption* 6, APPENDIX 3).

However, cleavage still occurred. In another attempt to reduce cleavage, we imposed bilateral symmetry (*Assumption* 7, APPENDIX 3) on the motion of the units by averaging the coordinates of left and right mirror image units after each increment of notochord elongation. Rather than solving the cleavage problem, this created special difficulties with the units on the midline. However, symmetrization became of importance after the cleavage problem was solved, and was thus retained.

We have indicated above the desirability of retaining the net of connections as a planar graph. Despite our attempts to do this, when the distortions produced by the notochordal region became large, *tangles* or *crossed bonds* did develop. We interpreted these tangles as meaning that shear was occurring and could only be relieved by allowing a change of neighbors. Thus we created an algorithm to detect such tangles and undo them. The search for crossed bonds is limited in the following way, in order to minimize computing time: each bond is checked for crossing bonds only between nearest neighbors of the two units at its ends. The longer of two crossing bonds is broken. New bonds are then formed provided the units involved are within the relative cut-on distance of each other *and* bond formation would not cause a crossing. The operations of untangling and establishing bonds are alternated repeatedly until no tangles remain. More than one iteration is sometimes necessary because of the locally restricted extent of checking for tangles. Checking is done in random order. A "flag" or indicator is set for each unit found to be involved in a bond crossing. Only the flagged units are rechecked in the next iteration, further speeding the computation.

The operations of breaking and making bonds represent a crude model for the mechanism of cell rearrangement.

All the above factors contributed to our understanding of how to simulate the neural plate, but did not solve the problem of cleavage by the notochord. The answer lay in what we had thought was the independent problem of rate of convergence.

(7) *Numerical convergence and relaxation*

The rate of convergence of a numerical calculation representing a spatial process by discrete units can vary with the order in which the units are considered (Smith, '65). It was for this reason that we shifted from the slowly convergent simultaneous motion of the units (Equation (1.10)) to the use of packing centers.

When a spatial process has a localized energy input, it is best to use an order for considering the units which starts at the energy source and works out from it (M. Klee, personal communication). For instance, the computation of the wake of a ship should start from the ship, rather than from the shoreline. By analogy with this situation, we introduced a special form of *repacking from the notochord*. Instead of taking a single unit as packing center, all the units of the notochord perimeter are initially placed in the first ring. A point must still be chosen as the packing center. It is chosen at random on the line between the blastopore and the anterior end of the notochord. By using only repackings from the notochord we were finally able to eliminate cleavage of the neural plate.

We assume that the neural plate relaxes after each increment of lengthening of the notochordal region (*Assumption* 8, APPENDIX 3). This means that if notochordal lengthening stopped and the neural plate cells stopped shrinking, the sheet would

come to rest in a time short compared to the total time of plate formation. Relaxation is simulated by repacking as many times as necessary to bring the units to rest, before elongating the notochordal region another increment.

For the simulation, relaxation at every step means that the exact force modelled by the "equation of motion," Equation (1.13), is of little consequence. (We are simulating the dynamics rather than the kinematics of neural plate formation.)

We had considerable difficulty in designing a criterion for convergence, apparently for the following two reasons. First, the repacking algorithm adjusts units one pair at a time with some degree of random choice of the pairs. Thus in consecutive repackings a unit may be moved first towards one neighbor, then towards another. Second, the packing center exerts a systematic pull. Thus, since the packing center is chosen randomly along the length of the notochordal region, all units are tugged first one way, then another. These factors are partially absorbed by the following criterion for convergence.

Let the *mean relative displacement* at the qth repacking be the vector

$$v_x^q = \frac{1}{N} \sum_{i=1}^{N} sgn(x_i^q)\,(x_i^q - x_i^{q-1})/r_i$$
$$v_y^q = \frac{1}{N} \sum_{i=1}^{N} (y_i^q - y_i^{q-1})/r_i \qquad (1.21)$$

where

$$sgn(x) = \begin{cases} 1 & \text{if } x \geqslant 0 \\ -1 & \text{if } x < 0 \end{cases} \qquad (1.22)$$

and N is the number of shrinkage units.

The *sgn* function is needed so that the bilateral symmetry of the form will not cause v_x^q to always be near zero. (The origin for the coordinate system is at the blastopore, with the positive y-axis going through the notochord.) Let the *running average* of the mean relative displacement be the vector

$$\bar{v}_x^q = \frac{1}{q} \sum_{k=1}^{q} v_x^k$$
$$\bar{v}_y^q = \frac{1}{q} \sum_{k=1}^{q} v_y^k \qquad (1.23)$$

The running average tends to smooth out any oscillatory movements. Repackings are stopped when the length of either (v_x^q, v_y^q) or $(\bar{v}_x^q, \bar{v}_y^q)$ is less than some constant, which was chosen as $0.1\,\bar{r}/r_0$, where $\bar{r}$ is the current average radius of the units. (Fewer than 10 repackings per step were needed.)

Each increment of notochordal lengthening is kept at approximately $r_0/3$, where r_0 is the initial radius of the units. Thus the number of such steps is proportional to the $\sqrt{N}$. Since the repacking algorithm is local in its operation, the total computing time is proportional to $N\sqrt{N} = N^{3/2}$.

(8) *Summary of the SHRINK computer program*

We shall now describe the operation of the final version of the SHRINK program. Each shrinkage unit is described by its coordinates, radius, height program and bonds to nearest neighbors. The computer program records the trajectory of the unit and the number of times it changes nearest neighbors (a measure of *shear*). The computers we used allow one to display line drawings on a cathode ray tube. Thus we created a number of display modes:

(1) *Hexagons.* Each unit is displayed as a hexagon centered at its (x,y) coordinates. The size of the hexagon is chosen so that it would circumscribe a circle with the current radius of the unit. Hexagons are used only because they require less computing time to display than circles.

(2) *Nearest neighbors.* Lines are drawn between the centers of units bound to one another. One way connections are indicated by dashed lines which originate from the unit sending out the bond.

(3) *Height programs.* The appropriate digit 1 through 9 is displayed at the coordinates of the unit.

(4) *Shear.* The number of changes of nearest neighbors for each unit.

(5) *Trajectories.* The paths of the centers of selected units are displayed.

(6) *D'Arcy Thompson grid.* A record is kept of the *initial* left and right nearest neighbors of each unit. Lines are drawn connecting the center of a unit to the centers of its initial left and right neighbors and to the midpoints between the pairs of units which were initially above and below it. The result is a rectangular grid which is seen to distort as the simulation proceeds. The rectangles of the grid start out with a height to width ratio of $\sqrt{3}$.

All display modes can be observed dynamically, although this slows the compu-

tation considerably. The press of a key allows one to switch between modes, or turn the display on and off. Any part of the pattern may be enlarged to any extent. (This feature was crucial for successful debugging.) The program may be stopped and two or more display modes superimposed, or enquiries may be made about the state of any unit.

The program records the parameters of the units periodically on a magnetic disc file. It may be run in a *review* mode to generate displays from the file. The simulation may also be restarted from any recorded time.

The general flow of the SHRINK program is as follows:

(1) Interactively set the values of all parameters.

(2) Calculate new radii for each height program (Equation (1.7)).

(3) Calculate the current mean radius of the units.

(4) Lengthen the inverted parabola representing the notochordal region and narrow its width so the area is unchanged (*Assumption* 9, APPENDIX 3). If the spacing of the units along the notochordal perimeter is too large relative to the mean unit radius, intercalate new units between them. Then make a bond from each new unit to the nearest units on the same side. Also form the bonds across the notochord.

(5) Distribute the notochordal units evenly along the parabola defining the notochordal region.

(6) Displace each non-notochordal unit attached to the notochordal region by a vector equal to the average motion of its notochordal neighbors since the last repacking. (This simulates zero relative velocity of the boundary layer.)

(7) Choose a packing center and repack the units from that center outwards. (See details below.)

(8) Calculate the running average vector of the net displacement of the units since the last repacking, Equation (1.21) and (1.23). (Repeat steps 7 and 8 until the convergence criterion is met.)

(9) Invoke bilateral symmetrization, if called for.

(10) Break crossed bonds (tangles).

(11) Attempt to create bonds between units with less than their full complement of bonds and their second nearest neighbors, but only if no bonds are crossed in the process. (Repeat steps 10 and 11 until no more crossed bonds are found, or until the possibilities for new bonds are exhausted, but no more than ten times.)

(12) Record all current coordinates, radii, and connections on magnetic disc.

(13) Increment the time and go to step 1 unless the notochord has reached its final length.

The following are details of the repacking algorithm:

(1) Fill a list for ring 1 with either the unit chosen randomly as the packing center or with all the notochord units. If the latter, take the packing center to be a point chosen at random along the midline of the notochord.

(2) Fill the list for ring 2 with the nearest neighbors of the units in ring 1, which are not in ring 1.

(3) For each unit α in the first ring, chosen in random order:

(A) Calculate its displacement since the last repacking.

(B) Set a flag anchoring unit α.

(C) For each unanchored nearest neighbor β, considered in random order:

(a) List its neighbors (not already in rings 1, 2 or 3), in ring 3, and move them to preserve local structure. (A flag is set so that for each unit this local displacement occurs only once per repacking.)

(b) Move unit β toward unit α along the line towards the packing center if β is in ring 2, (Equations (1.13), (1.17) and (1.18)), or along the line between their centers if both α and β are in ring 1 (Equation (1.13)). In either case the motion of β is restricted so that it remains within the polygon of its nearest neighbors (Equations (1.19), (1.20)).

(4) The list for ring 1 is discarded. Ring 2 becomes ring 1, ring 3 becomes ring 2, then step 3 is repeated, unless the list for ring 2 is now empty.

A few devices are incorporated into the computer program to meet special conditions:

Each unit is allowed to have a maximum of six bonds from itself to its nearest neighbors. (It may receive more than six.) The *initially unsatisfied* bonds of the units at the edge of the disc are blocked to prevent

the edge from folding on itself. One block is removed if such a unit receives a new bond.

After each increment of notochord elongation the unit at the anterior end of the notochord is made to sever its longest bond, if all six are satisfied. This gives it an opportunity to attach to the unit anterior to it, which it may otherwise overlap.

When tangles are being removed, no unit is allowed to lose more than two bonds. This prevents units from becoming isolated. For a similar reason no more than two bonds crossing a given bond are broken at once.

(9) *Future computational procedures*

The reason for repacking the shrinkage units is to bring neighboring units as close to contact as possible. We have accomplished this by adjusting the distances between pairs of units. An alternative (C. Peskin, personal communication) would be to use a measure of the total deviation of all pairs from their relaxed spacings, such as

$$\Delta = \sum_{\substack{\text{nearest} \\ \text{neighbor} \\ \text{pairs } (i,j)}} (\delta_{ij} - 1)^2 \qquad (1.24)$$

This may be generalized to use any function of δ_{ij} representing a potential whose minimum occurs when all pairs are relaxed. The problem would then be, given the radii of the units $\{r_i(t)\}$, at time t, and the nearest neighbor connections, find a set of coordinates $\{(x_i,y_i)\}$ which *minimizes* Δ.

With this formulation we would obtain a set of simultaneous nonlinear equations which may be solved by iterative methods (Hildebrand, '56; Ortega and Rheinbold, '70). Equations (1.10) actually represent a similar iterative procedure.

The disadvantage of such a straightforward minimization procedure is that it does not account for the appearance of crossing bonds.

Minimization could be used, however, to give a more accurate representation of a contiguous sheet of cells than a set of circles. We would initially divide the sheet into a number of *triangular* shrinkage units and let $\{(x_i,y_i)\}$ refer to the *vertices* of the triangles. Thus the *whole* sheet would be covered without gaps. We would have to design a function to be minimized. We might, for instance, place each set of three vertices about a given area so as to give the minimum perimeter. Mathematically we would then have an *isoperimetric* problem. Since each shrinkage unit decreases in area, each perimeter would also have to decrease. If the shrinkage units were regarded as the cells themselves, we can see that this involves untested assumptions about the behavior of the perimeter and area of cells' apical membranes.

Equations for the areas of the triangles may be written as functions of the coordinates of the vertices (Hodgman, '43). These equations become side constraints and necessitate the introduction of Lagrangian multipliers to solve for $\{(x_i,y_i)\}$. Our feeling is that such a minimization procedure using vertices instead of the centers of shrinkage units may turn out to be the best computational approach.

APPENDIX 2

The mathematics of morphogenesis: Morphodynamics

Mathematical analysis has made a contribution to our understanding of the shaping of the newt neural plate, which we shall now outline. But more importantly, as in the nature of mathematics, the analysis will be seen to be of general applicability to morphogenesis. For this reason we have called the mathematics which follows *morphodynamics*.

We will begin with general considerations on mappings of the plane into itself, then introduce physical considerations by examing two dimensional Lagrangian hydrodynamics. This will provide a basis for relat-

ing our work to that of others using D'Arcy Thompson grids, and for discussing the relationship between our computer simulation and the mathematical analysis. Finally we shall outline a general three dimensional morphodynamics of developing embryonic tissues.

(1) *Mappings of the plane: Topology*

Some of the definitions, results, and limitations of topology have a bearing on our approach to the morphogenesis of sheets of cells. A *mapping* of the plane is a transformation which moves each point on the plane from one location to another. For example, for each time t, Equations (1.4) represent a mapping of the plane, each point (x_0,y_0) being mapped into (x,y). We shall assume that within the domain defined by the boundary of the neural plate this mapping is *one-to-one*.

Such an assumption is mathematically convenient and would follow immediately if we could identify "points" of the plane with the centers of the cells. This would clearly not be adequate if one were attempting a spatially continuous description of the interactions between adjacent cells. Moreover, in the presence of cell division, the one-to-one nature of the mapping could only be preserved if daughter cells remained attached to one another. We have obtained some evidence for shearing over the notochord and possibly at the neural ridge. In general, we cannot expect a morphogenetic mapping to be precisely a one-to-one transformation. (See *A General Approach to Morphodynamics* below.)

If a mapping of a convex domain of the plane into itself has the property that the distance between any two points decreases, (a *contraction* mapping), then the mapping will have a unique *fixed point*, i.e., a point which remains in its original location (Saaty and Bram, '64; Kantorovich and Akilov, '64). For the neural plate isolated without the notochord, we know that because of the shrinkage any two neighboring cells come closer to one another. It may be shown (B. Kellogg, personal communication) that a convex domain undergoing such a *local* contraction is also undergoing a *global* contraction, so that the isolated neural plate without notochord should have a fixed point.

We may define a *stationary point* as a point of zero velocity. We have observed a stationary point on the neural plate, as did Manchot ('29). Insofar as the intact embryo topologically approximates a sphere (say, as a blastula), we may apply to it a theorem which states that winds or flow on the surface of a sphere must have a stationary point (Milnor, '65).

For each time t we have a distinct mapping. However, if we assume that $(x(t), y(t))$ is a continuous function, then the set of stationary points for consecutive times t, taken together, should describe some trajectory over the plane, as we have observed.

(2) *Mappings of the plane: Conformal mappings*

A *conformal* mapping is one which preserves local angles. Thus two straight lines meeting at a given angle in the plane will intersect at the same angle after such a transformation (even though the lines themselves may rotate, deform, and become arced). Infinitesimal triangles will be geometrically similar to their transforms, and small circles will transform into circles. Knowing whether or not a D'Arcy Thompson grid transformation is conformal can help in uncovering the driving forces.

A conformal mapping has a number of useful properties. It obeys the Cauchy-Riemann equations

$$\frac{\partial x}{\partial x_0} = \frac{\partial y}{\partial y_0}$$

$$\frac{\partial x}{\partial y_0} = \frac{-\partial y}{\partial x_0} \qquad (2.1)$$

and the mapping may be described as an analytic function $z(z_0,t) = x + iy$ of the complex variable $z_0 = x_0 + iy_0$. Further differentiation of the Cauchy-Riemann equations leads to

$$\frac{\partial^2 x}{\partial x_0^2} + \frac{\partial^2 x}{\partial y_0^2} = \frac{\partial^2 y}{\partial x_0^2} + \frac{\partial^2 y}{\partial y_0^2} = 0 \qquad (2.2)$$

so that x and y are solutions of Laplace's equation.

We have assumed that each neural plate cell exerts an *isotropic* force on the rest of the cells, pulling them equally from all directions by an amount that depends only on the distance away. In the absence of external forces, to a first approximation it

seems reasonable to expect that each cell would retain its apical shape, so that the transformation would be conformal. For this reason we took the lack of conformality, (some angles are *not* preserved, fig. 4), as evidence of an external shearing force, which we attributed to the notochordal region. On the other hand, the isolated neural plate without notochord experiences no external forces, so that its transformation should be approximately conformal. Quantitative experiments are needed to determine to what extent the isolated neural plate actually undergoes a conformal change of shape. (The mathematical conditions under which isotropic forces rigorously imply a conformal transformation have yet to be worked out. Any conformal transformation may be described in terms of an equivalent shrinkage pattern.)

(3) *Two-dimensional Lagrangian hydrodynamics*

We may think of the deformation of the developing neural plate as a two dimensional *flow* of material. Hydrodynamics and the more general continuum mechanics are branches of science dealing with the flow of materials. Two coordinate systems are in general use in hydrodynamics. Calculations are usually done in *Eulerian* (*spatial*) coordinates, in which one asks for the velocity, pressure, etc., in a fluid at a given point in space, as the fluid moves by that point. Since hydrodynamicists ordinarily deal with fluids which are chemically homogeneous, such an approach generally leaves nothing out. However, we expect to find spatial gradients of properties between our *fluid elements*, which may be regarded as the individual cells. When each fluid element may differ from the next, it is more natural to use a coordinate system which allows us to follow each one. Such *Lagrangian* (*material*) coordinates move with the fluid elements:

> "This apparently very convenient method proves to be very troublesome and difficult in practice, when solutions to definite problems have to be found, though it is very powerful, to be sure in the few cases where it can be carried through. . . ."—Prandtl and Tietjens ('34).

Thus the very nature of morphodynamics forces us to work at the limits of the hydrodynamicists' art, even with the current availability of high speed computers.

The morphodynamics of a sheet of cells is solved in Lagrangian terms if we can find formulae for $x(x_0,y_0,t)$ and $y(x_0,y_0,t)$ (Equations (1.4)) in terms of the time course of the behavior of the individual cells. ("Behavior" of a cell includes its change of shape in response to internal and external forces, as well as differentiation and motility, if any.) Equations (1.5) provide initial conditions.

When we place a D'Arcy Thompson grid over a developing sheet of cells and follow the cells at the grid points, we are directly recording the motion in Lagrangian coordinates. This has been done by Avery ('33), Holman and Robbins ('47), Erickson ('66) and Burnside and Jacobson ('68). The analysis of growing tobacco leaves by Richards and Kavanaugh ('45) took Avery's ('33) data, which was in Lagrangian form, and changed it to Eulerian coordinates. Thus, except near time $t = t_0$ (when the two coordinate systems are equivalent), they could not have related the changes of shape of the leaves to cellular behavior, if they had tried.

da Riva Ricci and Kendrick ('72) have presented an elegant analysis in effectively Lagrangian terms of hyphal tip growth in fungi by nonuniform stretching. Their problem is greatly simplified by the organism's cylindrical symmetry, so that they only have to calculate the motion of points on a line representing the profile of the tip.

We will now show how physical considerations may be introduced into two dimensional Lagrangian morphodynamics. For a sheet of cells we can define a *surface density* (mass of protoplasm per unit area) $\rho(x_0,y_0,t)$ which may vary from place to place and with time. For instance, for a monolayer of abutting cells, such as the neural plate

$$\rho(x_0,y_0,t) = \frac{V(x_0,y_0,t)\, d\,(x_0,y_0,t)}{A(x_0,y_0,t)} = h(x_0,y_0,t)d(x_0,y_0,t) \qquad (2.3)$$

where d is the three dimensional mass density of a cell. (In our case d is probably constant. It would vary in a vacuolating leaf.) A sheet of cells acts as if it were a *compressible* two dimensional fluid, because the surface density ρ may vary. Since ρ is defined as a function of the initial

coordinates (x_0,y_0), it is a Lagrangian variable carried along with each cell as it moves.

Consider a particular rectangular area at time t_0 located at (x_0,y_0) with sides of lengths Δx_0 and Δy_0 whose density is initially $\rho_0 = \rho(x_0,y_0,t_0)$ (fig. 46). (The rectangle is assumed to be small enough so that the surface density ρ varies only slightly across it.) At a later time t, the rectangle will be deformed and rotated, now being located at (x,y). To a first approximation its shape will be that of a rhombus whose corners lies at the coordinates shown in figure 46. The displacements of the corners from (x,y) are given, for instance, by the rate of change of x with a change in x_0, $\partial x/\partial x_0$, times the amount of change in x_0, Δx_0. The area of this rhombus may be calculated in terms of three of its vertices, which form a triangle covering half of the area (Hodgman, '43). The result is

$$a = \Delta x_0 \Delta y_0 \left(\frac{\partial x}{\partial x_0}\frac{\partial y}{\partial y_0} - \frac{\partial x}{\partial y_0}\frac{\partial y}{\partial x_0} \right) \qquad (2.4)$$

If the volume of protoplasm under the area we are following does not change, and there is no net mass change, then we have that the amount of protoplasm before and after transformation is constant:

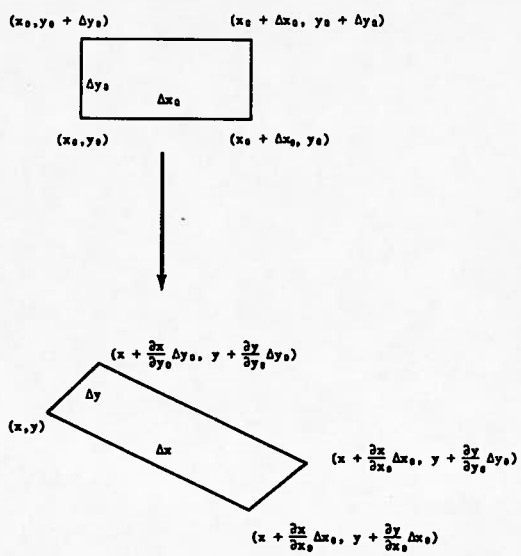

Fig. 46 Rectangular region of a plane before and after deformation and rotation to a new position.

$$\rho_0 \Delta x_0 \Delta y_0 = \rho a \qquad (2.5)$$

or

$$\frac{\rho(x_0,y_0,t_0)}{\rho(x_0,y_0,t)} = \frac{\partial x}{\partial x_0}\frac{\partial y}{\partial y_0} - \frac{\partial x}{\partial y_0}\frac{\partial y}{\partial x_0} \equiv J(x,y,x_0y_0) \qquad (2.6)$$

This is the two dimensional *equation of continuity* in Lagrangian terms. J is called the *Jacobian* of x and y with respect to x_0 and y_0.

Let us suppose that the motion of the sheet were conformal, in which case we can combine the Cauchy-Riemann Equations (2.1) with the equation of continuity to obtain two nonlinear partial differential equations in our two unknown functions x and y:

$$J = \left(\frac{\partial x}{\partial x_0}\right)^2 + \left(\frac{\partial x}{\partial y_0}\right)^2$$

and

$$J = \left(\frac{\partial y}{\partial x_0}\right)^2 + \left(\frac{\partial y}{\partial y_0}\right)^2 \qquad (2.7)$$

By combining Equations (2.3), (2.6), and (2.7), we obtain the *morphodynamic equations for the isolated neural plate* (without notochord):

$$\frac{h(x_0,y_0,t_0)}{h(x_0,y_0,t)} = J \qquad (2.8)$$

with J's from Equations (2.7).

Note that all quantities in this morphodynamic equation are measurable, so that it could be subject to a rigorous experimental test. The major assumption is that the mapping is conformal, which is also subject to an independent direct experimental test.

(4) *Mappings of the plane: Quasiconformal mappings*

We do not yet understand how the notochordal region changes shape, causing the neural plate to undergo a nonconformal transformation. However, we may attempt to describe the effects of this active elongation mathematically. Let us assume that a group of cells in the notochordal region elongates its apical area in a given direction. Thus a small circle of radius r_0 at time t_0 would be transformed to an ellipse with half axes $a(x_0,y_0,t)$ and $b(x_0,y_0,t)$, oriented at angle $\Theta(x_0,y_0,t)$ (figs. 24, 47). a, b and Θ are assumed to be Lagrangian properties, like h, of the initial coordinates (x_0,y_0), and not of the current position (x,y), because we assume that a cell could only

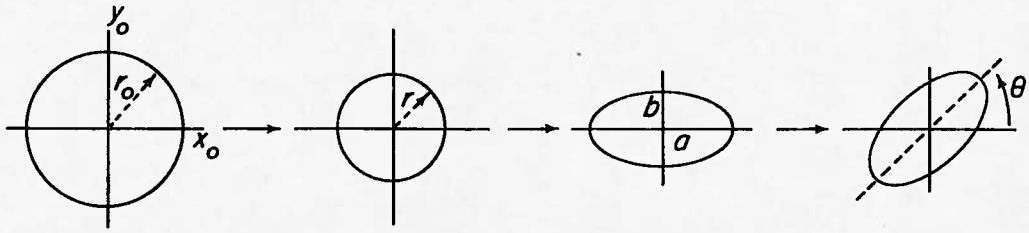

Fig. 47 Mathematical steps in transforming a small circle to a shrunk and rotated ellipse to derive the quasiconformal morphodynamic Equation (2.10).

ascertain its orientation relative to its neighboring cells.

A transformation of the plane which takes small circles into small ellipses of finite nonzero axial ratio or *stretching*

$$s(x_0,y_0,t) = \frac{a(x_0,y_0,t)}{b(x_0,y_0,t)} \qquad (2.9)$$

is called a quasiconformal mapping (Lehto and Virtanen, '73). By a derivation similar to that for Equation (2.8), we obtain the *morphodynamic equations for neural plate with notochord*

$$J = \frac{h(x_0,y_0,t_0)}{h(x_0,y_0,t)} = \frac{1}{s}\left[\left(\frac{\partial x}{\partial x_0}\cos\Theta + \frac{\partial y}{\partial x_0}\sin\Theta\right)^2 + \left(\frac{\partial x}{\partial y_0}\cos\Theta + \frac{\partial y}{\partial y_0}\sin\Theta\right)^2\right] \qquad (2.10)$$

$$= s\left[\left(\frac{\partial x}{\partial x_0}\sin\Theta - \frac{\partial y}{\partial x_0}\cos\Theta\right)^2 + \left(\frac{\partial x}{\partial y_0}\sin\Theta - \frac{\partial y}{\partial y_0}\cos\Theta\right)\right]$$

These equations reduce to Equations (2.8) when $s \equiv 1$ and $\Theta \equiv 0$.

For an arbitrary two dimensional tissue the more general relations of Equations (2.3) and (2.6) should be used on the left side of Equation (2.10).

We have not yet attempted to directly solve the morphodynamic Equations (2.8) and (2.10). However, insofar as they are equivalent to the computer simulation, we already have a numerical procedure for solving them. The equivalence is crude, especially for the notochordal region, which is treated more as a moving boundary than as a quasiconformal region by the simulation. A direct approach would be to solve the Lagrangian difference equations (Schulz, '64), which, however, suffers from "bond crossing" problems.

(5) *A general approach to morphodynamics*

The morphodynamics equations derived above leave out a number of physical phenomena, such as the stresses set up in the tissues, the viscoelastic response of the tissue to these stresses, and the possible existence of slippage (cf. fig.28). However, the weight of our evidence is that all of these factors exert only secondary effects on the form. The geometry of the neural plate is primarily generated by the changing geometry of its individual cells and by quasiconformal rearrangements of cells in the notochordal region. Equations (2.8) and (2.10) are primarily geometrical in nature.

Nevertheless, we would like to sketch the components of a more general theory of morphodynamics. In continuum mechanics there are four major equations which must be taken into account:

(1) conservation of mass (also called the equation of continuity);

(2) balance of linear momentum;

(3) balance of moment of momentum;

(4) constitutive relations (stress as a function of the local deformation or *strain*).

These equations must include the following features to be usefully descriptive of a developing organism:

(1) The equations should be expressed and solved in Lagrangian (material) coordinates.

(2) Most morphogenetic movements are slow enough so that the equations can be reduced to the case of creeping motion (Happel and Brenner, '65).

(3) The equations must include the active, anisotropic forces generated by the cells, such as shape changes generated by microfilaments and microtubules, and by oriented cell division.

(4) Surface forces, such as those involved in the sorting out of reaggregated cells, may be of considerable importance, and are likely to be anisotropic.

(5) The parameters describing cell behavior are both space and time dependent, and may depend on chemical interactions among the cells (Turing, '52).

(6) Some tissues may provide moving boundaries for others, and in any case there will be free boundaries.

(7) Mass changes due to cell growth and cell death must be taken into account.

There is an additional subtle factor which must be carefully analysed, namely the scale at which a continuum description is applicable (Lin and Segel, '74). Clearly, phenomena due to the behavior of spatially separated single cells, such as cell migration, cannot be described by a continuum model, except occasionally in a statistical sense. Cells in a continuous sheet probably have limits beyond which they may not be deformed. To some extent such limits could be incorporated into a nonlinear constitutive relationship between stress and strain. However, a strain may be reached at which cells must change their relationships to neighboring cells. Gordon et al. ('72) have shown that such slippage at the cellular level may be described macroscopically as a *tissue viscosity*. This viscosity is distinct from the viscous component of the viscoelastic stress/strain relationship expected in a sheet of contiguous cells whose neighbors are not changing. Of course, in tissues such as the neural plate over the notochord, both phenomena may occur simultaneously.

(6) *The general equation of continuity*

As a simple example of the mathematical richness of morphodynamics, consider the equation of continuity for a three-dimensional growing system, whose mass changes with time:

$$d(x_0,y_0,z_0,t)J(x,y,z,x_0,y_0,z_0,t) = d(x_0,y_0,z_0,t_0) + \int_{t_0}^{t} g(x_0,y_0,z_0,t)J(x,y,z,x_0,y_0,z_0,t)dt \qquad (2.11)$$

where d is the mass density and g is the rate of growth in mass of a Lagrangian volume element at (x_0,y_0,z_0). Equation (2.11) may be called the *morphodynamic equation of continuity with growth*. What is most interesting about this equation is that in terms of the Jacobian J it is an integral equation of the first kind, rather than an explicit equation for $J(t)$, such as Equation (2.6).

If the mass density d is constant, Equation (2.11) shows how the motion of a tissue is driven by its growth g. If there is no growth ($g \equiv 0$ everywhere), Equation (2.11) reduces to the ordinary equation of continuity (cf. Equation (2.6)). If d and g are both nonzero constants, Equation (2.11) reduces to

$$J(t) = J(t_0)\, e^{g/d} \qquad (2.12)$$

which implies that each volume element will expand exponentially, (or shrink, if g is negative).

(7) *Constitutive equation: Viscoelasticity*

At this time we can only draw qualitative conclusions about the stress/strain relationship in neural plate. While temporary elastic stresses are created, as shown by the gaping experiments described above, it is clear from the experiments on isolated neural plates that these stresses are not essentially involved in the final key-hole form. Thus the neural plate does not act as an elastic sheet, but rather "gives" in response to the generated tensions. Its behavior is both elastic and viscous, that is, viscoelastic.

There are two major idealized models for viscoelastic substances, called the *Maxwell*

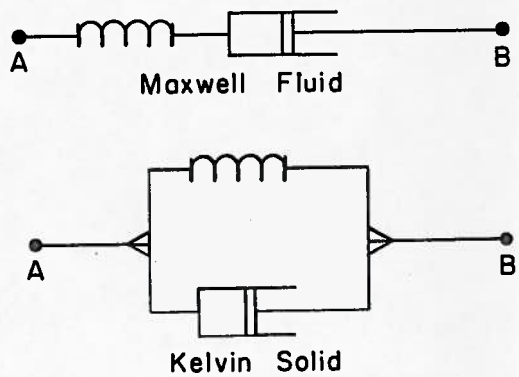

Fig. 48 In the two simplest models for viscoelasticity two points in a substance respond to forces as if they were connected by a spring (the elastic component) and a dashpot or piston (the viscous component) connected either in series (Maxwell fluid) or parallel (Kelvin solid). Most viscoelastic substances require more complex models.

fluid and the *Kelvin solid* (Flügge, '67). In a Maxwell fluid two neighboring points react to forces pushing or pulling them apart as if they were connected by a spring and dashpot in series (fig. 48). (A dashpot is a cylinder containing a viscous fluid which resists the motion of the piston.) A persistently applied force leads to greater and greater elongation, during which there is always an elasticity which would be released if a cut were made. A Kelvin solid may be represented by a spring and dashpot in parallel. It has a limit to its maximum distensibility.

Much more complicated models are possible, combining springs and dashpots in various ways (Flügge, '67), or by introducing nonlinearities into the parameters. The most we can conclude now is that a single cell probably behaves more like a Kelvin solid, being of finite distensibility, whereas the neural plate acts more like a Maxwell fluid. As such, if the forces are applied very slowly, the elastic stresses should relax. This is exactly what happens in the isolated neural plate with or without notochord, and in its computer simulation. (Such slowly applied forces cause the motion to be quasistatic.)

The slower relaxation of tensions in the intact embryo, compared to isolated neural plate, may be due to the epidermis being stretched over a whole sphere, or to friction against the underlying mesoderm.

APPENDIX 3

Justification of assumptions

Some of the important assumptions underlying the arguments in previous sections are justified and amplified here.

Assumption 1. The cells of the neural plate maintain a constant volume from stage 13 to stage 15

This assumption is justified on two grounds, directly from measurements of cell volume at the two stages, and indirectly from measurements of the volume of the entire nervous system.

Whether the neural plate increases its volume during neurulation has always been a fundamental question for the understanding of neurulation. Glasser ('14, '16) came to the conclusion that neural plate cells enlarged during neurulation after measuring "comparable" sections from different embryos of different ages. He measured ten non-consecutive cross sections taken from the middle of each of three embryos. Since cells are displaced in the embryo during neurulation, he could not have compared the same cell groups at different stages. He also failed to take into account changes in the number of cells per unit of cross-sectional area which must be evaluated before judging that a cell has gotten bigger because it is taller. His ideas of neurulation involving uptake of water at the basal ends of plate cells were based on false assumptions.

Gillette ('44) made measurements of the volume of the *total* ectoderm during neurula stages of *Ambystoma maculatum* and found little or no volume change. If anything, there was a decrease in volume from stage 13 to later stages.

Burnside and Jacobson ('68) mapped the displacement and changes in area of squares of a coordinate grid superimposed on the neural plates of *Taricha torosa* embryos recorded by time-lapse cinematography. The amount of decrease of an area correlated with the increase in height of cells in that area.

Burnside ('73a) has been able to measure cell volumes in areas of the neural plate at stage 13 and in the same displaced areas at stage 15. She made height and diameter measurements of 20 cells each from serial sections of embryos at stage 13 and stage 15, then calculated apical surface area and volume by assuming the cells were cylindrical. In two regions so measured she found the volumes of the cells remained relatively constant between the two stages. The change in apical surface area matched the change in area of the region of the coordinate grid (-40% compared to -46% in one case; -31% compared to -27% in another), and the apical surface area was inversely proportional to the cell heights just as we have proposed (Equation (1.2), APPENDIX 1).

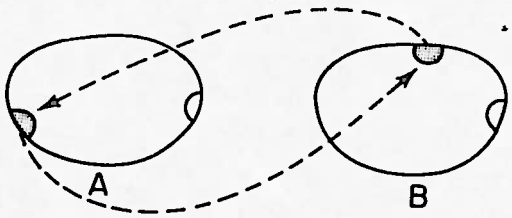

Fig. 49 At stage 13, prospective epidermis (shaded, A) was reciprocally exchanged with prospective neural plate (shaded, B). Results are shown in figures 50, 51, 52. Blastopores at right.

We have measured the volume of the entire nervous system at stages 13, 14 and 18. Embryos were fixed at various stages in Kahles F.A.A. fixative (60 ml H_2O, 32 ml 95% ethyl alcohol, 16 ml formalin, 2 ml glacial acetic acid) which Harris ('64) says causes minimal shrinkage of the tissues (less than 0.5%). Each section of the serial cross sections of entire embryos at stages 13, 15 and 18 was projected through a drawing tube of a microscope and the volume measured, as described in Section II. The weight of the pieces of paper representing the images of the section of the nervous system should be proportional to the volume of the nervous system. The weights for each stage were: stage 18, 84.5 grams; stage 15, 71.3 grams, and stage 13, 90.1 grams.

Previous measurements of the external diameters of ten stage 13 embryos (Burnside and Jacobson, '68) gave a diameter of 2.4 ± 0.1 mm. This standard deviation in diameter can be converted to volumes of whole embryos by calculating volumes of corresponding spheres:

D = 2.3 mm	V = 6.4 mm^3
D = 2.4 mm	V = 7.2 mm^3
D = 2.5 mm	V = 8.2 mm^3

The ratios of larger and smaller variations are 8.2/6.4 = 1.28. This is a dimensionless ratio that can be compared to the weight variations of cutouts representing nervous system volumes. The ratio of the largest to smallest of these is 90.1/71.3 = 1.26. It appears that the variation seen in measured nervous system volumes is within the range of variation expected among different embryos.

Each cell of the nervous system thus must maintain its volume, with the exception of those that divide, assuming no net mass transfer among cells. The two daughter cells of a divided cell probably have a total volume equal to the volume of the cell from which they came. There are not many cell divisions in the nervous system between stages 13 and 15. We estimated that a stage 13 neural plate contains n_0 = 6,600 cells and a stage 15 neural plate about n = 10,000 cells, corresponding to a mean of 0.6 doublings per cell.

We assume the two daughter cells that result from a cell division would together have apical surface areas and total lengths

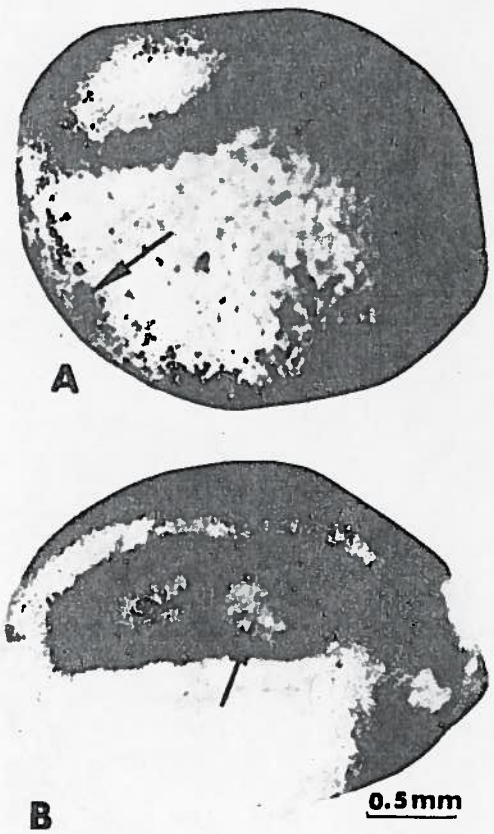

Fig. 50 Results, at stage 15, of the reciprocal transplantations done at stage 13 shown in figure 49. A. The neural plate transplanted into the epidermis (arrow) appears as a black area because the cells are much taller than surrounding epidermal cells and the apical pigment is concentrated. B. The epidermis transplanted into the neural plate has expanded in this foreign site distorting the shape of the spinal cord region.

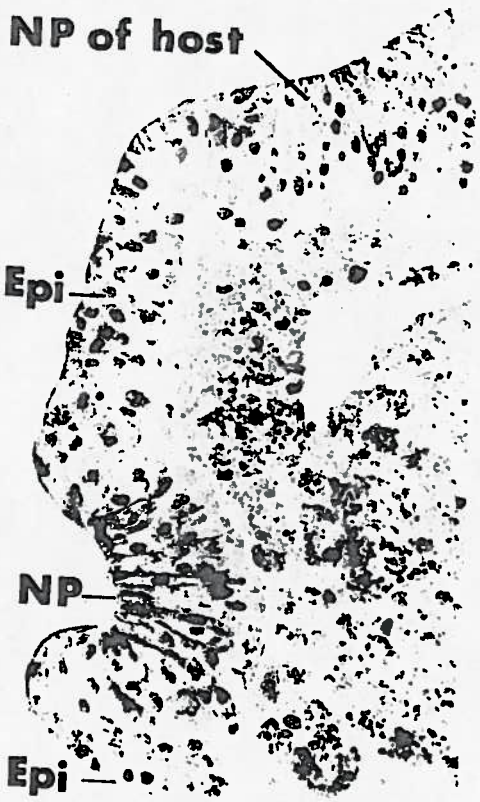

Fig. 51 Section through the implanted neural plate in the epidermis shown in figure 50A. The thicker pseudocolumnar neural plate cells (NP) are surrounded by a lower epidermis (Epi). × 150.

equivalent to the mother cell from which they arose, though this remains to be observed. If this is correct, mitosis could have no role in shaping the neural plate.

It is doubtful that there is any transfer of material needed for growth from one cell to another until the heart begins to beat. That first occurs at larval stage 34. Then, certainly, many regions of the embryo begin to grow at the expense of food stuffs transferred from the large endodermal cells that line the gut.

The increase in cell number by mitosis in a region is without consequence to the volume of that region until growth is possible. However, once growth commences, the numbers of cells in different regions would represent a store of morphogenetic potential. Then a region with greater numbers of cells is poised to grow rapidly as the cells enlarge.

Gillette ('44) found at stage 13, and at all subsequent stages of development of *Amblystoma maculatum*, that the anterior cells of the embryo (and of the neural plate) were smaller in volume than the posterior cells (about 7,000 cubic microns per cell at the anterior end versus about 10,700 cubic microns per cell at the posterior end). He believed this difference was an expression of the animal-vegetal gradient in cell size that originated during cleavage.

Assumption 2. The dorsal presumptive neural ectoderm of a late gastrula (stage 13) may be represented as a flat disc

At late stage 13 cross sections show that the prospective neural plate is mostly flat (Burnside and Jacobson, '68: their fig. 3). In the intact embryo, however, the future plate does bend sharply at its edges. Since the plate can be cut off the embryo, together with the underlying notochord, and laid flat in culture on a bed of agar where it transforms into a keyhole shape, it seems reasonable to model it starting as a disc.

Assumption 3. The cells of the forming neural plate are in close contact with one another along their lengths

Burnside ('68, '71) examined the *Taricha torosa* neural plate by electron microscopy. She found the columnar cells of the neural plate tightly attached near their apical surfaces by dense close junctions (100 Å gap) and desmosomes. Desmosomes also attach adjacent cells at other points along their length, but none are seen at the basal ends of the cells. The columnar cells are roughly parallel with contact between adjacent cells ranging from typical 200–250 Å gap to larger spaces, occasionally traversed by filapodia. By light microscopy, adjacent cells appear to be in close contact along their lengths (fig. 7).

Assumption 4. The future course of cell height changes of regions of the neural plate are programmed by stage 13

Evidence that cell height changes are programmed and independent of their contiguous tissue environment comes from the following experiments.

Fig. 52 Section through the epidermis implanted in the neural plate shown in figure 50B. A. Low power view across the entire neural plate showing thick neural tissue at the edges of the plate and the thin implanted epidermis in the center. B. Higher magnification to show cellular detail. Bars = 0.1 mm.

Embryos at the beginning of stage 13 were operated on in Holtfreter's solution at 17°C. Reciprocal transplantations of parts of the nervous system, and of epidermis and neural plate, were made (fig. 49).

An extreme test of the determination of height programs for displaced cells is seen in transplants of epidermis into the neural plate and neural plate into the epidermis at stage 13 (fig. 49). The epidermis in the neural plate expands while the contiguous neural plate cells shrink (fig. 50). The reciprocal transplant of neural plate tissue into the expanding epidermis also continues to shrink (fig. 50). The greater height of the neural plate cells embedded in the epidermis is especially evident in section (fig. 51). The low epidermis within the thick neural plate is seen in section in figure 52.

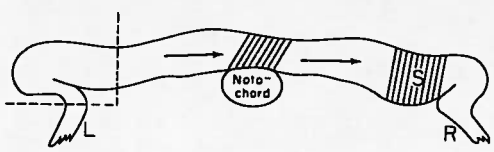

Fig. 53 Only the cells of the neural plate above the notochord are attached at their basal ends. When one side of the plate shrinks more than the other motion is translated across the notochordal area by tilting of the cells attached to the notochord. Normally the right and left halves of the neural plate shrink about the same amount, so tilting of cells over the notochord is only transient. Dashed line indicates region removed to produce a permanent tilt (see text).

Reciprocal transplantations between anterior and posterior regions within the prospective neural plate were made at stage 13. If the height programs are determined, the anterior piece transplanted to the posterior neural plate should shrink more than the surrounding region, and the posterior piece transplanted to the anterior neural plate should shrink less than the surrounding region. This was observed in the three cases done.

Holtfreter ('46, '47) isolated single cells

from salamander neural plates (*Ambystoma maculatum*). He observed that these cells retained their columnar shapes and continued to elongate in culture. This demonstrated that the elongation of a cell is an intrinsic behavior of the single cell, not requiring continuing cellular communication at this stage. Holtfreter's observations have been repeated by Burnside ('73b).

Assumption 5. Waves of repacking propagate across the region of the neural plate attached to the notochord

Observations on high magnification time-lapse movies confirm that this assumption is correct. Only neural plate cells over the notochord are anchored at their basal ends. These cells can sway to the right and left when pulled unequally by shrinkage from one of the two sides, but they are not displaced off the notochord (fig. 53). We deprived some embryos of their left prospective neural folds and some adjacent neural plate cells at stage 13. These embryos were fixed at stage 15 and cross-sectioned. Since the two sides of the plate would now shrink asymmetrically, we predicted that, if the above assumption were correct, the cells attached to the notochord would be permanently tilted toward the intact right side. Examination of the sections proved this to be the case. The cells over the notochord were tilted at an angle of 23°.

Assumption 6. The line of neural plate cells (and of shrinkage units) just off the region attached to the notochord move along with the cells attached to the notochord during elongation

This assumption is directly confirmed by observation of forming neural plates in time-lapse movies.

Assumption 7. The neural plate is bilaterally symmetric

This was shown to be true in detail by Burnside and Jacobson ('68: p. 540). Time-lapse movies of cell displacements in the neural plate were analysed frame-by-frame. Cell movements on each side of the midline were found to be accurate mirror images of one another. Normal neural plates always appear to be bilaterally symmetrical.

Assumption 8. The neural plate relaxes after each increment of motion of the notochordal region

Essentially we assume that motion of the notochord is instantaneously accommodated by cell movements or stretching, that there is no residual momentum. Gordon et al. ('72) have calculated momentum among sorting cells and found it to be insignificant.

One consequence of assuming fast relaxation is that the form depends only on the amount of notochordal lengthening and not on its rate. It is not necessary to assume that the notochordal region lengthens linearly even though, for the most part, it does (fig. 5). Fast relaxation may be an important general embryological principal: the rate of growth could vary with fluctuating temperature, without altering the sequence of forms. With slow relaxation, different growth rates could produce different forms.

We have observed that embryos grown at different temperatures, at which notochord lengthening would proceed at very different rates, all achieve the same shape. Embryos of *Taricha torosa* raised at temperatures ranging from 5° to 25°C form perfectly normal neural plates though the rates of formation vary widely with temperature. For example, it takes the embryo 25 days to go from stage 1 to stage 16 at 5°C, but only three days at 25°C (Jacobson, '58).

Assumption 9. The area of the notochordal region is constant

The notochordal region of the neural plate is visible in color movies of neural plate development, distinguishable by subtle color differences and by position and behavior. The area of the notochordal region was determined at stages 13 and 15 by projecting movie frames, outlining the notochordal region on paper, and cutting out and weighing the drawings. Actual length and width were calculated using a magnification factor obtained by projecting movie frames of a stage micrometer taken through the same optical setup.

In two of the films that show the notochordal areas best, the weights of cut-out notochordal regions were:

Film 1, stage 13 — 0.228 g; stage 15 — 0.239 g.

Film 2, stage 13 — 0.151 g; stage 15 — 0.150 g.

The small differences in weight at the two stages are well within the error due to drawing and cutting.